

**ROBUSTNESS ASSESSMENT OF A NOVEL 4D OPTIMIZATION APPROACH FOR
LUNG CANCER RADIOTHERAPY**

By

Shahad M. Al-Ward

Bachelor of Science with Honours

Medical Physics

Ryerson University, 2012

A thesis

presented to Ryerson University

in partial fulfillment of the

requirements for the degree of

Master of Science

in the Program of

Medical Biophysics

Toronto, Ontario, Canada
© Shahad M. Al-Ward, 2015

Author's Declaration

I hereby declare that I am the sole author of this thesis. This is a true copy of the thesis, including any required final revisions, as accepted by my examiners.

I authorize Ryerson University to lend this thesis to other institutions or individuals for the purpose of scholarly research.

I further authorize Ryerson University to reproduce this thesis by photocopying or by other means, in total or in part, at the request of other institutions or individuals for the purpose of scholarly research.

I understand that my thesis may be made electronically available to the public for the purpose of scholarly research only.

Abstract

ROBUSTNESS ASSESSMENT OF A NOVEL 4D OPTIMIZATION APPROACH FOR LUNG CANCER RADIOTHERAPY

Shahad M. Al-Ward

Master of Science, Medical Biophysics, Ryerson University, 2015

One of the main challenges to treatment of lung cancer with radiation therapy is the tumor motion due to respiration. Previously, a novel approach was developed to generate treatment plans which compensate for respiratory motion and its variations. The worst case method is based on combining two intensity maps from two 4D plans optimized on the two worst cases of motion variations. The worst case planning method was previously tested on simulated motion variations. The goal of this project was to further test the worst case approach on realistic patient motion variations and treatment planning data. Two approaches to combining worst case plans were investigated: the first method takes the average of the two intensity maps, and the second method takes the maximum intensity of the two intensity maps. The robustness of worst case plans was compared with ITV plans and nominal 4D plans on three different motion variation scenarios. Study 1 and 2 investigated the robustness of the worst case methods on amplitude variations and patient motion variations on simulated image data. Study 3 investigated the robustness of the worst case methods on patient motion variations using real patient image data. The average intensity worst case method was only robust to Study 3 motion variations. The maximum intensity worst case method, the margin based, and the nominal approaches were not robust to any of the motion variations. Further evaluation over a wide range of tumour sizes, motion amplitudes and variability is required to determine the clinical applicability of the worst case planning method.

Acknowledgments

I would like to express my deepest appreciation to my supervisor Dr. Emily Heath for her guidance, time, support and her constant feedback.

I would like to thank my committee members Dr. Claire McCann of Sunnybrook Health Sciences Center, Dr. Michael Kolios of Ryerson University, and Dr. Carl Kumaradas of Ryerson University for their time and valuable feedback.

I would also like to thank my colleague Chandra P. Pokhrel for his help and support throughout this project.

This project was funded by the NSERC Collaborative Health Research Program (PI: Dr. Tim Chan, University of Toronto).

To

my dear mother, father, brother, and to

my soul mate

Table of Contents

Chapter 1	Introduction.....	1
1.1	Background.....	1
1.2	Radiation therapy	2
1.3	Concept of radiation dose and the physics of dose deposition	2
1.4	Medical Linear Accelerators.....	5
1.6	External beam radiation therapy techniques employed in NSCLC	9
1.6.1	3D Conformal Radiation Therapy (3DCRT)	9
1.6.2	Stereotactic Body Radiation Therapy (SBRT).....	10
1.6.3	Intensity Modulated Radiation Therapy (IMRT).....	10
1.7	Respiratory motion in radiation therapy of lung cancer	11
1.7.1	Effects of organ motion on imaging for treatment planning.....	12
1.7.2	Effects of organ motion on treatment delivery	13
1.8	Current respiratory motion management in radiation therapy.....	14
1.8.1	4D computed tomography (4DCT).....	14
1.8.2	Breath Hold.....	15
1.8.3	Gating.....	16
1.8.4	Tumor Tracking	16
1.8.5	Margin Approach.....	17
1.8.6	Mid-ventilation planning approach.....	17
1.10	Respiratory motion and anatomical variations during lung cancer radiation therapy	18
1.11	Robust 4D optimization.....	21
1.12	Previous work: A novel approach to generate robust plans.....	22
1.13	Hypothesis and Objectives	25
1.14	Thesis organization.....	25
Chapter 2	Materials and Methods.....	26
2.1	Materials	26
2.1.1	Phantom data.....	26
2.1.2	Patient data.....	28
2.1.3	Virtuos.....	28

2.1.4	KonRad	31
2. 2:	Treatment planning methods.....	34
2.2.1	4DCT image generation and processing (Simulated image data).....	36
2.2.2	Treatment planning in Virtuos	36
2.2.3	Deformable image registration.....	38
2.2.4	Dose accumulation.....	38
2.2.5	The ITV plan.....	39
2.2.6	The Nominal 4D plan.....	39
2.2.7	Worst case plans.....	39
2.2.8	Evaluation of plan robustness	40
2.3	Experiments	40
2.3.1	Study 1: Amplitude variation study using XCAT image data	41
2.3.2	Study 2: Patient intra-fractional motion variation study using XCAT image data	43
2.3.3	Study 3: Patient intra-fractional motion variation study using patient image data	45
2.3.4	Study 4: Patient inter-fractional motion variation study using patient image data	49
Chapter 3	Results.....	52
3.1	Influence of KonRad optimization constraints	52
3.2	Study 1: Simulated amplitude variations applied to XCAT phantom images	55
3.2.1	Image registration parameters and assessment	55
3.2.2	ITV plan	57
3.2.3	Nominal 4D plan.....	58
3.2.4	Worst case plans.....	59
3.2.5	Comparison of dose statistics for different plans.....	63
3.3	Study 2: Patient motion variations applied to XCAT phantom images.....	66
3.3.1	ITV plan	67
3.3.2	Nominal 4D plan.....	68
3.3.3	Worst case plan	70
3.3.4	Comparison of dose statistics for different plans.....	74
3.4	Study 3: Patient motion variation study.....	77
3.4.1	Image registration parameters and assessment	78
3.4.2	ITV plan	80
3.4.3	Nominal 4D plan.....	81

3.4.4	Worst case plans.....	83
3.4.4	Comparison of dose statistics for different plans.....	85
3.5	Study 4: Patient inter-fractional motion variations using patient 4DCT data.....	88
Chapter 4	Discussion, Conclusions and Future work.....	89
4.1	Discussion.....	89
4.2	Limitations to the study.....	90
4.3	Conclusions.....	91
4.4	Future work.....	92
Bibliography.....		93

List of Tables

Table 2.1: XCAT phantom settings	26
Table 3.1: First set of KonRad constraints used to optimize a 4D plan on the 0.9 cm and the 1.6 motion amplitudes.....	53
Table 3.2: Second set of KonRad constraints used to optimize a 4D plan on the 0.9 cm and the 1.6 motion amplitudes.....	53
Table 3.3: Optimized plan dose statistics when using the KonRad constraints in Tables 3.1 and 3.2 on the 0.9 cm amplitude and the 1.3 cm amplitude 4D plans	53
Table 3.4: The optimal parameters used for registration of displacement-binned XCAT images using ANIMAL software	55
Table 3.5: 4DCT phase weightings for each 30 second interval of the patient trace as well as the average, standard deviation, and the coefficient of variance of phase weightings.	66
Table 3.6: The fraction of time each breathing phase spends in each 20 second interval. The average, standard deviation, and the coefficient of variance are also shown.	78
Table 3.7: The optimal parameters used for registration of patient 4DCT images using the ANIMAL software.....	78

List of Figures

Figure 1.1: The relationship between dose and collisional Kerma with respect to depth in the tissue [5].....4

Figure 1.2: Schematic diagram of a linac [7].....6

Figure 1.3: 120 leaf multi-leaf collimator [8]6

Figure 1.4: Target volumes defined in ICRU report 62 [12].8

Figure 1.5: Comparison of beam intensity profiles for 3DCT and IMRT [18]..... 11

Figure 1.6: Examples of breathing induced image artifacts in 3DCT images (coronal): (a) overlapping structures and smearing of the right diaphragmatic dome, (b) overlapping structures and smearing of the caudal part of the tumor in the right lung, (c) duplicate structures and smearing of the caudal part of the tumor in the right lung [21]. 12

Figure 1.7: Dose profiles showing the blurring effect due to motion. The dashed line shows the dose profile of a static tumor. The solid lines show the dose profile to a tumor in motion. As seen in this figure, if the tumor is in motion, then it will be under-dosed at the periphery and the surrounding tissue is over-dosed [23]. 13

Figure 1.8: Labeling of a respiration trace with points belonging to (a) the same amplitude bin and (b) the same phase bin [26]. 15

Figure 1.9: Patient respiratory trace measured using a RPM system..... 19

Figure 1.10: Tumor regression [44] 19

Figure 1.11: Anatomical response [44]..... 20

Figure 1.12: The nominal pmf (non-bold line) along with the upper and lower envelopes which encompass the pmfs measured for a population of patients (bold line) [47] 22

Figure 1.13: Simulated amplitude variations. The number of exhaling and inhaling phases are equal in all scenarios [49]	23
Figure 1.14: More time inhaling / exhaling variations. The amplitude of tumor motion is fixed at 18 mm in all scenarios [49].....	23
Figure 1.15: CTV DVHs for amplitude variation scenario (a) average pdf approach (b) worst case approach [49]	24
Figure 1.16: CTV DVHs for more time inhaling vs. exhaling scenario (a) average pdf approach (b) worst case approach [49].....	24
Figure 2.1: Male (left) and female (right) anatomy generated by the XCAT software [50].....	27
Figure 2.2: Transverse (left), coronal (middle), and sagittal (right) views of a lung lesion in a phantom generated by XCAT.	28
Figure 2.3: Screenshot of Image processing mode in Virtuos showing sagittal, axial and coronal views of a CT image with planning contours overlaid. The bottom right image is the Virtuos observer view, which shows a three dimensional model of the patient’s anatomy with additional therapy relevant information.....	29
Figure 2.4: Screen shot of Planning mode in Virtuos. Yellow lines indicate the boundaries of incident treatment beams. At bottom right is a three-dimensional view of the contoured lungs with incident beams show as tetrahedrons.....	30
Figure 2.5: Screenshot of Result mode in Virtuos. Shown at top left is a dose volume histogram (DVH) for the CTV (shown in pink). The right hand image shows the dose distribution and isodose lines overlaid on an axial slice of the CT image. The yellow dashed line represents the 95% isodose line	31
Figure 2.6: Illustration of how each treatment beam is divided into beamlets (labeled with index j) and the CT image is divided into voxels (labeled with index i). The dose deposited by beamlet j to voxel i is stored in the D_{ij} matrix [53].....	32

Figure 2.7: Screenshot of the KonRad GUI. The top right corner shows the DVHs for all structures (VOIs) specified in the constraint list at the bottom right. The bottom left portion of the KonRad GUI shows the progress of the objective function minimization33

Figure 2.8: A summary of the treatment planning procedure that was followed to create ITV, nominal 4D and worst case plans on both simulated and patient image data35

Figure 2.9: Illustration of the dose accumulation process. The dose is first calculated on phases 0-9 then each dose distribution is mapped to the exhale phase and summed. The last figure shows the accumulated dose distribution.....37

Figure 2.10: The simulated breathing traces for all amplitude variation scenarios. The dashed horizontal lines represent the displacement points where XCAT 4DCT images were available.42

Figure 2.11: The probability density function of each amplitude variation scenario.42

Figure 2.12: The breathing trace taken from a healthy volunteer showing up to 120s.....44

Figure 2.13: 30 second interval motion variations pdfs extracted from the breathing trace in Figure 2.1244

Figure 2.14: Tumor displacement along the superior-inferior direction.....46

Figure 2.15: Patient breathing trace for week 0 4DCT showing phases 0 and 4 (exhale and inhale respectively) bin displacement values, and exhaling phases (phases 5-9) bin displacement values ...47

Figure 2.16: Patient breathing trace for week 0 4DCT showing phases 0 and 4 (exhale and inhale respectively) bin displacement values, and inhaling phases (phases 1-3) bin displacement values48

Figure 2.17: Patient 20 second interval pdfs extracted from the breathing trace shown in Figures 2.15 and 2.16.....49

Figure 2.18: Patient breathing traces for weeks 0, 2, 4 and 7.50

Figure 2.19: Pdfs extracted from the full breathing traces presented in Figure 2.18.....51

Figure 3.1 : a) DVHs from the worst case approach using the average intensity method and constraints from Table 3.1 to optimize the 0.9 cm amplitude and the 1.6 cm amplitude 4D plans
 b) DVHs from the worst case approach using the average intensity method and constraints from Table 3.2 to optimize the 0.9 cm amplitude and the 1.6 cm amplitude 4D plans.....54

Figure 3.2: Example of visual assessment of image registration quality: (a) red/green overlay of the target XCAT image (red) on the reference XCAT image (green) before image registration and (b) the overlap of the target XCAT image (red) on the registered XCAT image (green) after registration.56

Figure 3.3: Dose volume histograms of the ITV plan applied to other motion amplitude scenarios showing dose coverage of both the CTV and the right lung.....57

Figure 3.4: Dose volume histograms of the nominal plan applied to different motion amplitude scenarios for the CTV and Right lung (tumor-bearing lung). The black dashed lines represent the ICRU minimum and maximum dose criteria of 57 Gy and 64.2 Gy, respectively.....58

Figure 3.5: Frontal view of the cumulative dose distributions of (a) the nominal 4D plan applied on 1.4 cm amplitude motion, and (b) the nominal 4D plan applied on 1.6 cm amplitude motion. The pink contours show the CTV, and the dashed yellow lines represent the 95% isodose (the volume covered by 95% of the prescribed dose).59

Figure 3.6: a) Dose volume histograms of the worst case planning using the average intensity method applied on the amplitude variation scenarios and (b) the worst case planning using the maximum intensity method applied on the amplitude variation scenarios60

Figure 3.7: Sagittal and frontal views of the cumulative dose distribution for worst case method plan applied to 1.6 cm amplitude case. The pink contours show the CTV, and the dashed yellow lines represent the 95% isodose. The inferior region of the tumor is under-dosed because it is not contained within the 95% isodose. (a) using the average intensity worst case planning method (b) using the maximum intensity worst case planning method62

Figure 3.8: Minimum and maximum CTV doses of different planning approaches on amplitude variation study. The dashed lines represent the minimum and maximum doses defined by the

ICRU criteria (57 Gy and 64.2 Gy respectively). Method 1 is the average intensity method, and Method 2 is the maximum intensity method..... 64

Figure 3.9: D99 of different planning approaches on amplitude variation study. The dashed lines represent the minimum D99 defined by lung cancer radiation therapy protocols in PMH (59.4 Gy). Method 1 is the average intensity method, and Method 2 is the maximum intensity method..... 65

Figure 3.10: V20 of different planning approaches on amplitude variation study. The dashed lines represent the minimum V20 defined by lung cancer radiation therapy protocols in PMH (30%). Method 1 is the average intensity method, and Method 2 is the maximum intensity method 65

Figure 3.11: Dose volume histograms for the ITV plan applied to other motion variation scenarios showing dose coverage to both the CTV and the right lung. 67

Figure 3.12: Cumulative dose distribution of the ITV plan on the 60s-90s segment. The blue dots represent the CTV contours at exhale, and the yellow dots represent the CTV contours at inhale. The dashed yellow lines represent the 95% isodose (the volume covered by 95% of the prescribed dose)..... 68

Figure 3.13: Dose distribution of the ITV plan applied on phase 8. The pink dots represent the CTV contours at exhale, and the blue contours represent the CTV at phase 8. The dashed yellow lines represent the 95% isodose (the volume covered by 95% of the prescribed dose)..... 68

Figure 3.14: Dose volume histograms of the nominal 4D plan applied to 30s segments of the healthy volunteer respiratory trace. Dose coverage of both the CTV and the right lung are shown. .. 69

Figure 3.15: Cumulative dose distributions of nominal 4D plan applied on the 60s-90s segment. The pink contours show the CTV and the dashed yellow lines represent the 95% isodose (the volume covered by 95% of the prescribed dose) 70

Figure 3.16: Cumulative dose distributions of nominal 4D plan applied on the 90s-120s segment. The pink contours show the CTV and the dashed yellow lines represent the 95% isodose (the volume covered by 95% of the prescribed dose) 70

Figure 3.17: Dose volume histograms of (a) worst case planning using the average intensity method and (b) worst case planning using the maximum intensity method applied on 30s motion segment 72

Figure 3.18: Cumulative dose distributions of worst case plans using (a) using the average intensity method and (b) using the maximum intensity method applied on the 120s-150s segment. The pink contours show the CTV and the dashed yellow lines represent the 95% isodose (the volume covered by 95% of the prescribed dose) 73

Figure 3.19: Minimum and maximum doses of different planning approaches on motion variation scenarios. The dashed lines represent the minimum and maximum doses defined by ICRU criteria (57 Gy and 64.2 Gy respectively). Method 1 is the average intensity method, and Method 2 is the maximum intensity method..... 75

Figure 3.20: D99 of different planning approaches on motion variation scenarios. The dashed lines represent the minimum D99 criteria (59.4 Gy). Method 1 is the average intensity method, and Method 2 is the maximum intensity method..... 76

Figure 3.21: V20 of different planning approaches on amplitude variation study. The dashed lines represent the minimum V20 defined by lung cancer radiation therapy protocols in PMH (30%). Method 1 is the average intensity method, and Method 2 is the maximum intensity method..... 77

Figure 3.22: (a) Overlap of the patient target image on the patient reference image before image registration. (b) Overlap of the patient target image on the patient registered image after registration 79

Figure 3.23: Dose volume histograms of the ITV plan applied to the 20s segments of the patient respiratory motion trace showing dose coverage to both the CTV and the right lung..... 80

Figure 3.24: Dose volume histograms of the nominal 4D plan applied to 20s segments of the respiratory motion trace. Dose coverage of the CTV and the right lung are shown..... 81

Figure 3.25: Cumulative dose distributions of the nominal 4D plan applied on a) 40s-60s b) 80s-100s segment of the patient respiratory motion trace. The pink dots represent the CTV contours

and the dashed yellow lines represent the 95% isodose (the volume covered by 95% of the prescribed dose). 82

Figure 3.26: Dose volume histograms of the (a) worst case planning using the average intensity method (b) Worst case planning using the maximum intensity method applied on the patient motion variation scenarios. 84

Figure 3.27: Cumulative dose distributions of the nominal 4D plan applied on the 20s-40s segment of the patient respiratory motion trace. The pink dots represent the CTV contours and the dashed yellow lines represent the 95% isodose (the volume covered by 95% of the prescribed dose) a) using the average intensity method and b) using the maximum intensity method..... 85

Figure 3.28: Minimum and maximum doses of different planning approaches on patient motion variation scenarios. The dashed lines represent the minimum and maximum doses defined by ICRU criteria (57 Gy and 64.2 Gy respectively). Method 1 is the average intensity method, and Method 2 is the maximum intensity method..... 86

Figure 3.29: D99 of different planning approaches on patient motion variation scenarios. The dashed lines represent the minimum D99 defined by lung cancer radiation therapy protocols in PMH (59.4 Gy). Method 1 is the average intensity method, and Method 2 is the maximum intensity method..... 87

Figure 3.30: V20 of different planning approaches on amplitude variation study. Method 1 is the average intensity method, and Method 2 is the maximum intensity method..... 87

Figure 3.31: Dose volume histograms of the ITV plan applied to the 20s segments of the patient respiratory motion trace showing dose coverage to both the CTV and the right lung..... 88

List of Abbreviations

3DCRT: Three Dimensional Conformal Radiation Therapy
3DCT: Three Dimensional Computed Tomography
4DCT: Four Dimensional Computed Tomography
ANIMAL: Automated Nonlinear Image Matching and Anatomical Labeling
CT: Computed Tomography
CTV: Clinical Target Volume
D99: The dose, in Gy, that covers 99% or more of the target volume
DICOM: Digital Imaging and Communication in Medicine
DVH: Dose Volume Histogram
EDW: Enhanced Dynamic Wedge
GTV: Gross Tumour Volume
GTV-N: Gross Tumour Volume- Nodal
GTV-T: Gross Tumour Volume- Tumour
GUI: Graphical User Interface
HU: Hounsfield Units
ICRU: International Commission on Radiation Units
IMRT: Intensity Modulated Radiation Therapy
ITV: Internal Target Volume
Kerma: Kinetic Energy Released Per Unit Mass
Linac: Linear Accelerator
LRC: Local Regional Control
MLC: Multi-leaf Collimator
MRI: Magnetic Resonance Imaging
NSCLC: Non-Small Cell Lung Cancer
OAR: Organ At Risk
pdf: Probability Density Function
PET: Positron Emission Tomography
PMH: Princess Margaret Hospital
pmf: Probability Mass Function
PTV: Planning Target Volume
RPM: Real-Time Position Management
SBRT: Stereotactic Body Radiation Therapy

SCLC: Small Cell Lung Cancer

V20: The percentage volume that receives a dose of 20 Gy or more

VOI: Volume Of Interest

XCAT: 4 Dimension Extended Cardiac-Torso

XRT: External Beam Radiation Therapy

Chapter 1 Introduction

1.1 Background

Lung cancer is the second most frequently diagnosed type of cancer. According to the 2013 statistics of the Canadian Cancer Society, 14% of newly diagnosed cases in males and 20% of all cancer cases in females are lung cancer. Annually, there are 13,300 new cases of lung cancer in males and 12,200 new cases of lung cancer in females in Canada. The percentage of cancer deaths attributed to lung cancer in both sexes is 27% [1].

There are two main types of lung cancer: Small Cell lung cancer (SCLC), and Non-small Cell lung cancer (NSCLC). 15% of lung cancer cases are SCLC while NSCLC accounts for 85% of all lung cancer cases [2]. There are three main types of NSCLC: squamous cell carcinoma, large cell carcinoma, and adenocarcinoma.

Lung cancer is staged according to tumor size and extent of invasion into nearby organs and lymph nodes. In *Stage IA* the tumor size is less than 3 cm and the tumor is confined to the lung only. *Stage IB* is the stage in which the size of the tumor is between 3 cm and 5 cm. In this stage the tumor grows into the bronchus or the pleura. Inflammation or partial collapse of the lung is common in this stage. *Stage IIA* is the stage in which the size of the tumor is between 5 cm and 7 cm. This stage also involves tumors that are less than 5 cm in size but have spread to nearby lymph nodes. *Stage IIB* is when the size of the tumor is between 5 cm and 7 cm and has spread to the nearby lymph nodes. *Stage IIB* also describes tumors that have grown into the chest wall, pleura, muscle layer below the lung and the heart. *Stage IIIA* describes tumors of any size in which the cancer cells have spread into the lymph nodes of the mediastinum, chest wall and the pleura. In *Stage IIIB* there are two or more tumors in one lung. It also describes tumors that have spread to the distal side of the chest or to the clavicle. Tumors that have spread to other structures such as the esophagus, the heart, the trachea, or main blood vessels are also considered *Stage IIIB*. Finally, *Stage IV* is the stage in which the cancer has spread to the other lung or to the rest of the body.

The current strategies for treating lung cancer depend on the type and stage of the cancer. The outcomes with current treatments for SCLC are poor. The majority of SCLCs are referred to palliation and, without treatment, survival rates for SCLC are the lowest when compared to NSCLC. The median survival time for SCLC from diagnosis is only 2-4 months and the 2 year overall

survival rates are 45 % and 5% for conformed (with a defined shape) and non-conformed (dispersed) SCLC, respectively [2].

According to the American Cancer Society (2014) [3], the overall 5 year survival rate for NSCLC depends on the stage of the cancer: 49% for stage IA; 45% for stage IB; 30% for stage IIA; 31% for stage IIB; 14% for stage IIIA; 5% for stage IIIB; and 1% for stage IV. Treatment strategies for NSCLC depend on the stage of the cancer. Conventional treatments for early stage NSCLC include surgery and radiation therapy while treatments for advanced NSCLC include radiation therapy combined with chemotherapy and/or surgery.

1.2 Radiation therapy

Radiation therapy is the use of ionizing radiation to kill malignant cells. Depending on the type of cancer, its stage, size and location in the body, the type of ionizing radiation used could be x-rays, gamma rays or charged particles such as electrons or protons. Ionizing radiation damages the DNA of the tumor cells which leads to cell death. There are two main modalities of radiation therapy: brachytherapy and external beam therapy. Brachytherapy uses radiation sources that are placed inside or next to the tumor. External beam radiation therapy (XRT), on the other hand, uses an external source to generate a radiation beam to treat a target inside the body. XRT sources include medical linear accelerators (linacs) which produce x-ray and electron beams, Cobalt-60 teletherapy units which deliver gamma rays and cyclotrons to generate proton beams. Typically, radiation therapy treatments are delivered overall several weeks, in daily fractions of smaller doses. In lung cancer radiotherapy, delivered typical fractionation regime is 30 – 35 fractions with a total dose of 60 Gy to the tumor [4].

1.3 Concept of radiation dose and the physics of dose deposition

To predict the outcome of a radiation therapy treatment, one needs to quantify the damage to the tissue caused by ionizing radiation. In terms of energy deposition, radiation can be directly or indirectly ionizing. Directly ionizing radiation, such as charged particles, deposit energy directly in the medium through ionizations and excitations. Indirectly ionizing radiation, such as x-rays and gamma rays, interact with the medium releasing charged particles, and these charged particles deposit their energy in the medium. The *Absorbed Dose* is defined as the energy E deposited in the medium by charged particles per unit mass m (Equation 1.1). Therefore, the unit of absorbed dose is J/Kg or Gray (Gy).

$$D = \frac{dE}{dm} \quad (1.1)$$

In the case of indirectly ionizing radiation, before energy is deposited in the medium by charged particles it needs to be transferred from incident photons to the charged particles. The total energy transferred to the charged particles E_{tr} per unit mass of medium is termed the Kerma (Kinetic Energy Released per unit Mass) (Equation 1.2). Kerma is further separated into collisional Kerma (K_c), and radiative Kerma (K_r) (Equation 1.3). Collisional Kerma describes the amount of transferred energy that is then deposited in the medium through ionization and excitation (collisional interactions). Radiative Kerma, on the other hand, refers to transferred energy that is lost through radiative interactions of electrons with the atomic nuclei. These radiative interactions result in the emission of Bremsstrahlung (x-ray) radiation. Therefore, collisional Kerma contributes to Dose deposition, while radiative Kerma is considered to be “lost” energy.

$$K = \frac{dE_{tr}}{dm} \quad (1.2)$$

$$K = K_c + K_r \quad (1.3)$$

Collisional and total Kerma are related to the energy fluence (Ψ) by Equations 1.4 and 1.5, respectively

$$K_c = \Psi \left(\frac{\mu_{ab}}{\rho} \right) \quad (1.4)$$

$$K_{tot} = \Psi \left(\frac{\mu_{tr}}{\rho} \right) \quad (1.5)$$

where (μ_{ab} / ρ) is the energy mass-energy absorption coefficient, and (μ_{tr} / ρ) is the mass-energy transfer coefficient. For a mono-energetic photon beam, the energy fluence is related to the particle fluence (Φ) by Equation 1.6

$$\Psi = h\nu \cdot \Phi \quad (1.6)$$

$$\text{where } \Phi = \frac{dN}{dA} \quad (1.7)$$

and dN is the number of photons that enter an imaginary sphere of cross-sectional area dA .

The relationship between Absorbed Dose and collisional Kerma is illustrated in Figure 1.1. When photons enter the medium, they transfer their energy to charged particles setting in motion secondary electrons which go on to deposit dose in the medium. Therefore, at the surface, there is minimum dose and maximum Kerma. As the photons go deeper into the medium they are attenuated, therefore Kerma decreases. However, the secondary charged particle fluence increases therefore the dose in the tissue increases. There is a point in the medium where charged particle equilibrium is achieved. At this point, the Kerma is equal to the dose, and the maximum dose in the medium occurs. This point is also defined as the depth of maximum dose or d_{max} . The depth of maximum dose depends on the energy of the incident photon beam. Low energy beams deposit most of their energy at the surface. This is useful for treatment of superficial tumors. High energy beams deposit most of their energy deeper in the medium than low energy beams. This is advantageous for treating deep seated tumors, such as lung tumors.

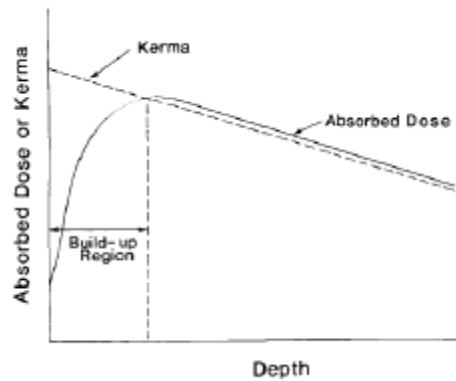


Figure 1.1: The relationship between dose and collisional Kerma with respect to depth in the tissue [5]

From Figure 1.1, there appears to be a direct linear relationship between dose and Kerma for depths greater than d_{max} . Therefore dose can be related to collisional Kerma through Equation 1.8

$$D = \beta K_c \quad (1.8)$$

In Figure 1.1, in the buildup region, the electron build up is incomplete; therefore, β is less than 1. At d_{max} , electronic equilibrium is achieved; therefore β is equal to 1 and the dose is equal to

the collisional Kerma. At depths greater than the maximum range of electrons, there is a region of quasi-equilibrium in which β is greater than one.

1.4 Medical Linear Accelerators

Medical linear accelerators (linacs) are the most commonly employed source of radiation beams used in external beam radiation therapy. Linacs are capable of producing high energy x-ray and electron beams with maximum energies ranging from 4-25 MeV. The typical radiation energy used in lung cancer radiation therapy is 6 MV. High energy beams (≥ 10 MV) are not suitable for treating lung lesions. This is because lungs have a low density, which causes an increased lateral electron transfer. The resulting electron disequilibrium causes a wider penumbra for high energy photons, as a result, the peripheral dose decreases. Also, high energy radiation beams produce neutrons which have different biological effects than photons, and they may not be modeled in the radiation therapy planning algorithm [6].

The schematic diagram in Figure 1.2 shows the major components of a linac. X-ray beams are generated by accelerating electrons and smashing them into a target which is composed of a high atomic number material. The electrons are emitted by an electron gun then they are accelerated in a waveguide using high frequency electro-magnetic fields. The accelerated electrons interact with either the electrons of the target atoms to generate characteristic x-rays or with the atomic nuclei to emit Bremsstrahlung x-rays. The x-rays emitted from the target are then collimated by a primary collimator. The intensity of the generated photons is higher in the center of the field; therefore, a cone shaped flattening filter is placed in the beam to make the beam intensity more uniform. The shape of the flattening filter is designed to give a flat dose profile at a specified depth in water, typically 5 or 10 cm. The size of the field is defined by two pairs of collimating jaws as well as by a multi leaf collimator (MLC). MLCs are made of multiple narrow leaves which are designed to move independently (Figure 1.3). The advantage of an MLC is that it allows the definition of irregular beam apertures.

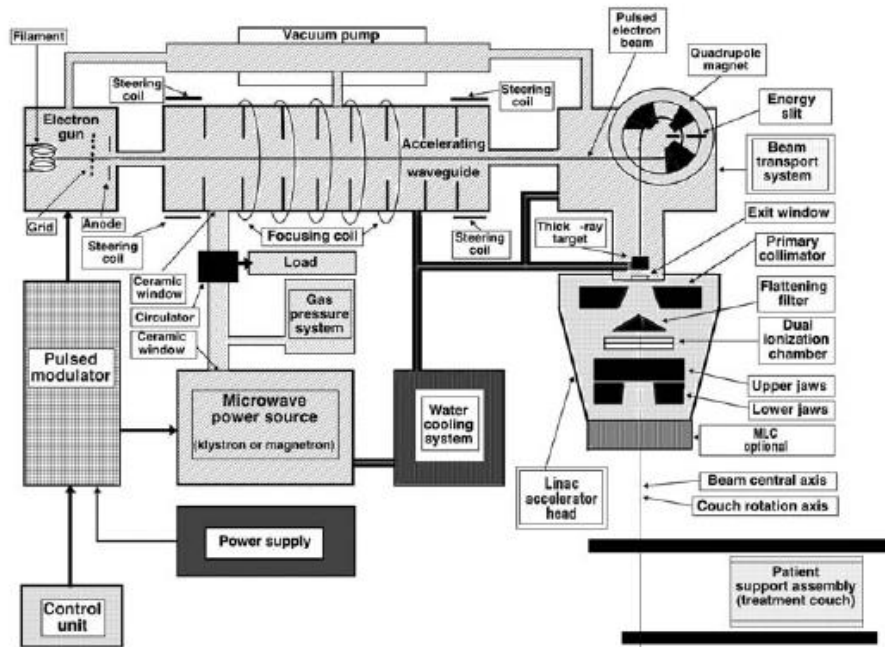


Figure 1.2: Schematic diagram of a linac [7]

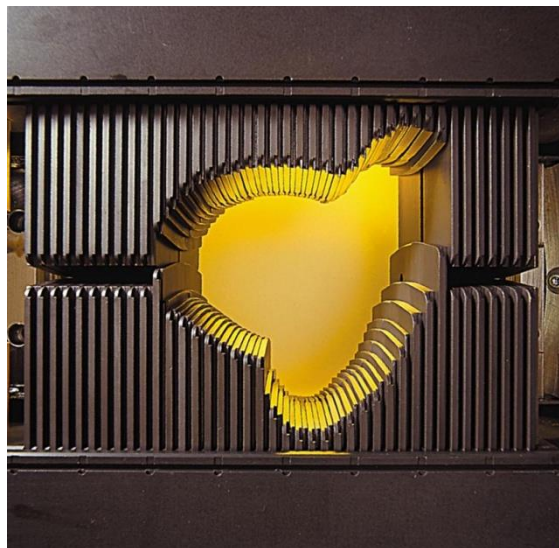


Figure 1.3: 120 leaf multi-leaf collimator [8]

1.5 Typical radiation therapy process for lung cancer

The radiation therapy process involves the participation of physicians, radiation oncologists, radiologists, medical physicists, technicians and physics associates. The process can be summarized in the following steps:

- 1- **Diagnosis and treatment decision:** Medical imaging modalities such as planar radiographs and CT scans are employed in the diagnosis and the staging of the disease. Based on the diagnosis, a decision to pursue either radical or palliative treatment is made. Radical treatments aim to eradicate or control the tumor while the goal of palliative treatments is to alleviate the symptoms of the cancer. Therefore, the radiation dose prescribed for a palliative treatment is typically lower compared to radical treatments. Once the decision is made to employ radiation therapy, a treatment plan must be designed.
- 2- **Imaging for treatment planning:** Modern treatment planning systems use 3D models of the patient anatomy to accurately predict the dose that will be delivered to the tumor and surrounding organs. These patient models are derived from 3D CT images of the patient in the same position as when he/she is treated. In lung cancer, a 4D CT image is typically acquired (to be described in Section 1.8.1) to measure the extent of the tumor motion due to respiration.
- 3- **Target volume localization:** Once the planning image is acquired, the target volumes to be treated are determined by the radiation oncologist. Radiation sensitive healthy tissue which may limit the dose that can be delivered should also be delineated. The target volumes (Figure 1.4) are defined by the International Commission on Radiological Units (ICRU) and include:
 - **Gross Tumor Volume (GTV):** This defines the extent of the tumor that is visible in the CT image. It can consist of both the primary tumor (GTV-T) as well as involved the lymph nodes (GTV-N).
 - **Clinical Target Volume (CTV):** This volume is defined as the GTV plus a geometric margin to account for microscopic malignant disease not visible in the CT image. Typical GTV-CTV margins in lung cancer are 5 mm.
 - **Internal Target Volume (ITV):** This is defined as the CTV plus an extra volume that accounts for uncertainties in the size and shape of the CTV due to internal organ motion. The ITV accounts for motion uncertainties *within* the patient; therefore the ITV excludes patient setup uncertainties.

- Planning Target Volume (PTV): An additional geometrical margin is added to the ITV to account for setup errors and motion of the patient between fractions.
- Organs at Risk (OARs): Refers to any critical structures or tissues that could suffer significant morbidity if over-irradiated. For example, the spinal cord, heart and lungs are considered organs at risk in lung radiation therapy. Lung treatment protocols differ from one cancer center to the other. These protocols determine the maximum doses to the OARs that should not be exceeded when treating the lung. At Princess Margaret Hospital, the volume (volume of the two lungs combined) that receives 20 Gy or more should not exceed 30%. The potential damage to the lung if this criterion is exceeded is radiation pneumonitis [9]. The maximum allowed dose to be received by the spinal cord is 45 Gy. The main biological effect resulting from exceeding the allowed dose to the spinal cord is paralysis. Radiation-induced spinal cord injury has been investigated in greater detail in mice models. In these models, the most predominant histopathologic change was necrosis to the white matter of the spine, which caused forelimb paralysis in mice [10]. The maximum allowed dose to be received by the heart is 40 Gy. The main side effect resulting from exceeding this dose limit is atherosclerosis [11].

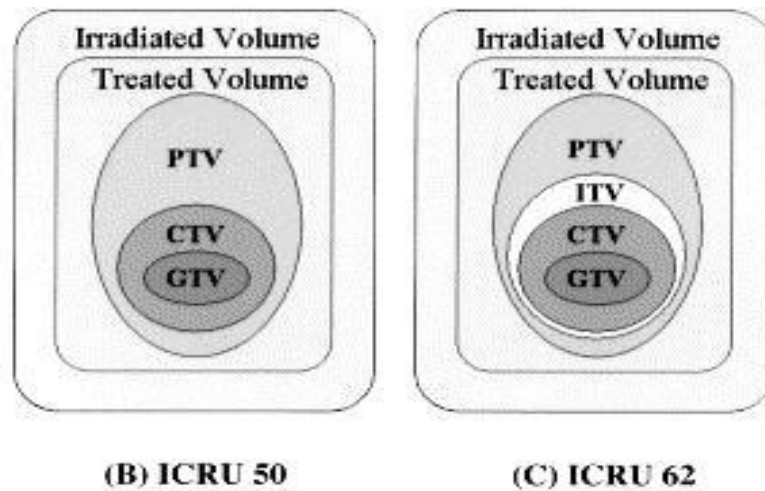


Figure 1.4: Target volumes defined in ICRU report 62 [12].

- 4- Treatment planning: The goal of treatment planning is to determine a beam arrangement which will deliver the prescribed dose to the PTV while keeping the dose delivered to OARs below critical tolerances. Depending on the XRT modality chosen, inverse planning or forward planning is performed. In the inverse planning approach, the user specifies dose criteria for each of the target volumes and the organs at risk and an optimization engine determines the beam intensities that result in a dose distribution which meets the specified criteria. In forward planning, the user manually adjusts the beam intensities in a trial and error approach.
- 5- Plan evaluation: The treatment plan is evaluated by verifying that the dose coverage to the target volumes and OARs meets the planning criteria. The dose coverage is typically evaluated by examining the cumulative dose volume histogram (DVH) for each planning structure. A cumulative dose volume histogram represents the volume of structure receiving greater than or equal to a certain level of dose.
- 6- Treatment verification and delivery: Before the first treatment delivery, the plan may undergo additional verification by comparing the dose computed by the treatment planning system to an independent measurement. At the time of treatment, the patient positioning is verified using in-room imaging and setup corrections are applied if necessary. Immobilization devices may be used to reduce setup errors, in which case they should also be used when the treatment planning image is acquired. The treatment is then delivered.

1.6 External beam radiation therapy techniques employed in NSCLC

Multiple delivery techniques exist in external beam radiation therapy and they differ in terms of fractionation, type of beam collimation used, and planning approach. The three main XRT treatment methods include 3D conformal radiation therapy (3DCRT); stereotactic body radiation therapy (SBRT); and IMRT.

1.6.1 3D Conformal Radiation Therapy (3DCRT)

3DCRT is a type of external beam radiotherapy in which multiple beams, with uniform fluence, are applied to achieve the desired dose distribution (Figure 1.5a). The planning is performed on a 3DCT image and the typical prescribed dose is 60-70 Gy delivered in 30-35 fractions for lung cancer. The beam apertures are defined by multileaf collimators (MLC) in order to conform to the shape of the PTV. Forward planning is used for 3DCRT.

1.6.2 Stereotactic Body Radiation Therapy (SBRT)

SBRT is used for the treatment of early stages of lung cancer with a tumor size typically less than 4 cm [13]. SBRT implies the use of a specialized stereotactic localization system which allows a much higher accuracy setup than conventional localization systems. In SBRT for NSCLC, tumor motion is typically reduced by using abdominal compression. Compared to 3DCRT and IMRT, SBRT uses smaller field sizes and fewer treatment fractions. A typical fractionation scheme is 10-20 Gy per fraction, delivered in 4-5 fractions [14]. SBRT is highly conformal as the PTV margin is smaller. Because of this, and the possible adverse effects of large doses per fraction, the delivery accuracy requirements are much higher compared to 3DCRT and IMRT.

1.6.3 Intensity Modulated Radiation Therapy (IMRT)

The major drawback of 3DCRT is that it does not achieve concave dose distributions. When compared to 3DCRT, IMRT is capable of “sculpting” the dose to create improved dose distributions to fit complex shapes. This is possible because IMRT delivers non-uniform beam fluence (Figure 1.5b). IMRT uses similar dose prescriptions and dose fractionation schemes as 3DCRT.

MLCs (multileaf collimators) are the primary method used to modulate the beam fluence. IMRT delivery techniques include the “step and shoot” method and the dynamic MLC, or “sliding window” method. In the “step and shoot” method, multiple static dose segments are delivered at each beam angle. The fluence from these delivered segments adds up to produce an intensity modulated field. In the dynamic MLC method the modulated intensity is achieved by moving the leaf pairs constantly across the field at varying speeds while the beam is on [15].

IMRT plans are usually created using inverse planning. The first step is to define the OARs and target volumes on the CT image. CT data sets may be fused with PET or MRI images to achieve more accuracy in volume delineation. The desired dose limits are defined for both target structures and OARs. Then, an inverse-planning algorithm determines the characteristics of the radiation beam to meet pre-specified criteria. The beam characteristics are constantly modified by the treatment planning software until the optimum treatment plan is achieved [16]. There are two main optimization approaches employed in IMRT: fluence-based optimization and direct aperture optimization. In fluence based optimization, each beam is divided into small beamlets and the dose distribution is computed for each beamlet and stored in a dose contribution matrix. The beamlet intensities are then optimized so that the resulting dose distribution meets the planning criteria. The optimization yields a non-uniform fluence map for each beam, however, the treatment plan cannot be

delivered until a leaf sequencing algorithm is applied to convert these fluence maps into a weighted sequence of deliverable apertures. Therefore, the constraints imposed by the MLC are accounted for in the leaf sequencing algorithm [17]. This means that the delivered fluence may not be the same as the optimized fluence. Direct aperture optimization, on the other hand, starts with a series of MLC-defined apertures for each beam and then optimizes the aperture shapes and weights. Therefore, all the MLC constraints are included in the optimization.

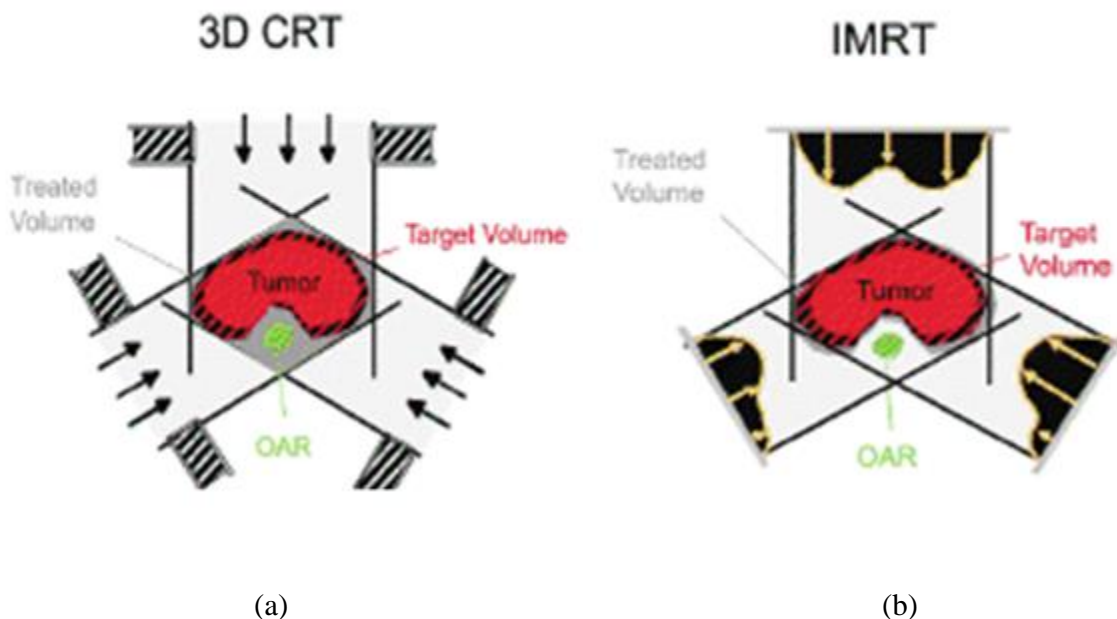


Figure 1.5: Comparison of beam intensity profiles for 3DCT and IMRT [18]

1.7 Respiratory motion in radiation therapy of lung cancer

Organ motion in radiation therapy has significant effects on imaging and treatment delivery. Respiratory motion is the most significant organ motion in lung radiation therapy and the amplitude of respiratory motion has been determined to be up to 50 mm in some patients [19]. This motion is mostly in the superior-inferior direction and it is more significant for tumors located in close proximity to the diaphragm.

1.7.1 Effects of organ motion on imaging for treatment planning

Patient motion during image acquisition is known to cause image artifacts. These artifacts lead to an inaccurate representation of the patient geometry and densities. This in turn leads to errors in treatment planning as the target volume and OAR delineation and dose calculation accuracy will be affected. Gagne *et al* studied the effects of motion artifacts on tumor delineation and found that the mean reconstructed density of a moving structure was on average less than that of the static structure by up to 38% [20].

Imaging of a moving object results in a blurred image. Further distortion can occur in CT imaging because of the slice by slice acquisition. Motion of anatomy in and out of the slices leads to consecutively acquired image slices being acquired of the tumor in different respiratory phases. This leads to a disjointed representation of the anatomy (Figure 1.6)

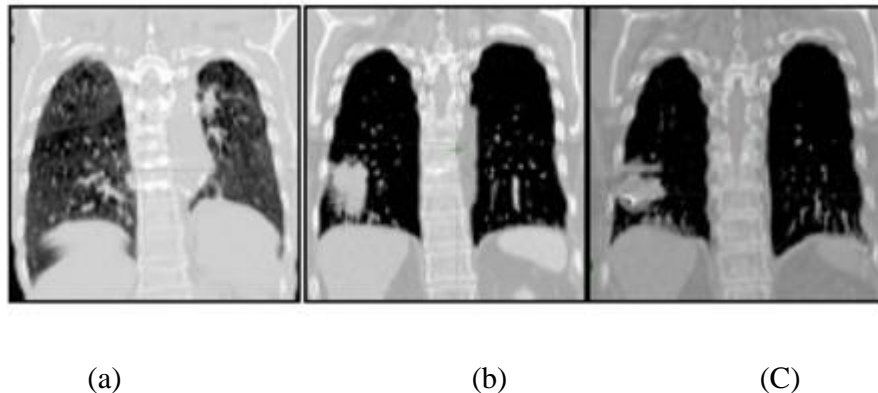


Figure 1.6: Examples of breathing induced image artifacts in 3DCT images (coronal): (a) overlapping structures and smearing of the right diaphragmatic dome, (b) overlapping structures and smearing of the caudal part of the tumor in the right lung, (c) duplicate structures and smearing of the caudal part of the tumor in the right lung [21].

To avoid motion artifacts, CT images can be acquired while the patient is holding his / her breath. 4DCT and gated CT (to be discussed in Section 1.8.3) can also be used to minimize motion artifacts. In all cases, a fast CT acquisition with a scan time of 0.1 seconds is required to minimize image blurring [22].

1.7.2 Effects of organ motion on treatment delivery

There are three main effects of organ motion on treatment delivery: dose blurring, deformations, and interplay effects. Dose blurring is considered to be the dominant effect (Figure 1.7) and it results in broadening of the beam penumbra and reduced conformity of the dose distribution to the tumor. The effect of dose blurring becomes more significant with increasing motion amplitude. Dose deformations are secondary motion effects which occur because the dose distribution varies spatially with displacement and deformation of internal anatomy. Interplay effects are specific to dynamic beam delivery techniques such as IMRT, enhanced dynamic wedge (EDW) and tomotherapy. If the tumor and MLCs are in motion during the treatment delivery, the beam directed to the tumor maybe blocked by the MLCs resulting in under-dosing of the tumor and over-dosing of the healthy tissue.

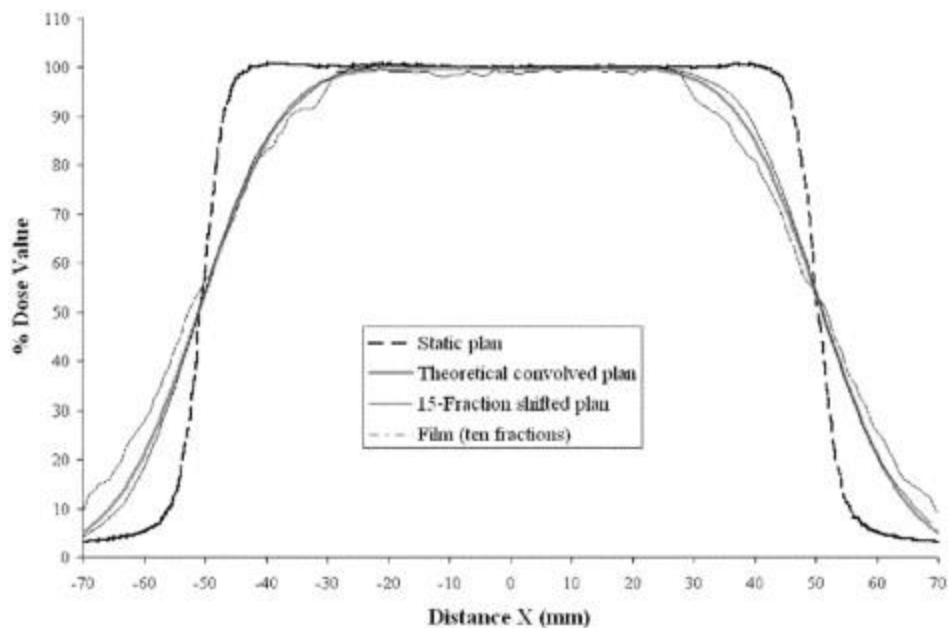


Figure 1.7: Dose profiles showing the blurring effect due to motion. The dashed line shows the dose profile of a static tumor. The solid lines show the dose profile to a tumor in motion. As seen in this figure, if the tumor is in motion, then it will be under-dosed at the periphery and the surrounding tissue is over-dosed [23].

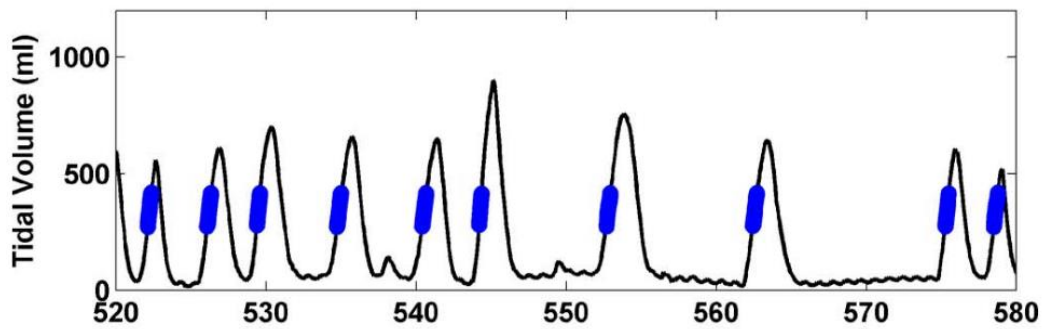
1.8 Current respiratory motion management in radiation therapy

Respiratory motion management methods are needed when the motion of the target is greater than 5 mm. Any motion management method is said to be appropriate if the patient can tolerate it and if it improves normal tissue sparing. Respiratory management techniques can be used during the planning and/ or delivery stage of the treatment [19].

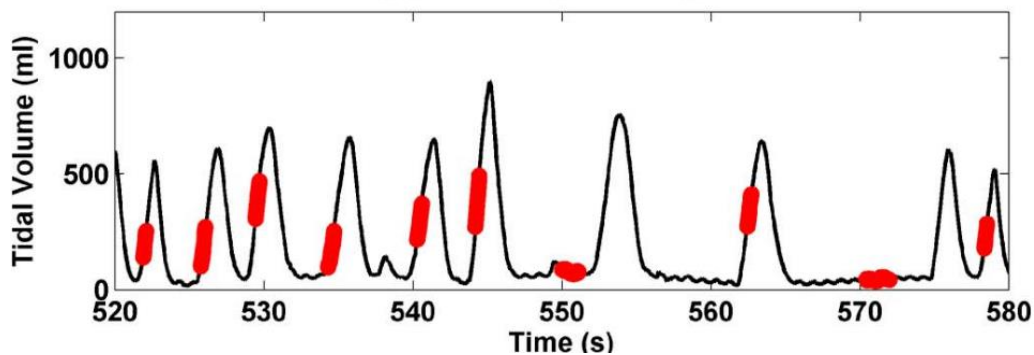
1.8.1 4D computed tomography (4DCT)

In radiation therapy planning, it is conventional to use three dimensional computed tomography. 3DCT is a three dimensional tomographic imaging technique that reconstructs 3D images from a large series of 2D projection images acquired at different angles. 3DCT does not account for patient respiratory motion. For example, an image slice might be obtained at one phase of the respiration cycle, and another image is acquired at another phase of the respiration cycle. This might not be a true representation of the patient's anatomy.

One way to minimize image artifacts is to use 4DCT. 4DCT is a dynamic image acquisition technique that allows for patient-specific measurement of respiratory motion. 4DCT imaging consists of slice acquisition with simultaneous respiration monitoring to label the slices. The slices are then sorted according to the respiration phase and volumetric images are reconstructed at each respiratory phase. There are two possible modes for 4DCT acquisition: ciné mode and helical mode. Ciné mode acquires repeated image slices at different couch positions. In helical mode, the table translates constantly during acquisition [24]. In 4DCT, the acquired image slices are sorted into their respective respiratory motion states by either phase binning or amplitude binning. In phase binning, each breathing cycle is divided into equal intervals of time. Each image slice is sorted into the closest bin corresponding to the phase of the respiratory trace at the time it was acquired. In amplitude binning, the respiratory trace is divided into equally spaced amplitudes. Each image slice is sorted, according to the amplitude of the respiratory trace at the time the slice was acquired, to the nearest amplitude bin [25]. Figure 1.8 illustrates the difference between phase and amplitude binning. In Figure 1.8b, it can be seen that slices acquired at different displacements maybe assigned to the same phase bin.



(a)



(b)

Figure 1.8: Labeling of a respiration trace with points belonging to (a) the same amplitude bin and (b) the same phase bin [26].

1.8.2 Breath Hold

The effect of respiratory motion on radiation therapy planning and delivery can be reduced by minimizing the tumor motion. The tumor position can be kept stationary if the patient holds his or her breath during the treatment delivery. This technique is only feasible if the patient is able to hold their breath for 10 seconds or longer [27]. Safe implementation requires patient training and coaching during treatment delivery through the means of audiovisual feedback or other devices. The patient's ability to maintain the breath hold may be monitored by spirometry [28] and [29], external markers [30], or imaging of an implanted fiducial [31]. The treatment is delivered at end-inhalation or end-

exhalation phases. Deep inspiration breath hold is preferred as lung density is reduced [28] and [29]. Moreover, the dose to the heart may be reduced using the deep inspiration breath hold technique. One disadvantage of using the breath hold technique is that it prolongs the treatment duration by a factor of two or more. Moreover, patient with poor pulmonary function may not tolerate holding their breath for more than 10 seconds.

1.8.3 Gating

Gated radiation therapy refers to delivering radiation only during a specific portion of the respiratory cycle. Similar to 4DCT imaging, gating can be amplitude or phase based. This technique is advantageous over the breath hold technique because patients with poor pulmonary function can tolerate it better than breath hold. Gated radiation therapy has been shown to reduce treatment margins, especially for highly mobile tumors [32]. One drawback of gated radiation therapy, however, is a reduction in treatment efficiency. This is because the beam is turned on for a fraction of the respiratory cycle. Therefore, a combined breath hold and gated radiation therapy technique may be preferable, if it can be tolerated by the patient [33].

To accurately deliver gated radiation therapy, a reliable respiration monitor with a fast response, minimal baseline drift and low signal-to-noise ratio is required. Respiration may be monitored by measuring the displacement of implanted gold markers or external markers placed on the abdomen. The use of implanted markers in lung patients raises a concern as the implantation procedure is risky and the marker may migrate to other parts of the body [34]. The use of external markers has the disadvantage that the motion of the external surface of the patient may not correlate with the internal tumor motion [35].

1.8.4 Tumor Tracking

In tumor tracking, the respiratory motion is compensated by synchronizing the motion of the radiation beam to the tumor motion trajectory. Tracking may be achieved using dynamic MLC motion or a robotic couch [36]. Tracking can also be performed using the CyberKnife, which is a commercially available compact linac that is mounted on a robotic arm [37]. Typically, for tracking an external marker is used to track the internal motion of the tumor and synchronize the MLC leaf motion with the motion of the target; however, an internal fiducial marker is preferred. Safety precautions involve shutting the beam off if there are large differences between the planned and the measured tumor trajectory. Moreover, it is important to provide patient breathing coaching to improve the accuracy of dynamic MLC treatment delivery [38].

1.8.5 Margin Approach

The most widely used approach to account for respiratory motion during the treatment planning process is to add an additional margin to the target volume. The most commonly used margin approach to account for respiratory motion is to use an ITV. The ITV can be constructed by fusing CTV contours at inhale and exhale. This approach produces a treatment plan that ensures coverage of mobile structures; however, it is overly conservative as it assumes that the tumor spends the same amount of time at each respiratory phase. Therefore, the use of an ITV is known to result in a larger volume of irradiated healthy lung tissue compared to other respiratory motion management techniques. Instead of using an ITV, margin recipes may also be used to determine the additional PTV margin required to account for motion of the CTV. For example, Van Herk *et al* described a margin recipe that accounts for random and systematic errors in the planning and delivery process [39].

1.8.6 Mid-ventilation planning approach

In the mid-ventilation approach, a plan is generated on the CTV of a single CT scan (mid-ventilation CT scan) which is selected from a 4DCT data set. This CT scan represents the time-averaged position of the tumor over the whole respiratory cycle [40]. Planning on the mid-ventilation phase reduces the size of the margin required for respiratory motion.

1.9 4D optimization

4D optimization is a treatment planning approach which is specific to IMRT, because IMRT permits modulation of beam intensities. A 4D-optimized plan compensates for respiratory motion by incorporating information about the patient's respiratory motion pattern into the treatment plan optimization. Trofimov *et al* [41] described different 4D optimization approaches. In the "motion kernel" method, the dose influence matrices were calculated on each phase of a 4DCT dataset. Instead of optimizing the dose on a single respiratory phase, this approach optimizes the cumulative dose that anatomical voxels receive as they move to different positions in different breathing phases. Therefore, a method for mapping voxels through the respiratory phases was used. The voxel grid defined for the inhale phase was chosen as the reference phase. Voxel based affine and non-rigid registration was used to obtain the voxel displacement vector fields. These voxel displacement vectors describe the displacement of voxel i to phase x relative to its position in the reference phase. The dose to anatomical voxel i at phase x is then interpolated at the actual position of the anatomical

voxel in phase x . The cumulative dose is the sum of the doses that a given voxel receives in each phase x . This is shown in Equation 1.9:

$$d_i = \sum_x d_i^{(x,0)} = \sum_x \sum_j D_{ij}^{(x)} w_j p(x) \quad (1.9)$$

where $D_{ij}(x)$ is the dose influence matrix calculated on phase x , and $p(x)$ is the weight given to phase x , or the fraction of the breathing cycle that is spent at that phase.

With the dose influence matrices calculated as described in Equation 1.9, one can perform an optimization that is similar to the 3D optimization except that the patient respiratory motion is accounted for. The results from Trofimov *et al* suggest that when using the motion kernel approach, the total dose to the target showed a high degree of homogeneity (small difference between the minimum and the maximum dose to the target) when compared to the instantaneous dose distributions calculated on single phases (inhale / exhale). In terms of OAR sparing, the results from the same paper show that the ITV approach delivers more dose to the liver and the spinal cord than the motion kernel approach when treating the liver and the lung, respectively. For example, V10 (the volume which receives 10 Gy or more) was 40% and 30% when using the ITV approach and the motion kernel approach respectively.

1.10 Respiratory motion and anatomical variations during lung cancer radiation therapy

Changes during radiation therapy are classified as either *intra*-fractional or *inter*-fractional. Intra-fractional changes refer to changes *within* a treatment fraction, while inter-fractional changes refer to changes that occur *between* treatment fractions. Respiratory motion variations have been shown to occur on an intra- or inter-fractional basis. Anatomical variations, such as tumor and normal tissue response, and tumor regression occur between treatment fractions.

The breathing pattern in a patient may vary in amplitude, period, and/or baseline shifts (Figure 1.9). The amplitude of tumor motion ranges from 6 mm to 18 mm during normal tidal breathing [42]. Breathing periods last from 2.7 s to 6.6 s, with an average of 5 s [42]. Figure 1.9 shows an example of a patient respiration trace measured during a single treatment session which shows motion variability.

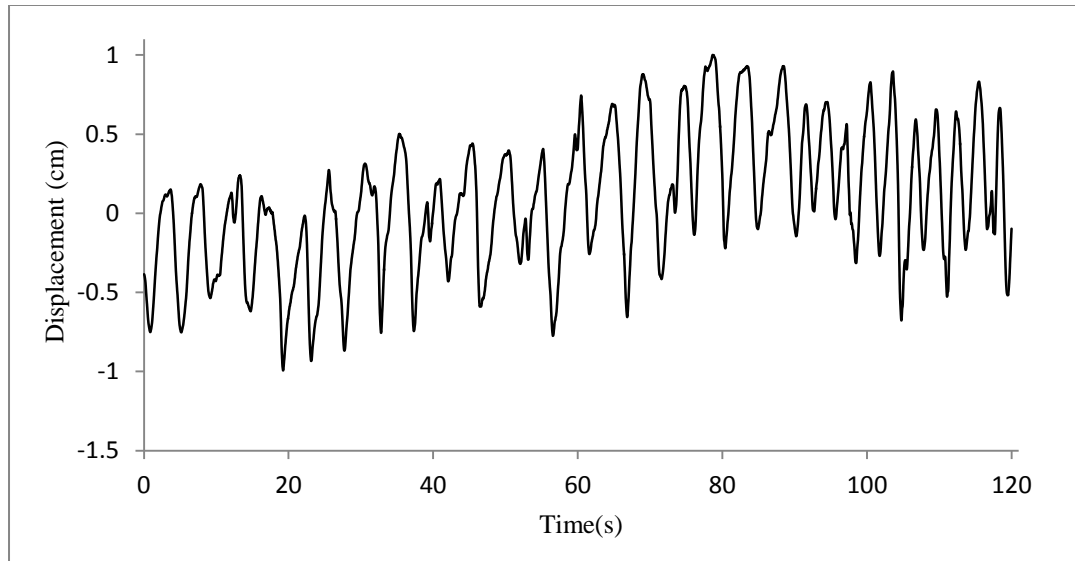


Figure 1.9: Patient respiratory trace measured using a RPM system.

Throughout the treatment course, most tumors shrink or regress (Figure 1.10). The regression rate varies between 0.6 %/day to 2.4 %/day [43]. Tumor regression potentially allows for reduction of the beam apertures which can reduce the dose to the OARs. However, shrinkage of the visible tumor does not necessarily mean that the CTV can be reduced [44]. Sonke *et al* [44] observed two types of tumor regression: 1) The surrounding lung tissue moves consistently with the tumor, 2) the tumor (CTV) regresses while the surrounding tissue remains in its original location.

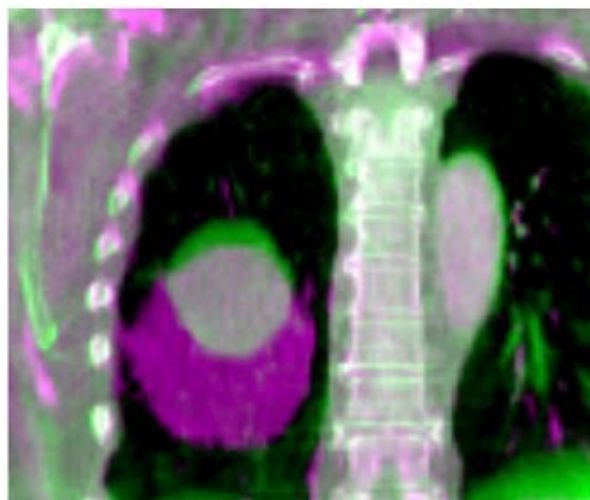


Figure 1.10: Tumor regression [44]

Furthermore, lung and other types of tissues can change shape with the 5-7 weeks from the start of the treatment. This occurs frequently in patients with tumors invading the central airways, atelectasis (lung collapse), plural effusion, and inflammation [45]. For example, when lung atelectasis is resolved, re-ventilation of the lungs due to reopening of air-ways occurs. This can change breathing patterns, regional lung and tumor configurations, and tumor and lymph node locations [44]. An example of an anatomical response is illustrated in Figure 1.11.

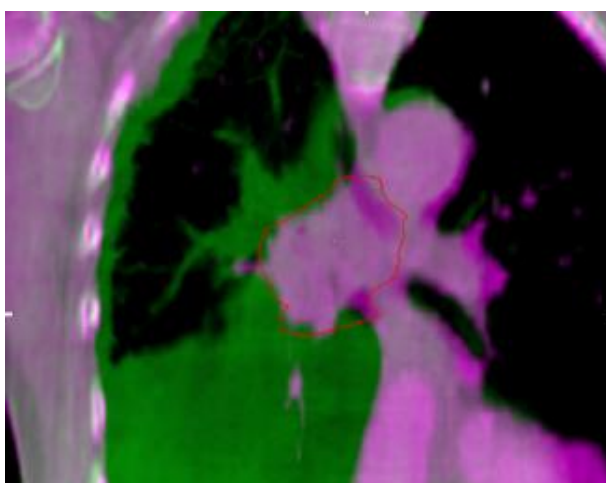


Figure 1.11: Anatomical response [44]

1.11 Robust 4D optimization

Motion management strategies applied during treatment planning should account for intra- and inter-fraction respiratory motion variations otherwise the tumor could potentially be under-dosed. 4D optimization accounts for the respiratory motion measured at the time of treatment planning however, it ignores variations in the motion during and between treatments.

Robust optimization approaches account for respiratory motion variability during the 4D optimization. There are many approaches to robust 4D optimization. One approach is to employ a quadratic objective function which minimizes variance of the dose in each voxel of the target volume due to respiratory motion variations [46]. This method is known as the variance minimization method. Another approach suggested by Heath *et al* (2009) [46] was the worst case optimization approach. In this approach a weighted combination of the nominal dose and the worst case dose is optimized. The worst case dose was determined by considering the minimum dose that a target voxel would receive over all possible respiratory motion variations.

Heath *et al* 2009 compared robust 4D optimized plans with margin based plans optimized on the mid-ventilation phase. In terms of target coverage, the margin plan and robust 4D optimized plans provided equivalent CTV coverage [38]. However, the margin approach appeared to irradiate more healthy tissue than the robust 4D optimized plans.

Another robust optimization approach, which was described by Chan *et al* (2006), is to account for variability in the time spent at each respiratory phase. In this approach, patient breathing traces were used to create probability mass functions (pmf) to describe the motion of the tumor due to breathing [47]. Then, data from past patients are used to create envelopes of the maximum and minimum motion. The pmf that was obtained from the patient is the ‘nominal’ pmf (Figure 1.12). The nominal pmf along with the upper and lower envelopes are incorporated in the optimization routine.

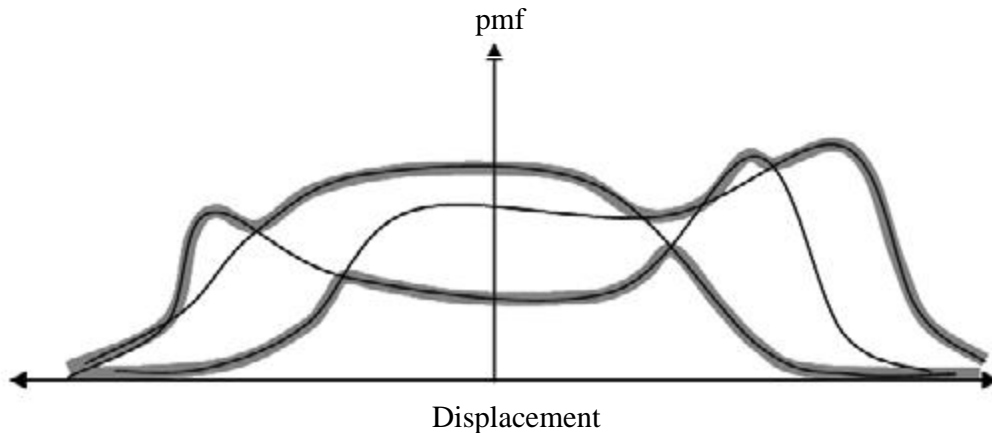


Figure 1.12: The nominal pmf (non-bold line) along with the upper and lower envelopes which encompass the pmfs measured for a population of patients (bold line) [47]

One of the potential applications for robust optimization is dose escalation. For the same lung dose, robust optimized plans can potentially deliver a higher dose to the target volume compared to margin-based plans. The motivation for dose escalation comes from recent studies which suggest that escalating dose to more than 70 Gy helps improve the overall survival rate. A higher dose helps increase the Local Regional Control (LRC). It is important to consider LRC because LRC failure correlates with poor survival rates. Machtay *et al* concluded that patients who were locally controlled had a median survival of 23.5 months, and patients who were not locally controlled had a median survival of 17.0 months [48].

1.12 Previous work: A novel approach to generate robust plans

Pokhrel and Heath (2013) previously developed and tested two novel 4D optimization approaches to generate treatment plans which are robust to respiratory motion and motion variations [49]. These approaches consisted of either optimizing a 4D plan on an “average” motion or combining two 4D plans optimized for “worst case” motion variations by averaging their beam intensity maps.

The robustness of these two planning approaches was evaluated using phase-binned 4DCT data generated with a numerical phantom for two different motion variation scenarios: amplitude variations and variations in time inhaling compared to exhaling. Figures 1.13 and 1.14 show the simulated motion variations. Figures 1.15 and 1.16 show the results of both approaches.

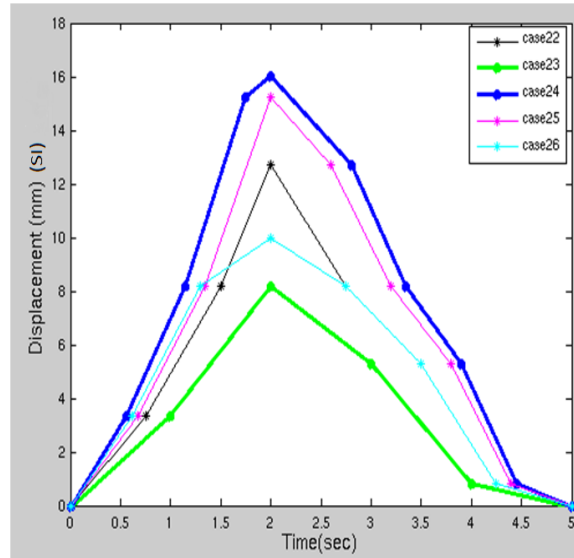


Figure 1.13: Simulated amplitude variations. The number of exhaling and inhaling phases are equal in all scenarios [49]

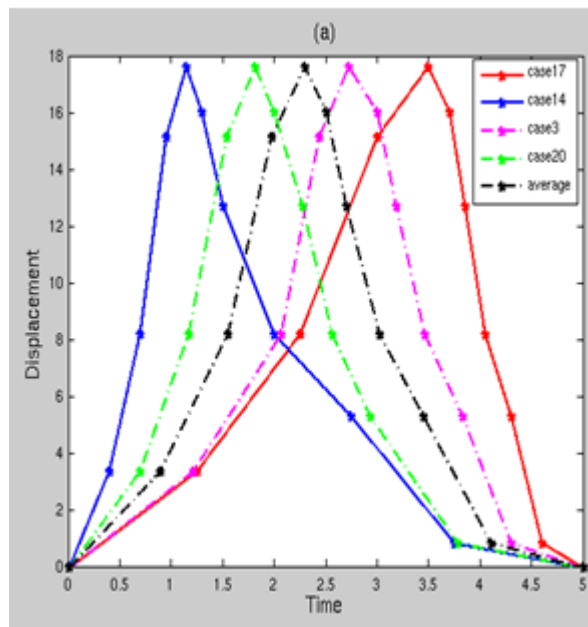
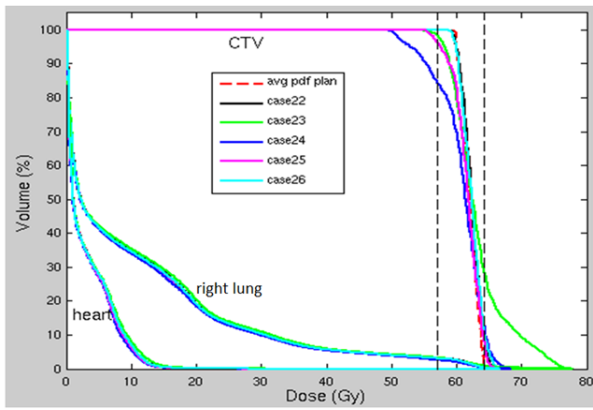
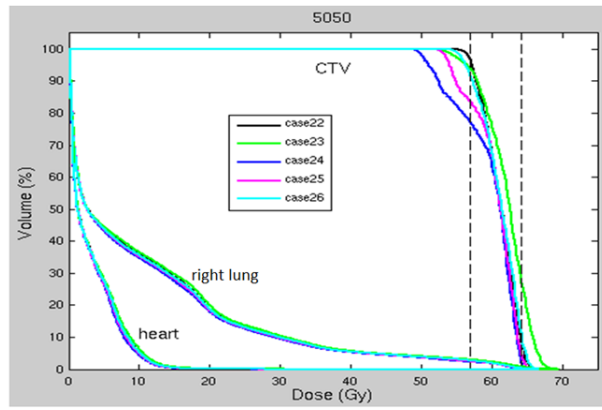


Figure 1.14: More time inhaling / exhaling variations. The amplitude of tumor motion is fixed at 18 mm in all scenarios [49]

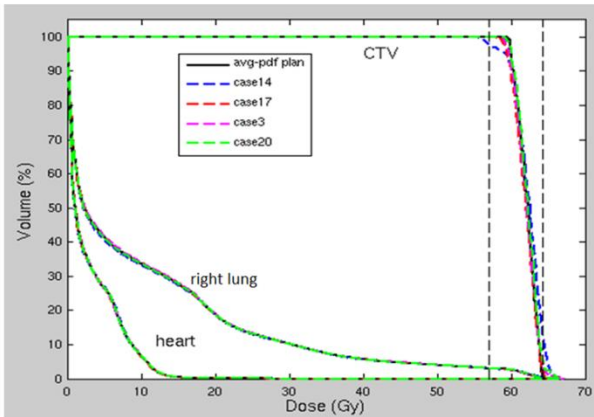


(a)

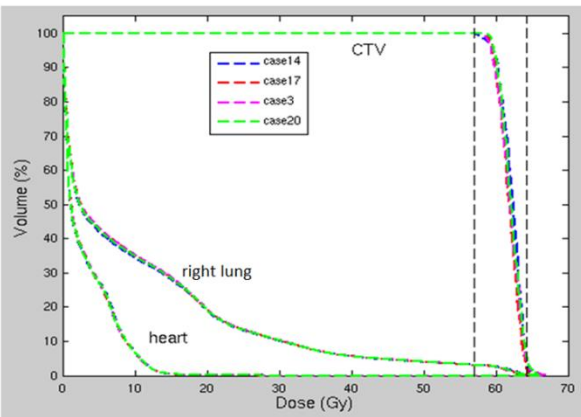


(b)

Figure 1.15: CTV DVHs for amplitude variation scenario (a) average pdf approach (b) worst case approach [49]



(a)



(b)

Figure 1.16: CTV DVHs for more time inhaling vs. exhaling scenario (a) average pdf approach (b) worst case approach [49].

The worst case approach was robust to amplitude variations of up to 3 mm. The results in Figures 1.15b and 1.16b show that the worst case approach appears to provide better dose coverage to the target volume than the average pdf approach and that neither approach was robust to amplitude variations. The limitation of this study was that only phantom data and simulated motion variations were evaluated. It is not known how robust the average pdf and worst case planning approaches would prove to be on clinical patient data and real patient motion variations. Also, phase binned simulated images were used to evaluate the robustness of the worst case plan on amplitude variations. Since the images were phased binned, amplitude variations did not occur in equal steps. Furthermore, it is possible that the robustness of the “worst case” approach could be improved by combining the beam intensity maps in a different way.

1.13 Hypothesis and Objectives

The objective of this project was to further investigate the robustness of the worst case planning approach using intra-fractional patient motion variation data. The specific objectives included: (1) re-evaluating the robustness to simulated amplitude variations using simulated displacement binned image data; (2) investigating whether plan robustness could be improved by modifying the approach used to combine the beam intensity maps; and (3) testing the robustness of worst case plans developed on clinical patient image data to measured patient intra-fraction motion variations.

We hypothesized that worst case 4D plans developed on clinical patient data would be robust to realistic patient intra-fractional motion.

1.14 Thesis organization

Chapter 2 of this document will describe the software used to generate image data, design treatment plans, and perform plan optimization. This chapter will also include a detailed description of the planning methods used and how plan robustness was evaluated as well as the different studies that were performed. Chapter 3 will present the results of the robustness of the different planning methods used. Chapter 4 will discuss the results as well as conclude the findings of this project, and provide suggestions for future work.

Chapter 2 Materials and Methods

2.1 Materials

In this section, the software used to generate image data (XCAT) and the software used in the planning system (Virtuos, and KonRad) are explained. Moreover, the characteristics of both patient image data and phantom image data are described.

2.1.1 Phantom data

This project investigated patient motion variation scenarios using both phantom and patient image data. Phantom image data was generated using the XCAT virtual phantom [50]. The software can be used to generate 4DCT images of realistic male and female torsos (see Figure 2.1). Both cardiac and respiratory motions are modelled. The respiratory motion characteristics are controlled by the respiration period, maximum anterior-posterior chest and diaphragm motions which can be adjusted by the user. Image parameters such as voxel size, slice thickness and number of frames can also be varied in XCAT. The XCAT settings that were used in this project are listed in Table 2.1.

Table 2.1: XCAT phantom settings

Parameter	Value
Pixel width	1.5625 mm
Slice width	3.125 mm
Maximum anterior-posterior expansion of the chest	1.2 cm
Diaphragm max motion	3 cm
Number of output frames	10 - 20
Respiratory period	5 seconds

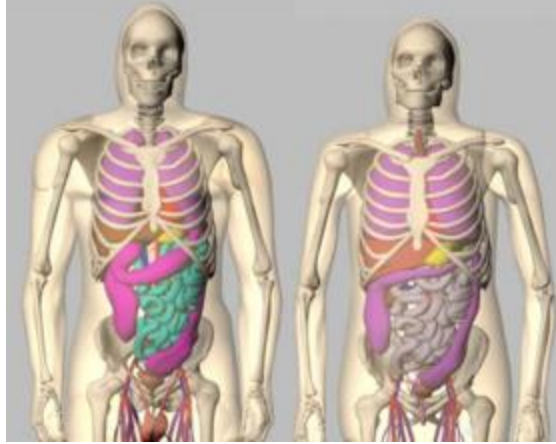


Figure 2.1: Male (left) and female (right) anatomy generated by the XCAT software [50]

The XCAT phantom outputs CT images at time points in the respiratory cycle that are determined by the requested number of frames. The image voxel intensities represent the linear attenuation coefficients of the tissues modeled by the phantom in units of 1/pixel. The attenuation coefficients must be converted into Hounsfield units (HU) before the images can be imported into a treatment planning system. The XCAT image intensities were converted to HU units using Equation 2.1

$$HU = 1000 \left(\frac{\mu_x - \mu_{water}}{\mu_{water}} \right) \quad (2.1)$$

where μ_{water} is the linear attenuation coefficient of water and μ_x is the linear attenuation coefficient of the imaged material. The value of μ_{water} for a given voxel resolution setting was obtained from the log file output by XCAT.

XCAT operates under different modes. In this project, only mode 0, which generates a 4DCT image of the phantom without the lesion, and mode 2, which generates images of the lesion only, were used. Therefore, to obtain a final 4DCT image, the phantom and lesion images were combined. XCAT was used to generate a spherical lung lesion with a diameter of 3 cm and maximum tumor motion amplitude of 16 mm (Figure 2.2).

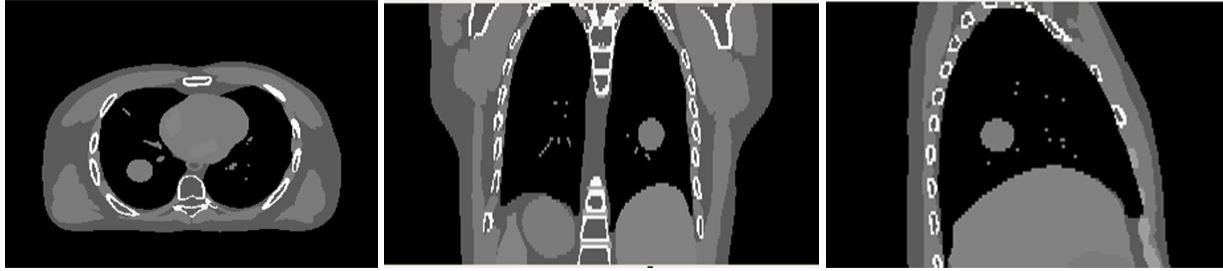


Figure 2.2: Transverse (left), coronal (middle), and sagittal (right) views of a lung lesion in a phantom generated by XCAT.

2.1.2 Patient data

Anonymized treatment planning data of a NSCLC patient was used, with ethics approval, in this project. This patient was previously treated at the Princess Margaret hospital with radiation therapy and chemotherapy. The data, which was provided in DICOM format [51], consisted of bi-weekly 4DPET/CT images, target volume and OAR contours and beam angles. The first set of images was acquired at the time of treatment planning. Two of the other 4DPET/CT datasets were acquired during the course of treatment and the final images were acquired after the completion of radiotherapy. The data also included bi-weekly respiratory motion traces acquired with an RPM system [8]. The tumor volume was 11.5 cm^3 , the nominal motion of the tumor was 7.5 mm and the tumor was located in the posterior upper right lobe.

2.1.3 Virtuos

Virtuos is a radiotherapy planning tool developed at the German Cancer Research Center in Heidelberg. In this project, Virtuos was used to design and evaluate treatment plans based on phantom and patient images [52].

There are four main modes, or functionalities, in Virtuos: Image processing, Planning, Result and Compare mode. Image processing mode (Figure 2.3) features DICOM image import and contouring tools. In Planning mode (Figure 2.4), the user can design a treatment beam arrangement and select incident beam parameters such as irradiation device, beam angle and energy and calculate the resulting dose distribution. The user can launch the KonRad inverse planning engine (to be described in the following section) from Planning mode. After the treatment plan has been optimized

in KonRad, the dose distribution can be viewed in Result mode (Figure 2.5). Isodose displays in Result mode allow the user to evaluate the target volume coverage. Isodose lines are lines that pass through points of equal doses and they are usually displayed in terms of a percentage of the prescription dose. Dose volume histograms for all contoured structures can also be viewed in Result mode. Compare mode allows the user to compare two treatment plans in terms of their DVHs and dose distributions.

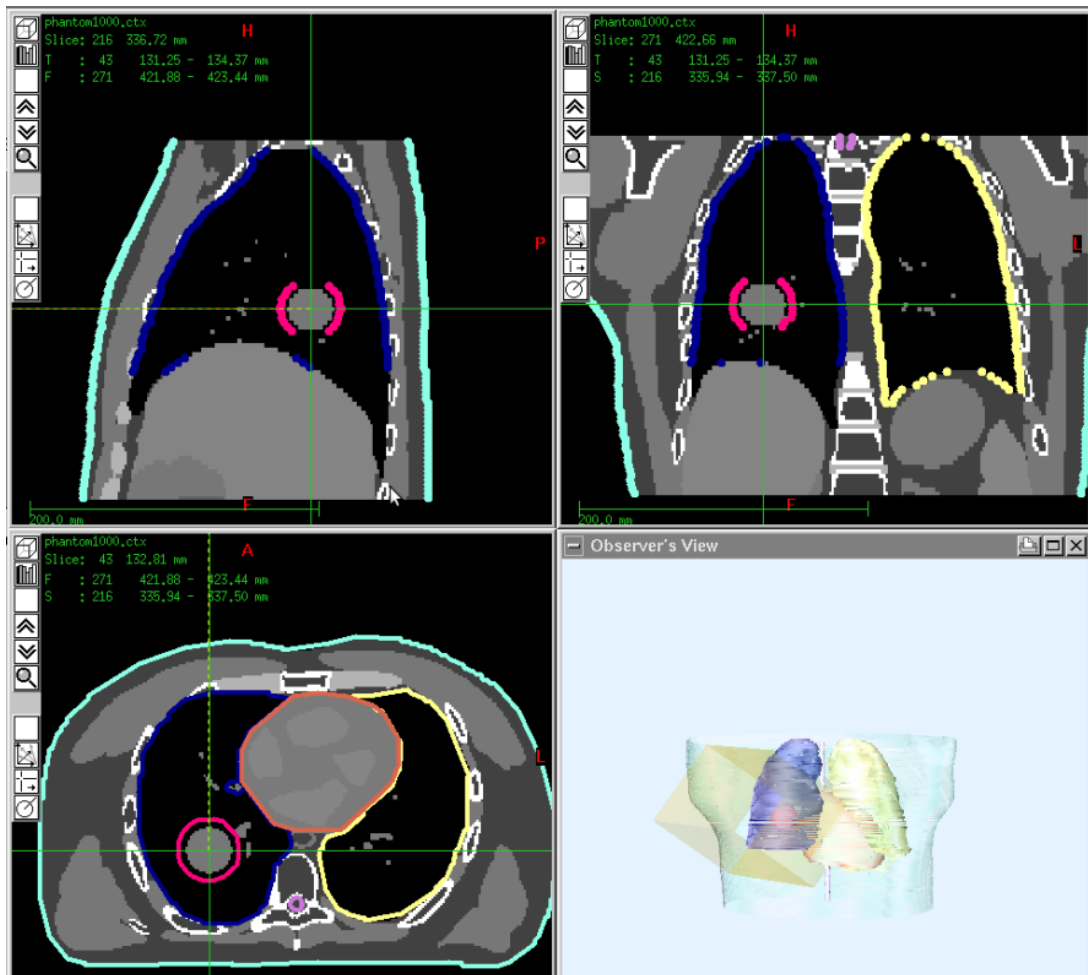


Figure 2.3: Screenshot of Image processing mode in Virtuos showing sagittal, axial and coronal views of a CT image with planning contours overlaid. The bottom right image is the Virtuos observer view, which shows a three dimensional model of the patient's anatomy with additional therapy relevant information.



Figure 2.4: Screen shot of Planning mode in Virtuoso. Yellow lines indicate the boundaries of incident treatment beams. At bottom right is a three-dimensional view of the contoured lungs with incident beams show as tetrahedrons.

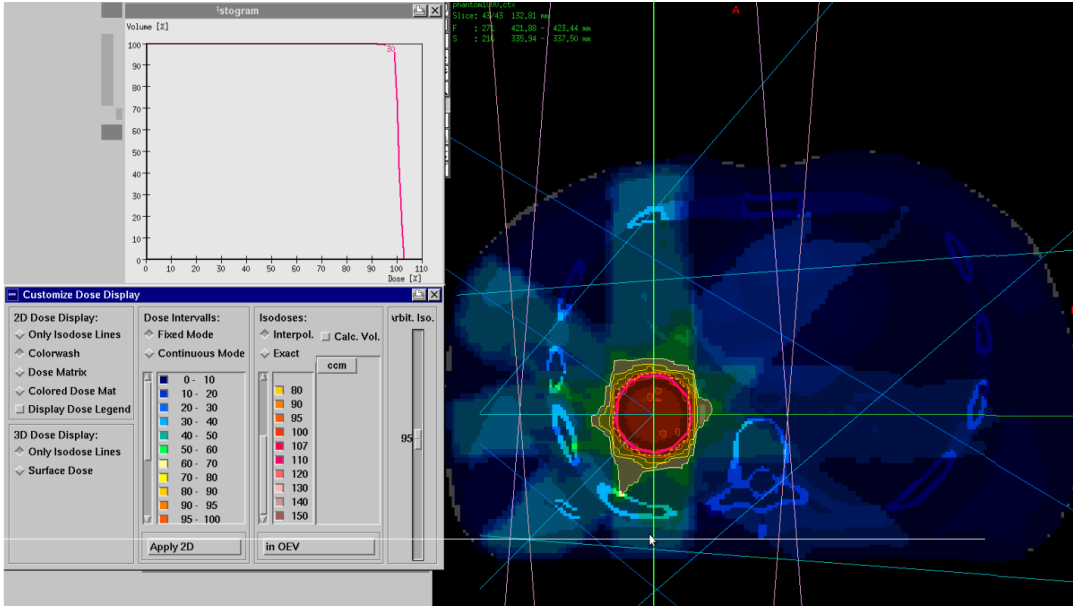


Figure 2.5: Screenshot of Result mode in Virtuoso. Shown at top left is a dose volume histogram (DVH) for the CTV (shown in pink). The right hand image shows the dose distribution and isodose lines overlaid on an axial slice of the CT image. The yellow dashed line represents the 95% isodose line

2.1.4 KonRad

KonRad is an inverse treatment planning tool that performs fluence-based optimization of intensity-modulated radiation therapy plans [53]. KonRad was used in this project to perform 3D and 4D optimization of treatment plans. KonRad requires as input CT images, planning contours and a treatment plan (incident beam angles, energies and irradiation device properties).

In KonRad the CT cube is divided into small cubic elements called voxels, each with a resolution of 2.62 mm. Each incident beam specified in the treatment plan is also sub-divided into smaller pencil beams with a cross-sectional area of size 5 mm^2 . These pencil beams are called beamlets. Figure 2.6 illustrates the relationship between the voxels and beamlets. For each beam, the dose delivered by beamlet j to voxel i is pre-calculated and saved in a D_{ij} matrix. Using this D_{ij} matrix, the dose delivered to a voxel D_i by a beam with intensity distribution w_j can be efficiently calculated following Equation 2.2

$$D_i = \sum_j^{N_j} D_{ij} w_j \quad (2.2)$$

where N_j is the number of beamlets in the treatment beam.

During the optimization process, KonRad uses a gradient descent method to search for the optimal weight of each beamlet in order to meet the plan constraints that are defined by the user in the KonRad GUI (Figure 2.7). The optimal weight for each beam is determined by minimizing the objective function F (Equations 2.3-2.5)

$$F = \sum_t^{N^{TARGET}} F_t + \sum_r^{N^{OAR}} F_r \quad (2.3)$$

$$F_t = \sum_i^{N_t} S_u^t [d_t^{min} - d_i]_+^2 + S_o^t [d_i - d_t^{max}]_+^2 \quad (2.4)$$

$$F_r = \sum_i^{N_r} S_o^r [d_i - d_r^{max}]_+^2 \quad (2.5)$$

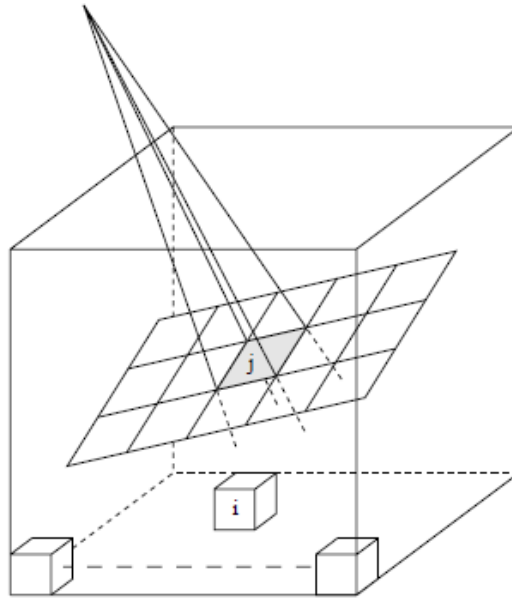


Figure 2.6: Illustration of how each treatment beam is divided into beamlets (labeled with index j) and the CT image is divided into voxels (labeled with index i). The dose deposited by beamlet j to voxel i is stored in the D_{ij} matrix [53]

where N^{TARGET} is the number of target structures, N^{OAR} is the number of organs at risk, F_t is the objective function for a target structure and F_r is the objective function for an organ at risk. The variables d_{min} and d_{max} are the minimum and maximum dose constraints for a given planning

structure that are specified by the user. The variables S_u and S_o are the user-specified penalties that are applied when a structure is under-dosed and over-dosed, respectively. The + sign in Equations 2.4 and 2.5 indicates that KonRad only penalizes positive values in the expression in the brackets.

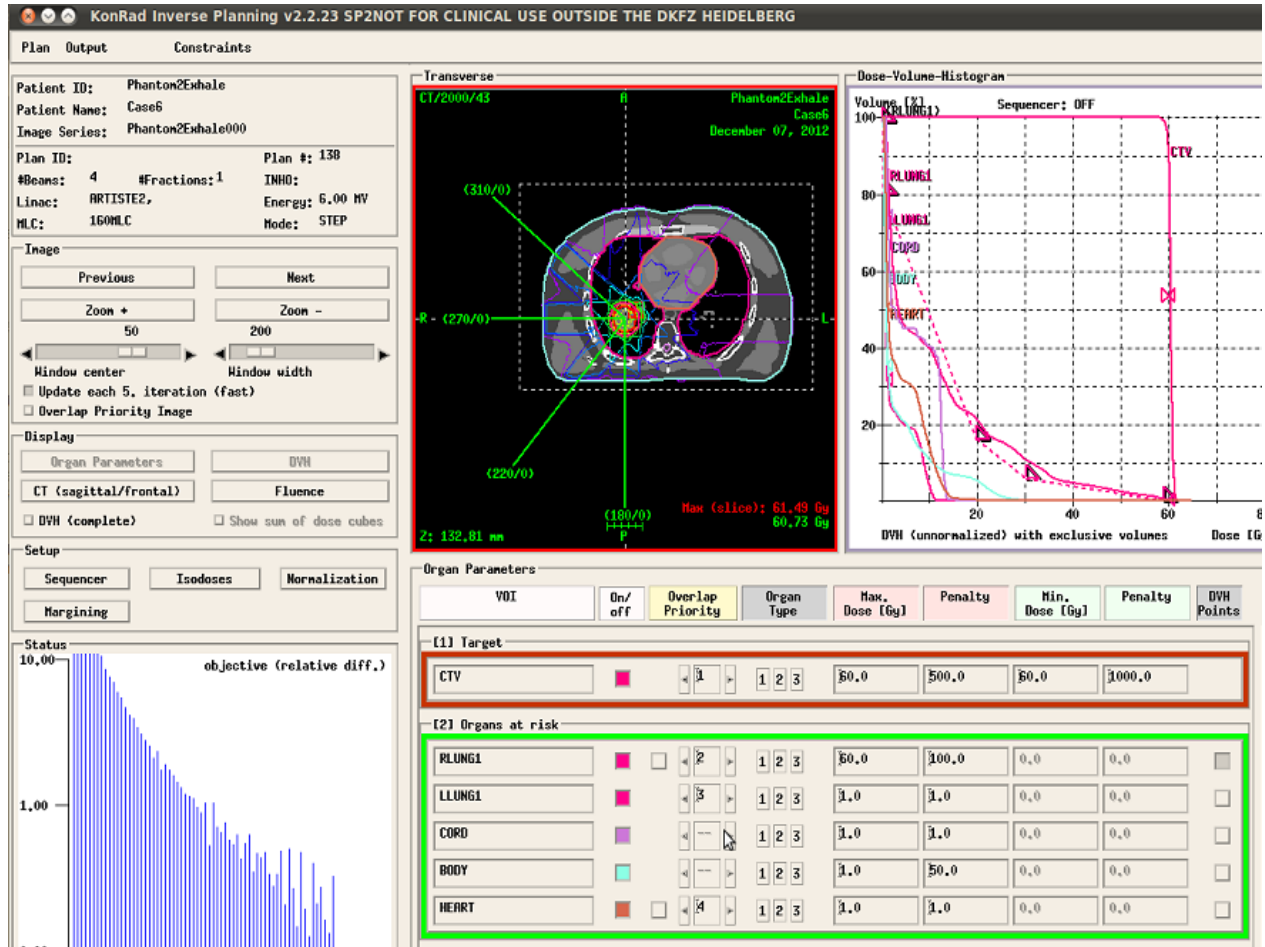
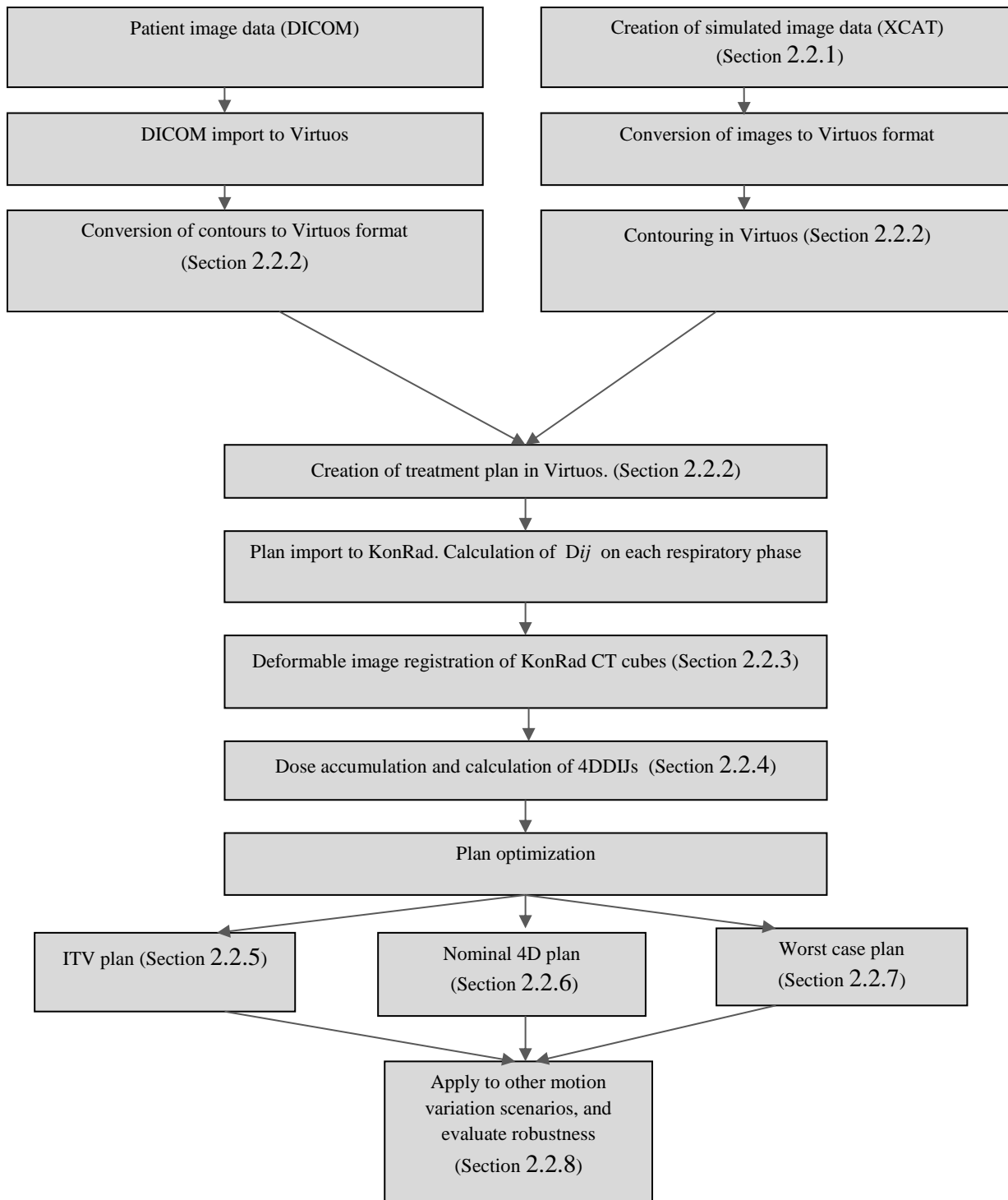


Figure 2.7: Screenshot of the KonRad GUI. The top right corner shows the DVHs for all structures (VOIs) specified in the constraint list at the bottom right. The bottom left portion of the KonRad GUI shows the progress of the objective function minimization

2. 2: Treatment planning methods

The following section describes in detail the process followed to generate the ITV plans, nominal 4D plans and the worst case plans for both simulated image data and patient image data. Figure 2.8 summarizes the treatment planning process.



2.8: A summary of the treatment planning procedure that was followed to create ITV, nominal 4D and worst case plans on both simulated and patient image data

2.2.1 4DCT image generation and processing (Simulated image data)

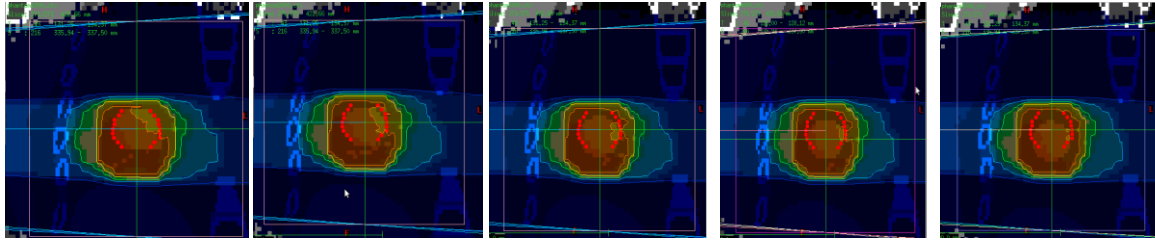
The XCAT software was used to generate a displacement-binned 4DCT dataset composed of 10 images with the tumor located at equally-spaced locations between the tumor location at exhale and inhale. To obtain the images that corresponded to the desired tumor positions, 4DCTs were generated with the number of frames set at 10 and 20. For each generated image the center of mass of the tumor was measured. The images where the center of mass of the tumor was closest to the tumor position for a given displacement bin were selected to form the 10-phase displacement-binned 4DCT.

2.2.2 Treatment planning in Virtuos

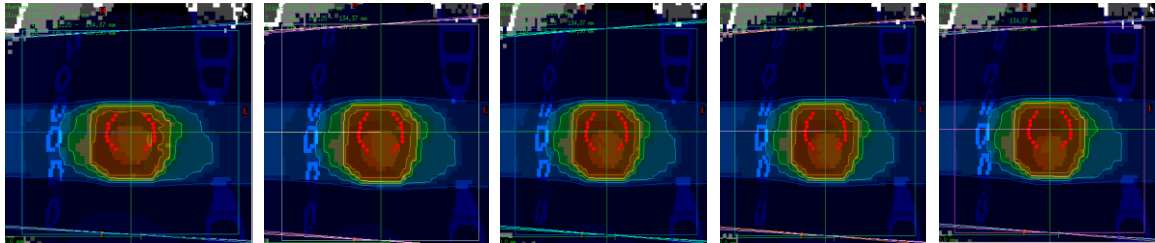
The XCAT images were converted to Virtuos format and then imported into Virtuos for contouring. The GTV, right and left lung, heart and spinal cord were contoured on the exhale image. Additionally, the GTV was contoured in the 9 other respiratory phase images and a CTV was created on each phase by expanding the GTV isotropically by a 5 mm margin.

In the case of the patient 4DCT images, the planning contours were provided along with the data. The contours had to be first converted from DICOM to Virtuos format using a MATLAB code provided by Alexander Runde, a graduate student from the German Cancer Research Center.

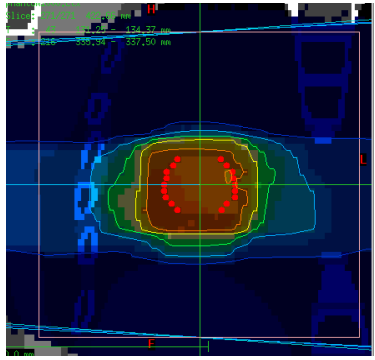
All treatment plans were designed using 6 MV photon beams. For the phantom studies, the beam angle arrangement that achieved the best dose distribution was 0° , 305° , 270° , 225° and 180° . For patient studies, the chosen beam angles were 51° , 103° , 154° , 206° , 257° , 309° and 360° .



0 1 2 3 4



5 6 7 8 9



Accumulated Dose

Figure 2.9: Illustration of the dose accumulation process. The dose is first calculated on phases 0-9 then each dose distribution is mapped to the exhale phase and summed. The last figure shows the accumulated dose distribution.

2.2.3 Deformable image registration

The Virtuos treatment plan was imported into KonRad and applied to each respiratory phase image. During this process, the KonRad CT cubes corresponding to each respiratory phase were output from KonRad for the purpose of deformable registration of each phase to the exhale image. Deformable image registration was performed using the ANIMAL software (Automated Nonlinear Image Matching Anatomical Labeling) [54]. ANIMAL outputs a 3D map of deformation vectors that join voxels in a reference image to the corresponding location of the voxel in the target image.

In the ANIMAL software, the image registration is controlled by different registration parameters including the step size, lattice diameter, sublattice diameter, number of iterations, stiffness, and weight. The procedure outlined in Heath *et al* (2007) was followed to select the optimal registration parameters for our images [55]. The quality of each image registration was visually checked by overlaying the registered image on the target image using the Register tool. The image quality was deemed acceptable if the difference between the target image and the registered image was small.

2.2.4 Dose accumulation

The vectors calculated in deformable image registration describe the transformation required to associate the voxels in the reference image (exhale) to the voxels in the target image. These vectors were used to map the dose calculated on each of the KonRad CT cubes, corresponding to the different respiratory phases, back to the exhale phase (Figure 2.9). First, the dose on each respiratory phase was calculated, according to Equation 2.2, using the corresponding DIJ matrix and setting the beamlet weights to 1. Next, the dose from a given phase $D(x)$ was mapped to the reference phase to get $D(x,0)$. The mapped doses for each respiratory phase were weighted by the time spent in that phase, which is specified by the motion probability density function $p(x)$, then summed and stored in a 4DDIJ matrix (Equation 2.6).

$$4DDIJ = \sum_{x=1}^{10} D_{ij}(x,0)p(x) \quad (2.6)$$

2.2.5 The ITV plan

In this thesis, we defined “3D plan optimization” to be the standard optimization approach in KonRad, as described in Section 2.1.4, which does not account for respiratory motion. An ITV plan is an example of a 3D optimized plan.

The ITV plan was optimized by choosing the ITV to be the target volume in KonRad. The optimization constraints were adjusted until the dose to the ITV was within the tolerances defined by the International Commission of Radiation Units [12]. The ICRU criteria state that the dose within the target structure must be fall between 95% and 107% of the prescription dose. Likewise, the volume of the target receiving 95% of the dose must be 100 % ($V_{95} = 100\%$). The criteria for dose to OARs differ from one institution to the other. In this project, we followed the OAR criteria from PMH lung radiotherapy protocol. The maximum dose limit for the body is 45 Gy. The maximum dose to the spinal cord is 45 Gy. Also, the dose to the heart must not exceed 40 Gy. To avoid healthy lung tissue over-dosage, the lung volume receiving 20 Gy or more must not be more than 30 %. An additional, more stringent criterion, was also used for target volume coverage which was that the dose that covers 99% of the volume must be at least 99% of the prescribed dose.

2.2.6 The Nominal 4D plan

The nominal 4D plan is a plan that accounts for tumor motion but ignores variability in the respiratory motion. We used the motion kernel approach described in Section 1.9 to create the nominal 4D plan. The accumulated dose corresponding to the nominal motion pdf was optimized, using the exhale image as the reference phase. KonRad only performs 3D optimization, therefore, to perform 4D optimization the DIJ matrices for each beam were replaced with the corresponding 4DDIJs which were calculated using the nominal motion pdf. As a starting point, the same optimization constraints were used as for the ITV plan. However, the constraints were adjusted as needed so that the plan criteria outlined in Section 2.2.5 were achieved.

2.2.7 Worst case plans

In this thesis, we used the term “Worst case plans” to refer to the approach tested by Pokhrel and Heath to generate robust 4D plans [49]. The worst case plans were generated by optimizing two nominal 4D plans based on the motion pdfs corresponding to “worst case” motion scenarios. These motion scenarios were chosen based on either how much the pdf weights varied from the nominal

motion pdf or whether that pdf resulted in the worst target volume coverage when the cumulative dose was calculated. More details about the selection of the worst cases will be given in Section 2.3.

Two methods to combine the beam weights were investigated: The average intensity method, which averages the beamlet intensities of each beam (Equation 2.7), and the maximum intensity method which takes the maximum of the two beamlet weights from the two intensity maps for each beamlet (Equation 2.8):

$$w_j^{Avg} = \frac{w_j(1)+w_j(2)}{2} \quad (2.7)$$

$$w_j^{max} = \max\{w_j(1), w_j(2)\} \quad (2.8)$$

2.2.8 Evaluation of plan robustness

To evaluate robustness of a certain planning approach, the plan was applied to the motion pdfs corresponding to the different motion scenarios and the cumulative dose was calculated for each scenario. To calculate the cumulative dose, the intensity maps corresponding to a given plan were applied to the 4DDIJs that were calculated using the different motion pdfs (Equation 2.9).

$$\langle D_i \rangle = \sum_j 4DD_{ij} w_j \quad (2.9)$$

where 4DDIJs were calculated according to Equation 2.6.

A plan was deemed robust if it fulfilled the criteria presented in Section 2.2.5.

2.3 Experiments

The following section describes the particular motion variation cases on which the robustness of the three different planning methods was investigated. Study 1 of the project evaluated the robustness of plans on simulated amplitude variations using displacement binned 4DCT image data generated with the XCAT phantom. Study 2 of the project evaluated plan robustness on patient motion variations using XCAT image data. Study 3 of the project evaluated plan robustness on patient motion variations using patient image data.

2.3.1 Study 1: Amplitude variation study using XCAT image data

In this study, XCAT was used to generate a 10 phase displacement binned 4DCT. Next, a simulated breathing trace was created for each amplitude variation scenario using the sinusoidal function described in Equation 2.10:

$$x = A \sin^2(2\pi t/T) \quad (2.10)$$

where A is the amplitude of motion, t is the time, and T is the breathing period which is 5 seconds.

Five motion amplitudes were chosen: 0.9 cm, 1.1 cm, 1.3 cm, 1.4 cm, and 1.6 cm. A pdf was then generated for each amplitude scenario by binning each breathing trace, generated using Equation 2.10, according to the displacements of the XCAT 4DCT images. Figure 2.10 shows the respiration traces for the 5 motion variation scenarios along with the bin centers corresponding to the XCAT 4DCT images. Figure 2.11 shows the resulting pdfs for each amplitude variation scenario.

An ITV plan, nominal 4D plan and a worst case plan were created. The ITV contour was created from the union of the GTV of phases 0 to 7, which encompasses the nominal motion amplitude of 1.3 cm, with an addition of a 5 mm GTV-CTV margin. The nominal 4D plan was optimized using the 4DDIJ based on the 1.3 cm pdf. The worst case plan was created by combining two 4D optimized plans: one on the 0.9 cm motion pdf, and one on the 1.6 cm motion pdf. These two amplitudes represent the motion outliers in Figure 2.10 and 2.11. The robustness of each planning method was evaluated by applying each plan (ITV, nominal, worst case) to the 5 4DDIJs to calculate the cumulative dose in each case. The dose statistics, DVHs, and dose distribution were all used to evaluate the robustness of each planning method. A plan was deemed robust if it met the criteria provided in Section 2.2.5.

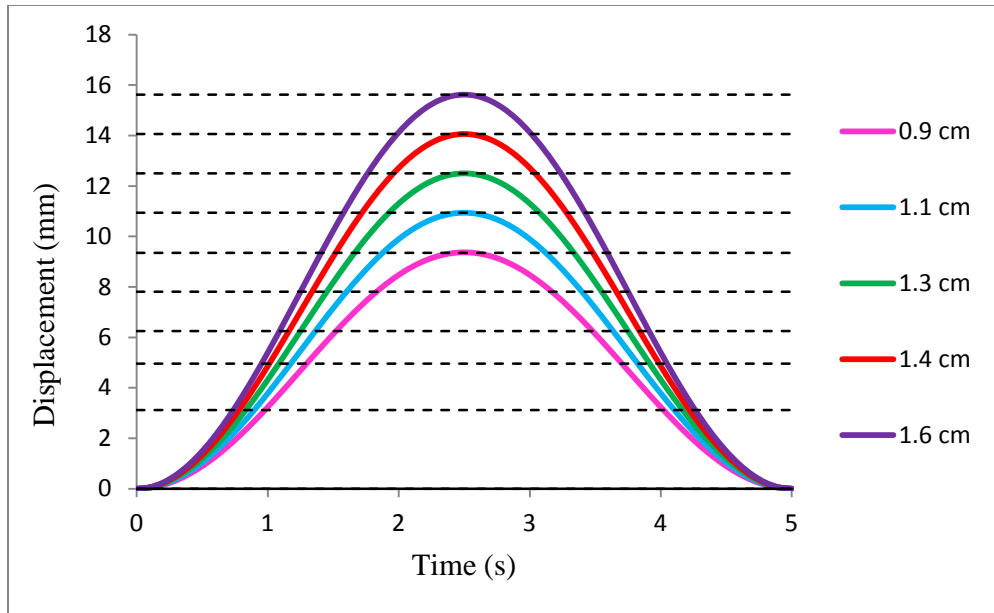


Figure 2.10: The simulated breathing traces for all amplitude variation scenarios. The dashed horizontal lines represent the displacement points where XCAT 4DCT images were available.

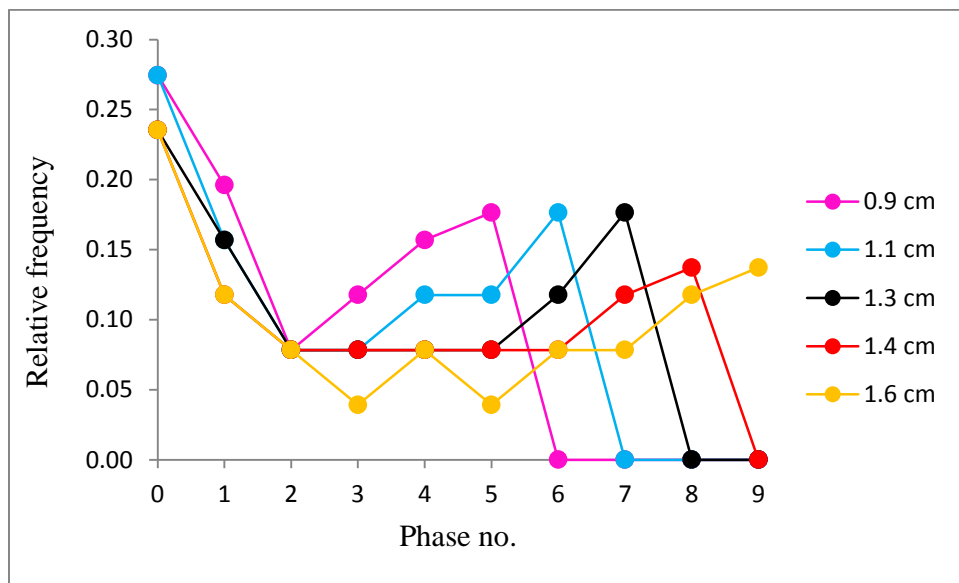


Figure 2.11: The probability density function of each amplitude variation scenario.

2.3.2 Study 2: Patient intra-fractional motion variation study using XCAT image data

The XCAT-generated displacement-binned 4DCT images were also used in this study. A 150s duration breathing trace was obtained from an external surrogate marker (RPM system, Varian Medical Systems) placed on the chest of a healthy volunteer who was asked to breathe irregularly (Figure 2.12). The breathing trace was divided into 30 second intervals. The maximum and the minimum displacement values on the trace were assumed to correspond to inhale and exhale, respectively. Ten equally spaced displacement binned were defined between the maximum and minimum displacement. Each bin was assigned a specific phase (phase0 – phase 9) of the 4DCT dataset and the displacements for each 30 second interval were binned to create 6 different probability density functions (pdfs). Figure 2.13 shows the pdfs extracted from the 30 second intervals of the trace shown in Figure 2.12.

An ITV plan, nominal 4D plan and a worst case plan were created. The ITV was created by fusing all GTVs from phases 0-9, and adding 5 mm margin to the fused GTV. The nominal 4D plan was optimized on the 0s-30s pdf. The worst case plan was created by combining two 4D optimized plans: one on the 0s-30s motion pdf, and one on the 60s-90s motion pdf. These two motion pdfs represent the pdf motion outliers in Figure 2.13. The robustness of each planning method was evaluated by applying each plan (ITV, nominal, worst case) to the 6 4DDIJs to calculate the cumulative dose in each case. The dose statistics, DVHs, and dose distribution were all used to evaluate the robustness of each planning method. A plan was deemed robust if it met the criteria provided in Section 2.2.5.

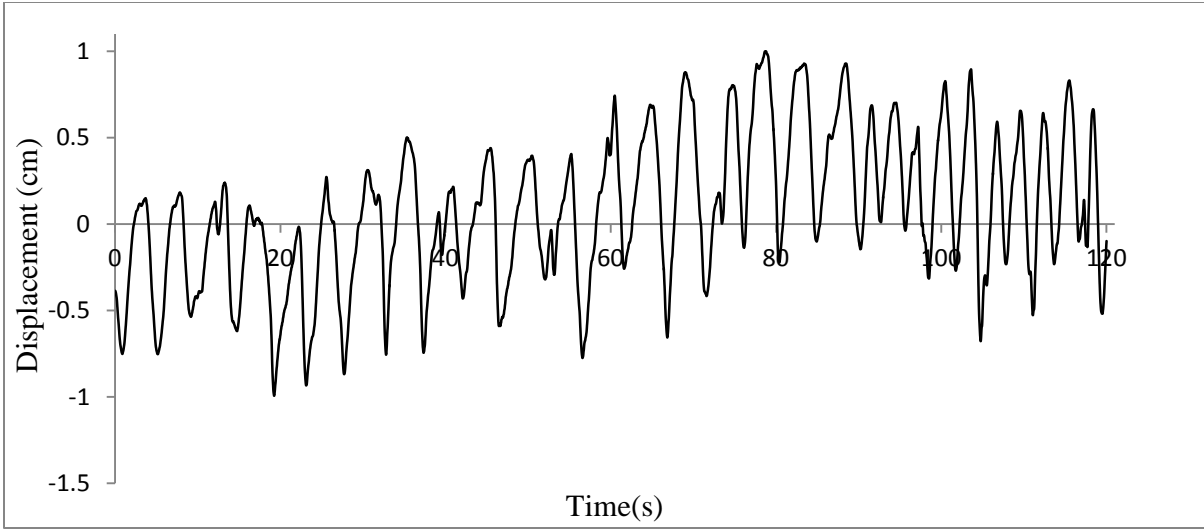


Figure 2.12: The breathing trace taken from a healthy volunteer showing up to 120s

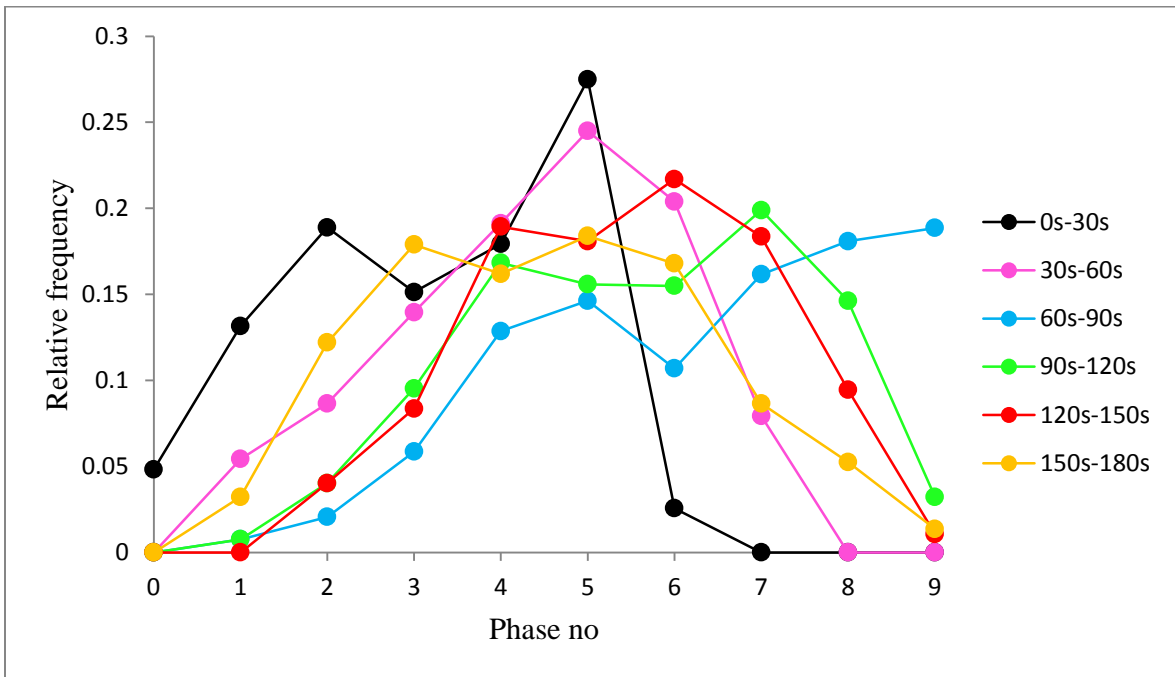
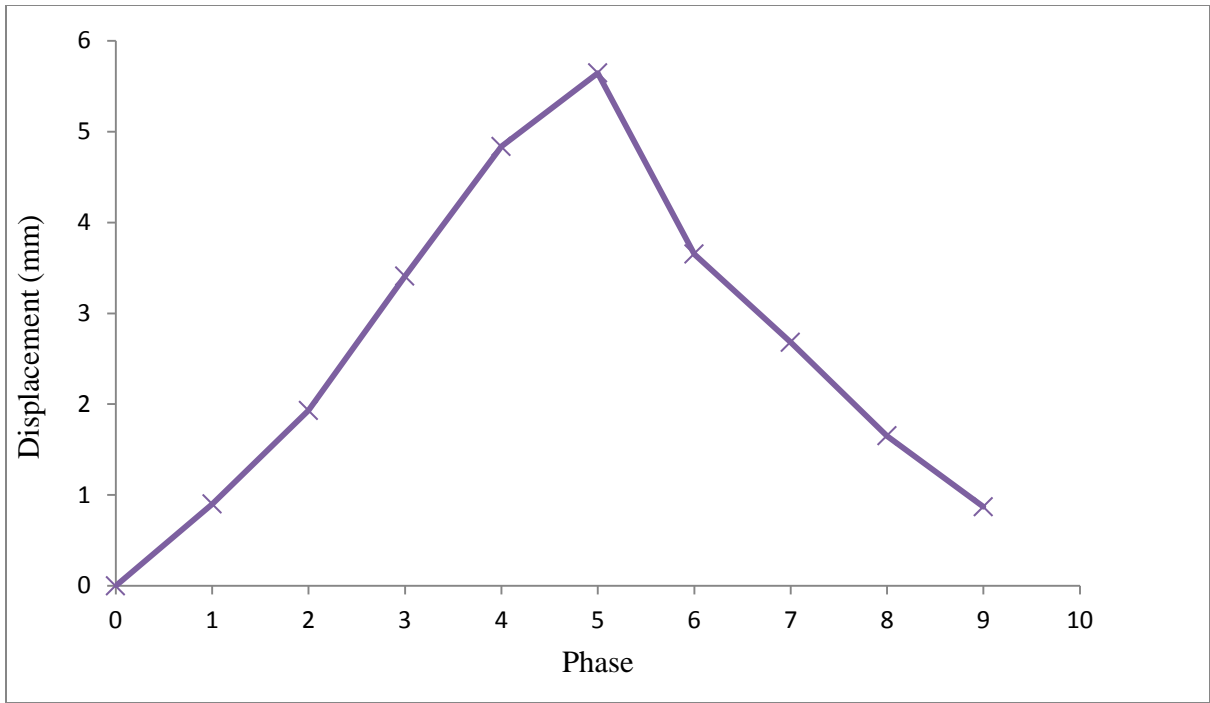


Figure 2.13: 30 second interval motion variations pdfs extracted from the breathing trace in Figure 2.12

2.3.3 Study 3: Patient intra-fractional motion variation study using patient image data

In this study, patient breathing traces and phase binned 4DCTs were used. It is important to note that for this patient the number of inhaling phases was not equal to the number of exhaling phases. Therefore, the inhaling phases were binned independently from the exhaling phases. Figure 2.15 and 2.16 show how each bin was defined. Also, for the patient 4DCT, the exhale phase was labelled phase 0, and the inhale phase was labelled as phase 4. Exhaling phases were phases 5, 6, 7, 8 and 9, and inhaling phases were phases 1, 2, and 3. The breathing trace was segmented into 20 second intervals. The maximum and the minimum displacement values on the trace were taken to be inhale and exhale points, respectively. Each 20s segment of the trace was then binned into 10 equally spaced displacement bins to determine the probability density function (pdf). Figure 2.17 shows the pdfs extracted from the 20 second intervals of the trace. This displacement binning approach was not consistent with the use of phase-binned 4DCT images. However, to model changes in amplitude it was necessary to use this approach. Figure 2.14 shows the tumor displacement along the superior-inferior direction. The amount of displacement between adjacent respiratory phases is almost equal.

An ITV plan, a nominal 4D plan, and a combined worst case plan were created. The ITV plan was based on the ITV contour provided by PMH. The nominal 4D plan was optimized on the 0s-20s pdf and the worst case plan was made by optimizing two 4D plans on the 0s-20s and the 80s-100s pdfs. These two pdfs represent the pdf motion outliers in Figure 2.17. The robustness of each planning method was evaluated by applying each plan (ITV, nominal, worst case) to the 4DDIIs calculated using the extracted 20s pdfs. The dose statistics, DVHs, and dose distribution were all used to evaluate the robustness of each planning method. A plan was deemed robust if it met the plan criteria described in Section 2.2.5.



2.14: Tumor displacement along the superior-inferior direction

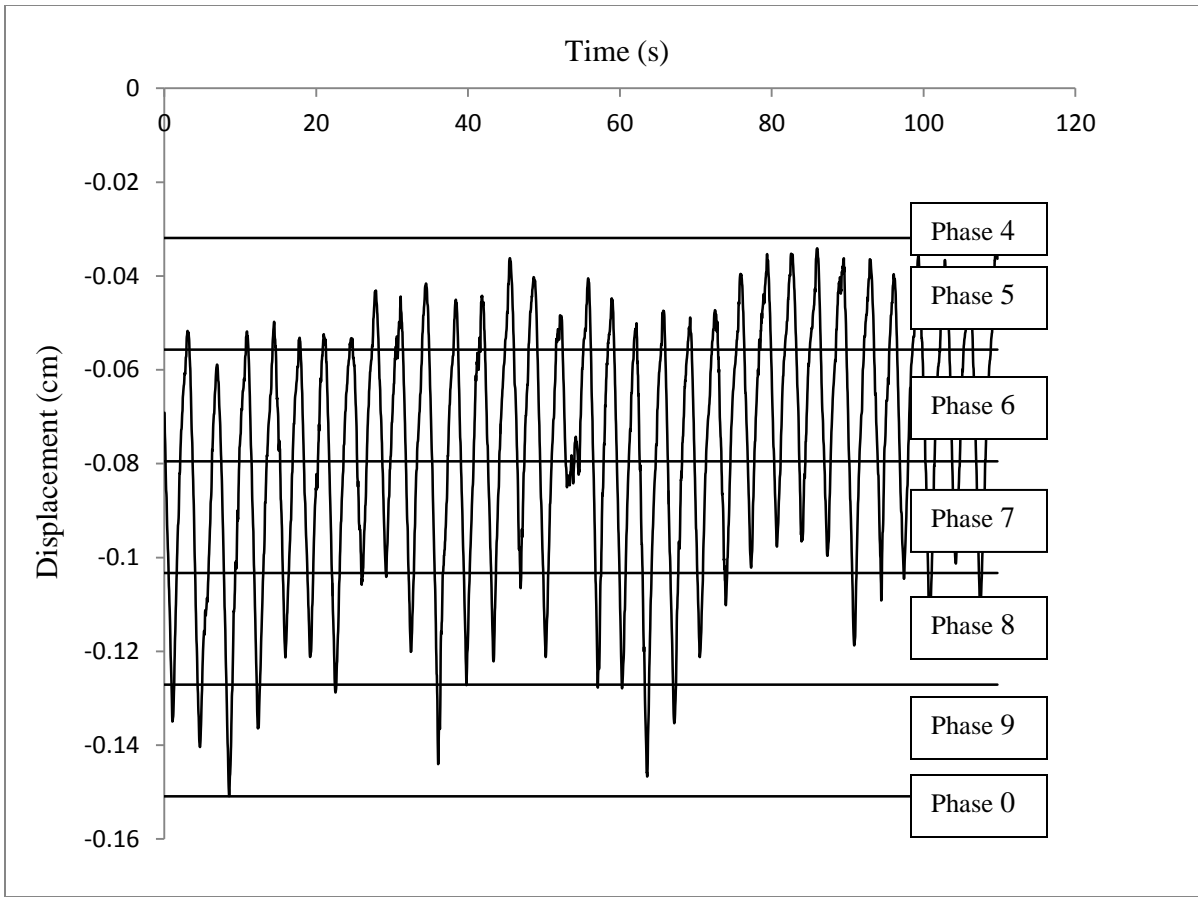


Figure 2.15: Patient breathing trace for week 0 4DCT showing phases 0 and 4 (exhale and inhale respectively) bin displacement values, and exhaling phases (phases 5-9) bin displacement values

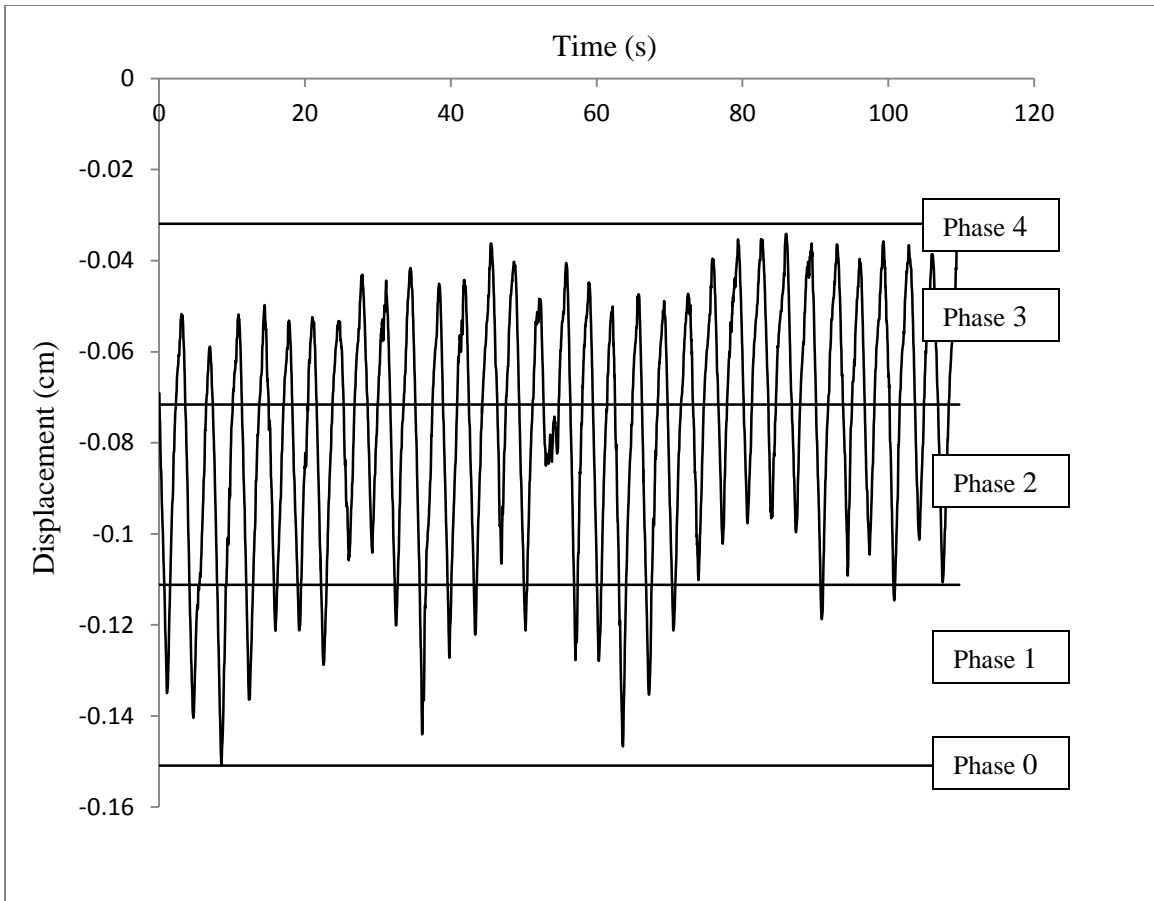


Figure 2.16: Patient breathing trace for week 0 4DCT showing phases 0 and 4 (exhale and inhale respectively) bin displacement values, and inhaling phases (phases 1-3) bin displacement values

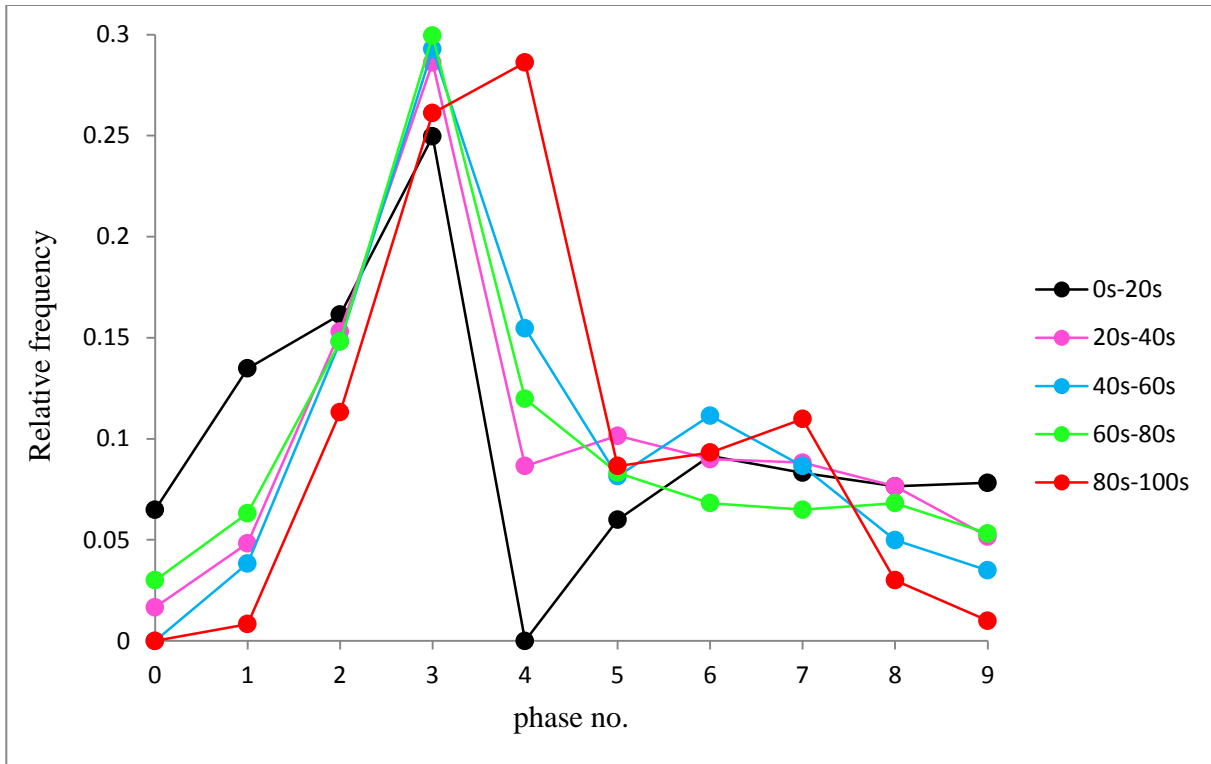


Figure 2.17: Patient 20 second interval pdfs extracted from the breathing trace shown in Figures 2.15 and 2.16

2.3.4 Study 4: Patient inter-fractional motion variation study using patient image data

In this study, patient breathing traces from weeks 0, 2, 4, and 7 and patient phase binned planning 4DCTs were used. Because no 4DCTs from weeks other than week 0 were used, this study excluded *anatomical* inter-fractional variations, and it only involved *respiratory motion* inter-fractional variations. The labeling for inhale/exhale and inhaling/exhaling was the same as the one presented in Section 2.3.3. The maximum and the minimum displacement values of each trace were taken to be inhale and exhale points, respectively. The breathing traces for each week are shown in Figure 2.18. Instead of segmenting the breathing trace into equal time intervals (as it was done in Study 2 and Study 3), the pdf of the full breathing trace was created. The pdf was created by binning the full breathing trace into 10 equally spaced displacement bins to determine the probability density function (pdf). Figure 2.19 shows the pdfs extracted from the full breathing traces presented in Figure 2.18.

The nominal 4D plan was optimized on the week 0 pdf which was extracted from the full breathing trace of week 0. No worst case plans, or ITV plan were created in this study. The robustness of the nominal plan was evaluated by applying the plan to the 4DDIJ's of the pdfs from weeks 2, 4, and 7.

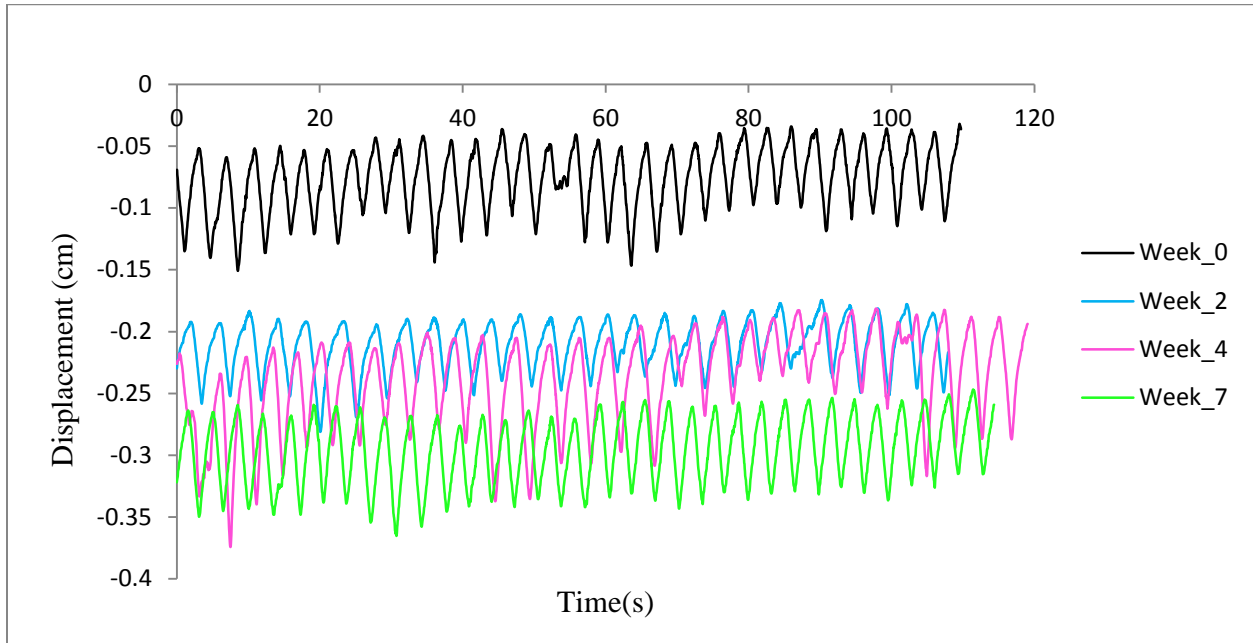


Figure 2.18: Patient breathing traces for weeks 0, 2, 4 and 7.

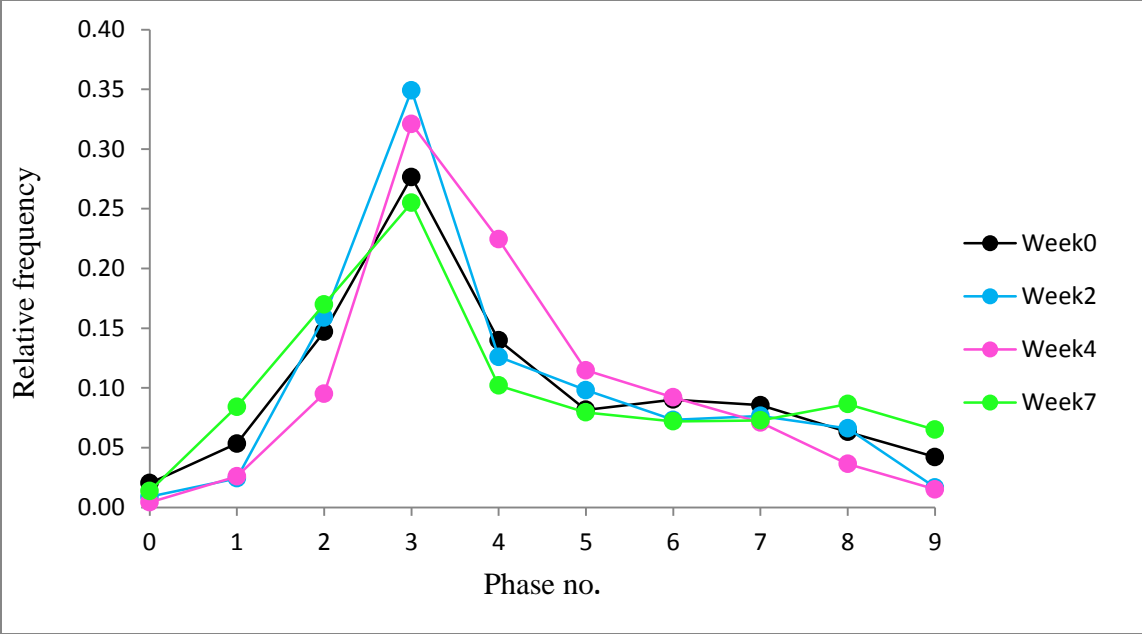


Figure 2.19: Pdfs extracted from the full breathing traces presented in Figure 2.18

Chapter 3 Results

This chapter will present the results from the robustness evaluation of the ITV, nominal 4D and the worst case plans on three different motion variation studies. Study 1 evaluated the robustness of the three different planning approaches on simulated amplitude variations applied to XCAT phantom images (Section 3.2). Study 2 evaluated the robustness of the three different planning approaches on intra-fractional patient motion variations applied to XCAT phantom images (Section 3.3). Study 3 evaluated the robustness of the three different planning approaches on intra-fractional patient motion variations using patient 4DCT image data (Section 3.4). Study 4 evaluated the robustness of the nominal plan of patient inter-fractional motion variations using patient 4DCT image data (Section 3.5).

3.1 Influence of KonRad optimization constraints

To optimize a plan in KonRad, the user needs to provide KonRad with optimization constraints for each planning structure. In this project, it was realized that the choice of optimization constraints affected the robustness of that 4D plan (or two combined 4D plans in the case of worst case planning) when applied to other motion scenario. For example, two different constraints were used to optimize two 4D plans on the minimum amplitude motion (0.9 cm) and the maximum amplitude motion (1.6 cm) scenarios for the Study 1 (Table 3.1 and 3.2). The two different constraints gave optimized plans that met the ICRU criteria (Table 3.3). However, when the 0.9 cm and the 1.6 cm plans were combined and applied to other motion amplitudes, the dose coverage and the DVH were different when using the constraints provided in Table 3.1 than the ones provided in 3.2 (Figure 3.1). It can be noted from Figure 3.1 that the constraints presented in Table 3.1 yielded better dose coverage than the constraints used in Table 3.2. Based on these results, the constraints presented in Table 3.1 were used consistently as a starting point for optimization of all plans.

Table 3.1: First set of KonRad constraints used to optimize a 4D plan on the 0.9 cm and the 1.6 motion amplitudes

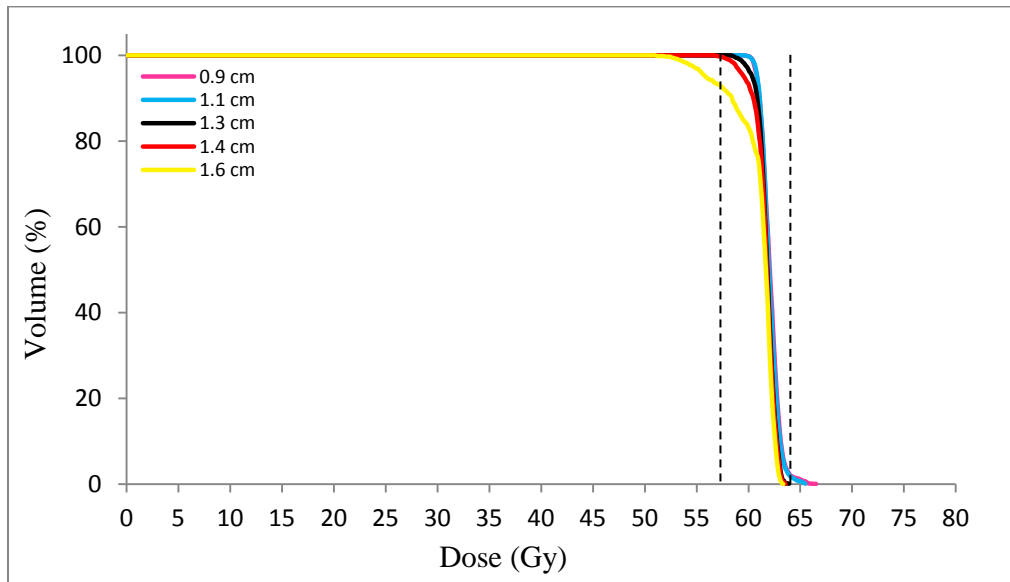
Target volume/ OAR volume	Maximum dose (Gy)	Penalty on maximum dose	Minimum dose (Gy)	Penalty on minimum dose
CTV	62.0	200.0	60.0	200.0
Right lung	60.0	1.0		
Left lung	60.0	1.0		
Cord	60.0	1.0		
External	20.0	40.0		
Heart	60.0	1.0		

Table 3.2: Second set of KonRad constraints used to optimize a 4D plan on the 0.9 cm and the 1.6 motion amplitudes.

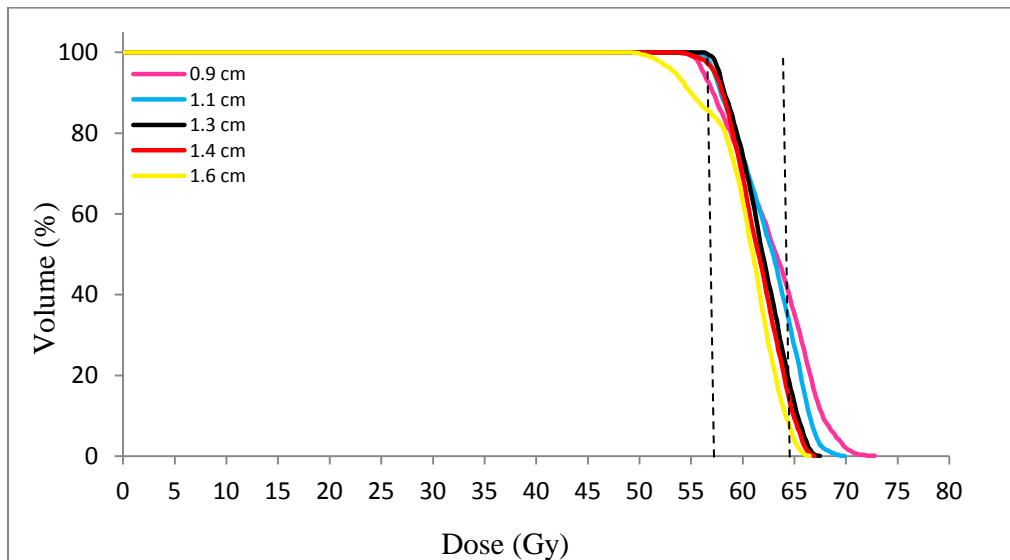
Target volume/ OAR volume	Maximum dose (Gy)	Penalty on maximum dose	Minimum dose (Gy)	Penalty on minimum dose
CTV	64.2	100.0	57.0	200.0
Right lung	60.0	1.0		
Left lung	60.0	1.0		
Cord	60.0	1.0		
External	60.0	20.0		
Heart	60.0	1.0		

Table 3.3: Optimized plan dose statistics when using the KonRad constraints in Tables 3.1 and 3.2 on the 0.9 cm amplitude and the 1.3 cm amplitude 4D plans

Plan	CTV minimum dose (Gy)	CTV maximum dose (Gy)	Heart maximum dose (Gy)	External maximum dose (Gy)
0.9 cm 4D plan using constraints from Table 3.1	59.80	62.10	26.80	40.10
1.6 cm 4D plan using constraints from Table 3.1	59.80	62.20	28.80	37.30
0.9 cm 4D plan using constraints from Table 3.2	57.00	64.20	30.18	39.48
1.6 cm 4D plan using constraints from Table 3.2	57.00	64.20	26.49	40.00



(a)



(b)

Figure 3.1 : a) DVHs from the worst case approach using the average intensity method and constraints from Table 3.1 to optimize the 0.9 cm amplitude and the 1.6 cm amplitude 4D plans b) DVHs from the worst case approach using the average intensity method and constraints from Table 3.2 to optimize the 0.9 cm amplitude and the 1.6 cm amplitude 4D plans.

3.2 Study 1: Simulated amplitude variations applied to XCAT phantom images

This study used displacement-binned 4DCT images generated using the XCAT software with realistic respiratory motion parameters. A nominal 4D plan and an ITV plan were designed for the nominal 1.3 cm motion amplitude. Two worst case plans were designed by combining 4D plans optimized for 0.9 cm and 1.6 cm amplitude motion. The robustness of all plans was tested by applying them to 5 different motion cases corresponding to amplitudes of 0.9 cm, 1.1 cm, 1.3 cm, 1.4 cm and 1.6 cm.

3.2.1 Image registration parameters and assessment

All image registrations were deemed to be acceptable by visual inspection. Table 3.4 shows the optimized parameters that were used for the deformable registration of the CT images of the 9 breathing phases (phase 1 – phase 9) to the exhale phase (phase 0). Figure 3.2 shows the overlap of the target image on the reference image before image registration, and the overlap of the target image on the registered image after registration.

Table 3.4: The optimal parameters used for registration of displacement-binned XCAT images using ANIMAL software

Target image	Step size (mm)	Lattice diameter (mm)	Iterations	Stiffness	Weight	Sublattice diameter
Phase 1	10.48	30	30	0.2	0.9	7
Phase 2	10.48	30	30	0.2	0.9	7
Phase 3	10.48	40	30	0.2	1.0	9
Phase 4	10.48	50	30	0.5	1.0	10
Phase 5	10.48	40	30	0.2	0.7	7
Phase 6	10.48	40	30	0.3	1.0	7
Phase 7	10.48	40	30	0.2	0.5	7
Phase 8	10.48	40	30	0.2	0.8	7
Phase 9	10.48	40	30	0.2	0.8	9



(a)

(b)

Figure 3.2: Example of visual assessment of image registration quality: (a) red/green overlay of the target XCAT image (red) on the reference XCAT image (green) before image registration and (b) the overlap of the target XCAT image (red) on the registered XCAT image (green) after registration.

3.2.2 ITV plan

The ITV was created by taking the union of the GTVs on phases 0-7 and adding a 5 mm margin to it. A static plan was then optimized using the ITV as the target volume. The optimized ITV plan met the ICRU criteria. The CTV minimum dose was 57.3 Gy and the CTV maximum dose was 63.8 Gy. The tight criterion was not met as the D99 was 58.1 Gy. All organs at risk received lower doses than the maximum allowed by treatment planning criteria with the exception of the right lung where the V20Gy was 32%. The ITV plan was then applied to all the motion amplitude scenarios. Figure 3.3 shows the DVHs of the CTV for each motion amplitude scenario. It can be noted from this figure that the ITV plan was robust to motion amplitude scenarios up to the nominal motion (1.3 cm). In the 1.4 cm and the 1.6 cm amplitude scenarios, the CTV was not fully covered by the ITV plan. The minimum dose to the CTV in these two cases was 55.1 Gy and 51.4 Gy respectively. The dose statistics for target coverage are shown in Figures 3.8 and 3.9.

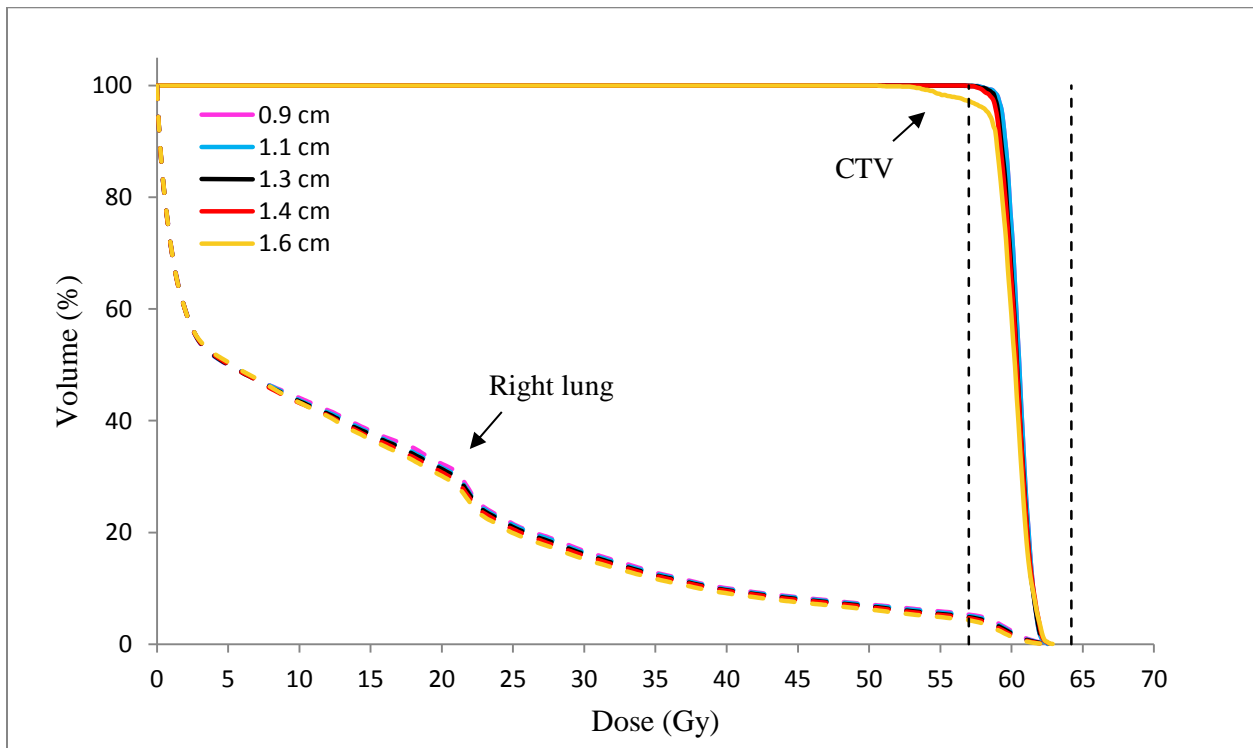


Figure 3.3: Dose volume histograms of the ITV plan applied to other motion amplitude scenarios showing dose coverage of both the CTV and the right lung.

3.2.3 Nominal 4D plan

A nominal 4D plan was optimized for the 1.3 cm motion amplitude scenario. The optimized plan met both the ICRU and the tight planning criteria. For example, the minimum CTV dose was 59.8 Gy, the maximum CTV dose was 62.1Gy and the CTV D99 was 60.0 Gy. All organs at risk received lower doses than the maximum allowed by ICRU criteria. 4DDIJs for the other amplitude variation scenarios were created based on the pdfs provided in Figure 2.11. Figure 3.4 shows the resulting DVHs when the nominal 4D plan was applied to other motion amplitude scenarios.

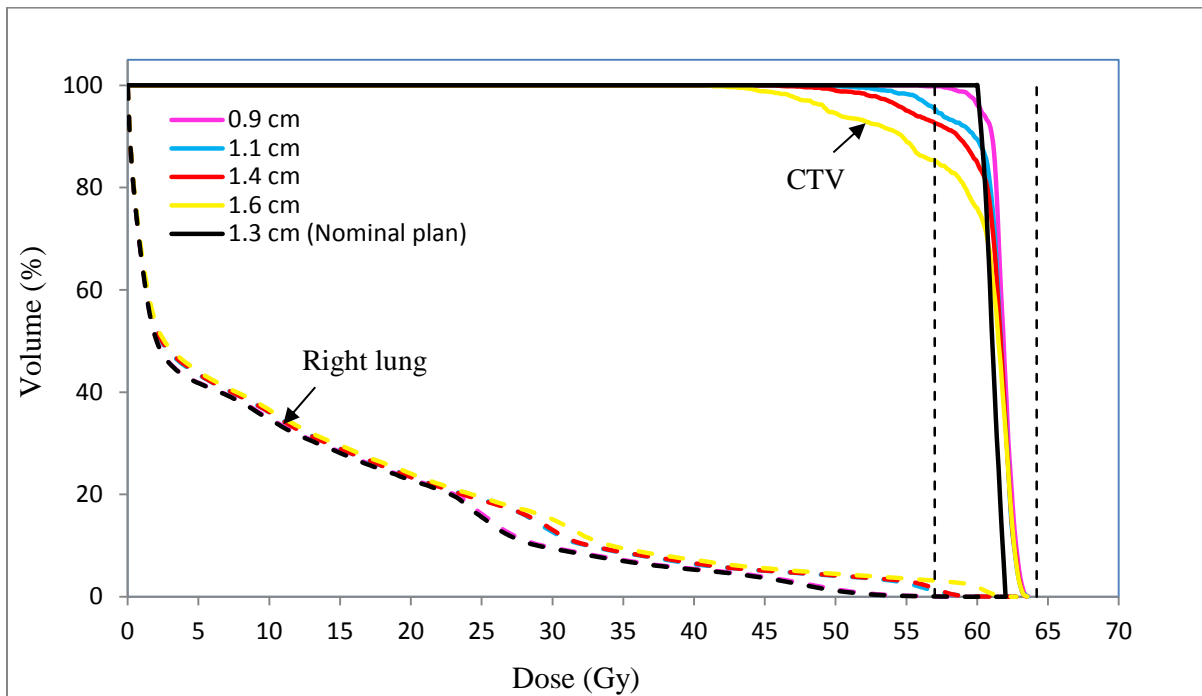
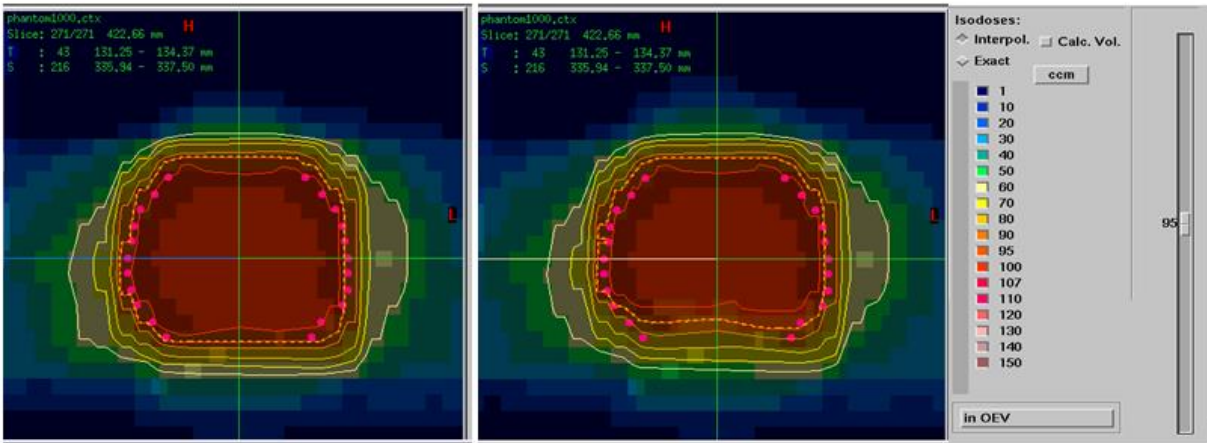


Figure 3.4: Dose volume histograms of the nominal plan applied to different motion amplitude scenarios for the CTV and Right lung (tumor-bearing lung). The black dashed lines represent the ICRU minimum and maximum dose criteria of 57 Gy and 64.2 Gy, respectively.

As seen in Figure 3.4, the two cases that yielded the worst CTV coverage are the 1.4 cm and the 1.6 cm amplitudes. Figures 3.5a and 3.5b show the dose distribution in Virtuos of the nominal 4D plan applied on 1.4 cm and 1.6 cm amplitude scenarios, respectively. Both Figures show that there is an under-dosage in the inferior portion of the tumor. The accumulated dose statistics for the different motion scenarios are summarized in Figures 3.8-3.10. From Figure 3.4 and Figure 3.8, it is noted that

the nominal plan is not robust to the amplitude variation scenarios, as the CTV is under-dosed when the motion amplitude is not the nominal amplitude.



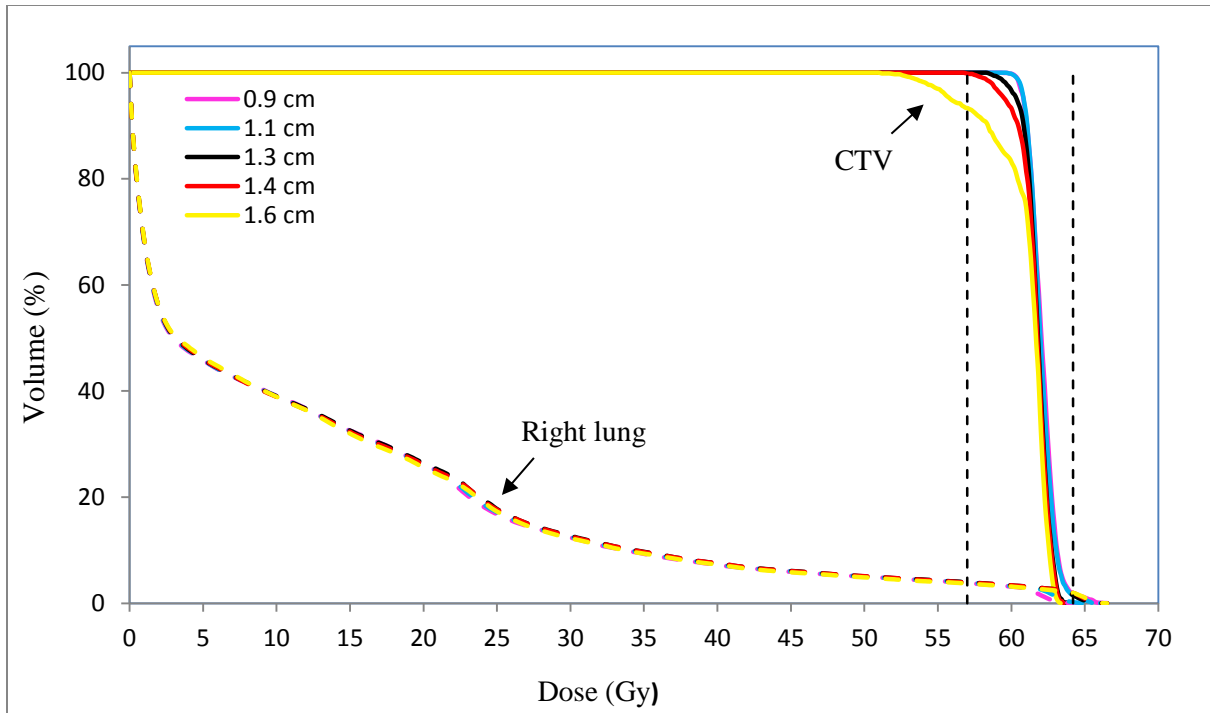
(a)

(b)

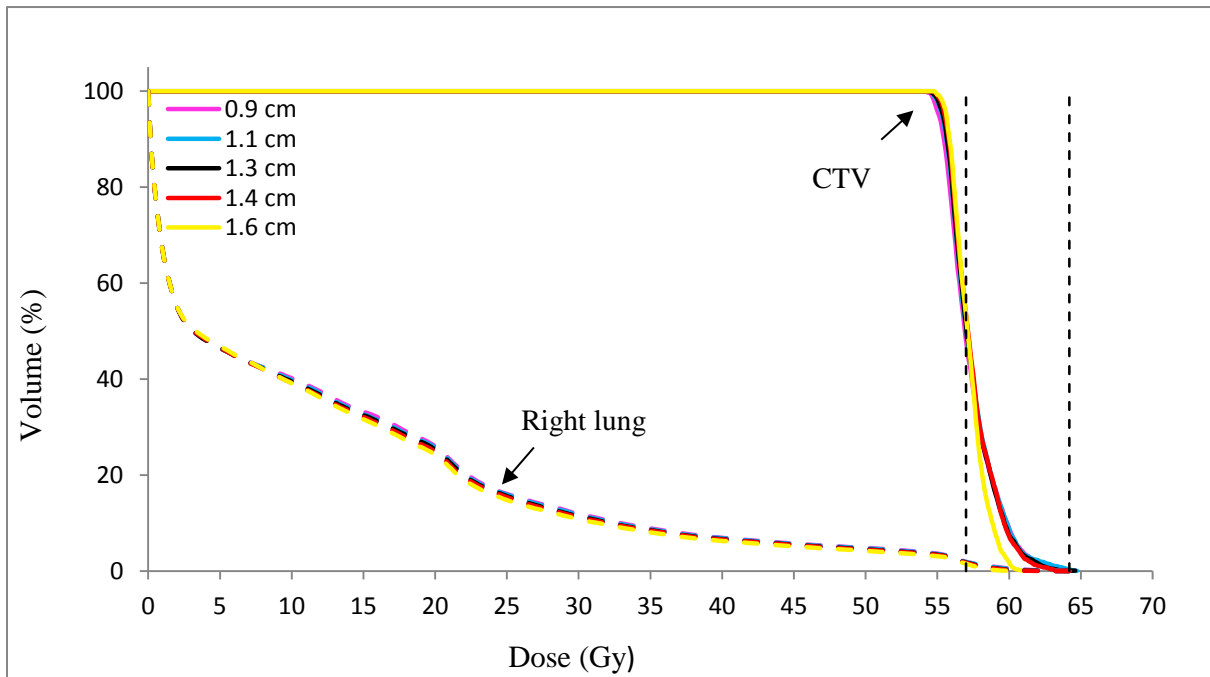
Figure 3.5: Frontal view of the cumulative dose distributions of (a) the nominal 4D plan applied on 1.4 cm amplitude motion, and (b) the nominal 4D plan applied on 1.6 cm amplitude motion. The pink contours show the CTV, and the dashed yellow lines represent the 95% isodose (the volume covered by 95% of the prescribed dose).

3.2.4 Worst case plans

Figure 2.11 indicates that the motion pdf outliers are the 0.9 cm amplitude and the 1.6 cm amplitude. Two 4D plans were optimized in KonRad: one on the 0.9 cm amplitude and one on the 1.6 cm amplitude. The intensity maps were combined using the average intensity method (Equation 2.7) and the maximum intensity method (Equation 2.8). The combined beam weights were then applied to the other motion amplitude scenarios. Figures 3.6a and 3.6b show the DVHs of the worst case plans applied to other motion amplitude scenarios.



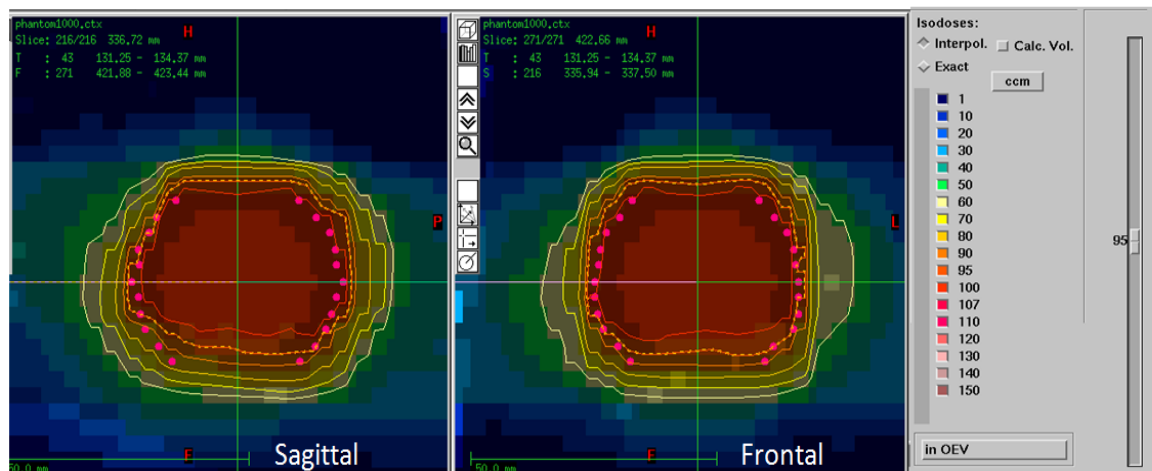
(a)



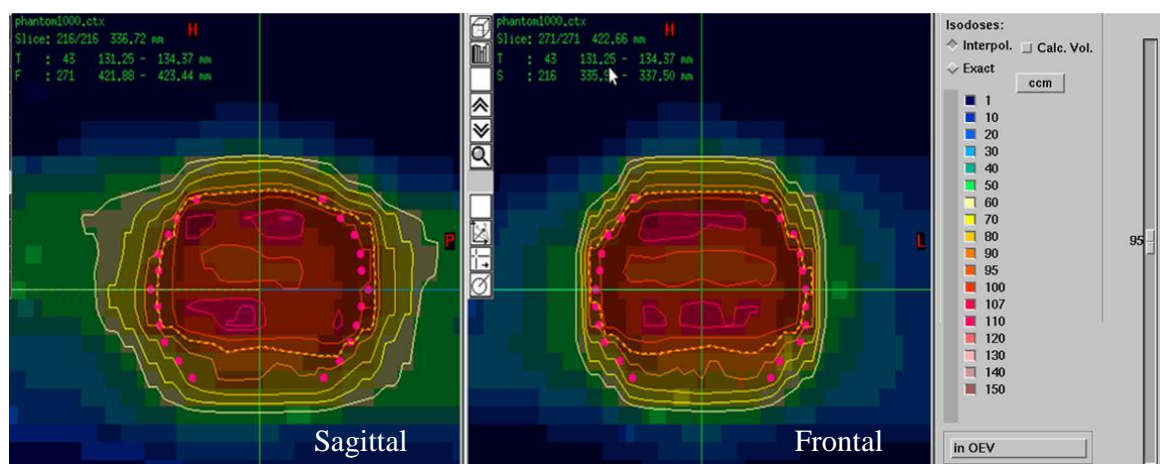
(b)

Figure 3.6: a) Dose volume histograms of the worst case planning using the average intensity method applied on the amplitude variation scenarios and (b) the worst case planning using the maximum intensity method applied on the amplitude variation scenarios

Figure 3.6a shows that the worst case plan obtained using the average intensity method was not robust for any of the motion amplitude scenarios. For example, when the plan was applied to the 1.6 cm motion amplitude, the ICRU minimum dose criteria were not met. The CTV minimum dose was 50.9 Gy. Figure 3.6b shows that the worst case using the maximum intensity method was not robust to any of the motion amplitude scenarios. The minimum dose to the CTV was 54.0 Gy, 54.4 Gy, 54.3 Gy, 54.6 Gy, and 54.7 Gy for the 0.9 cm, 1.1 cm, 1.3 cm, 1.4 cm, and 1.6 cm amplitudes, respectively. The maximum dose to the CTV was 66.5 Gy, 65.5 Gy, 63.6 Gy, 63.9 Gy, and 63.5 Gy for 0.9 cm, 1.1 cm, 1.3 cm, 1.4 cm, and 1.6 cm respectively. Figures 3.7a and 3.7b show the dose distribution of the worst case planning using the average and the maximum intensity, respectively, applied to 1.6 cm amplitude case. From Figure 3.7, it can be noted that the inferior of the CTV is under-dosed. It can also be noted from this figure that the dose distribution in Figure 3.7a (Average intensity method) is more uniform than the dose distribution in Figure 3.7b (Maximum intensity method).



(a)



(b)

Figure 3.7: Sagittal and frontal views of the cumulative dose distribution for worst case method plan applied to 1.6 cm amplitude case. The pink contours show the CTV, and the dashed yellow lines represent the 95% isodose. The inferior region of the tumor is under-dosed because it is not contained within the 95% isodose. (a) using the average intensity worst case planning method (b) using the maximum intensity worst case planning method

3.2.5 Comparison of dose statistics for different plans

Figures 3.8-3.10 summarize the dose statistics of all the planning approaches on the amplitude variation scenarios. It can be noted that when the nominal plan is applied to other motion amplitude variation scenarios, the CTV was under-dosed and the minimum dose criteria were not met. The nominal plan was not robust to any of the amplitude motion scenarios. The ITV plan was robust up to the nominal motion (1.3 cm). Worst case planning using the average intensity method was robust to 1.3 and 1.4 cm motion amplitudes. Worst case planning using the maximum intensity method was not robust to any of the amplitude variation cases as the average minimum dose to the CTV was 54.5 Gy.

Figure 3.9 shows the dose delivered to 99% of the CTV volume when the four planning methods were applied to different amplitude variation scenarios. It is noted that the ITV plan and the worst case plan using the maximum intensity method did not meet the D99 tight criteria when applied to any amplitude variation scenario. The nominal plan and the worst case plan using the average intensity method met the tight criteria for motion amplitudes up to 1.3 cm. From Figure 3.10, it can be noted that the V20 for the right lung was below 30% for all planning approaches for all amplitude variations scenarios, except for the ITV plan when applied to 0.9 cm motion amplitude.

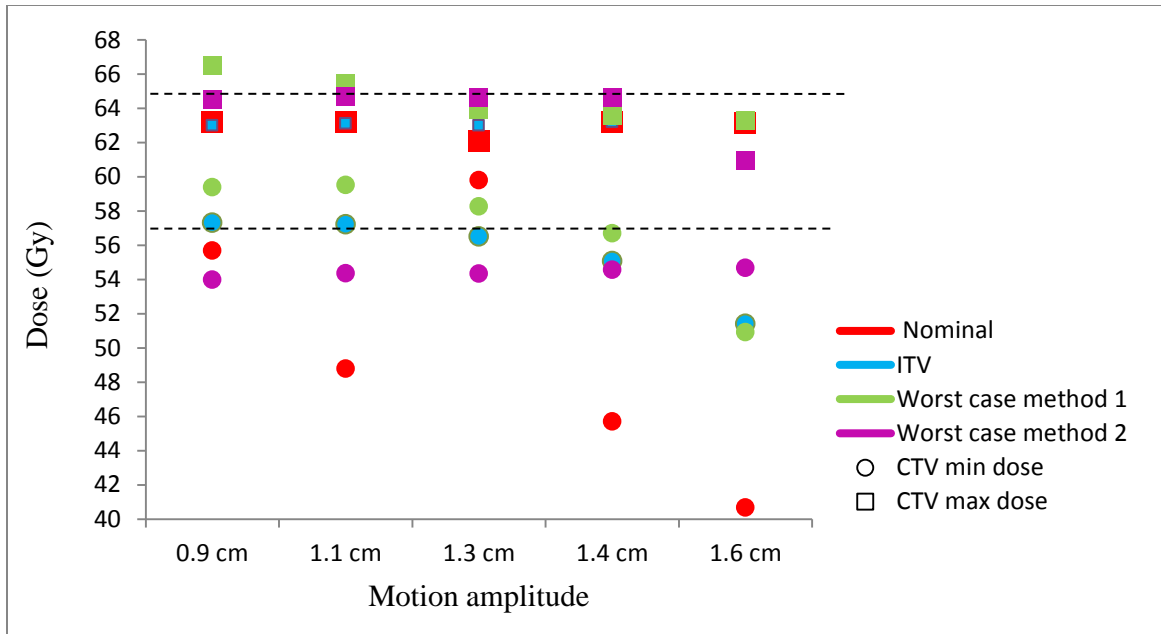


Figure 3.8: Minimum and maximum CTV doses of different planning approaches on amplitude variation study. The dashed lines represent the minimum and maximum doses defined by the ICRU criteria (57 Gy and 64.2 Gy respectively). Method 1 is the average intensity method, and Method 2 is the maximum intensity method

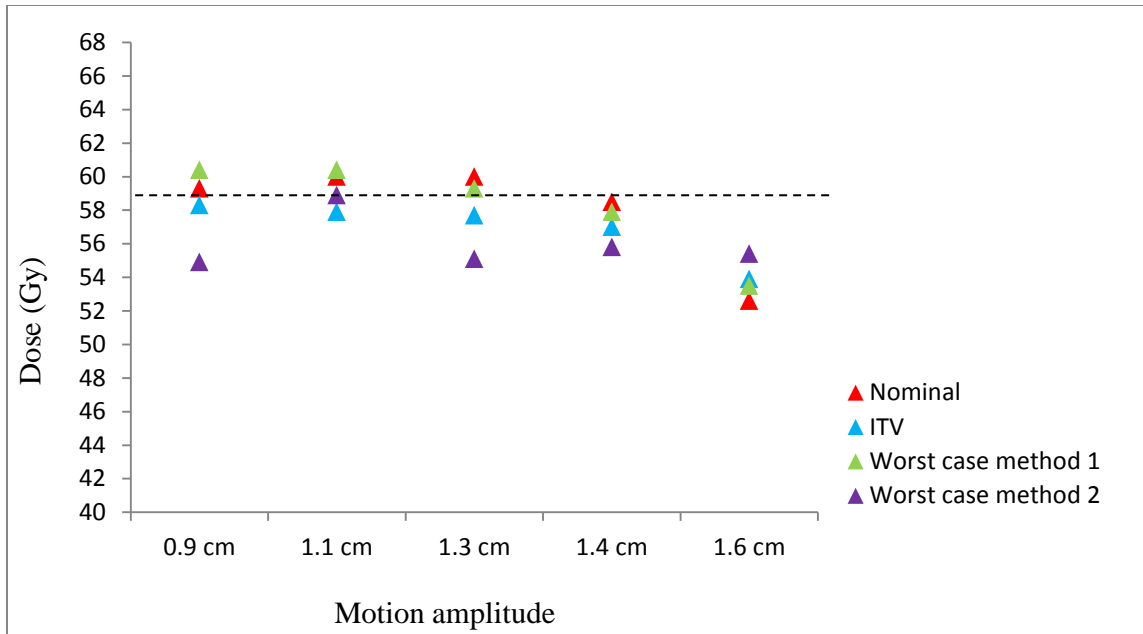


Figure 3.9: D99 of different planning approaches on amplitude variation study. The dashed lines represent the minimum D99 defined by lung cancer radiation therapy protocols in PMH (59.4 Gy). Method 1 is the average intensity method, and Method 2 is the maximum intensity method

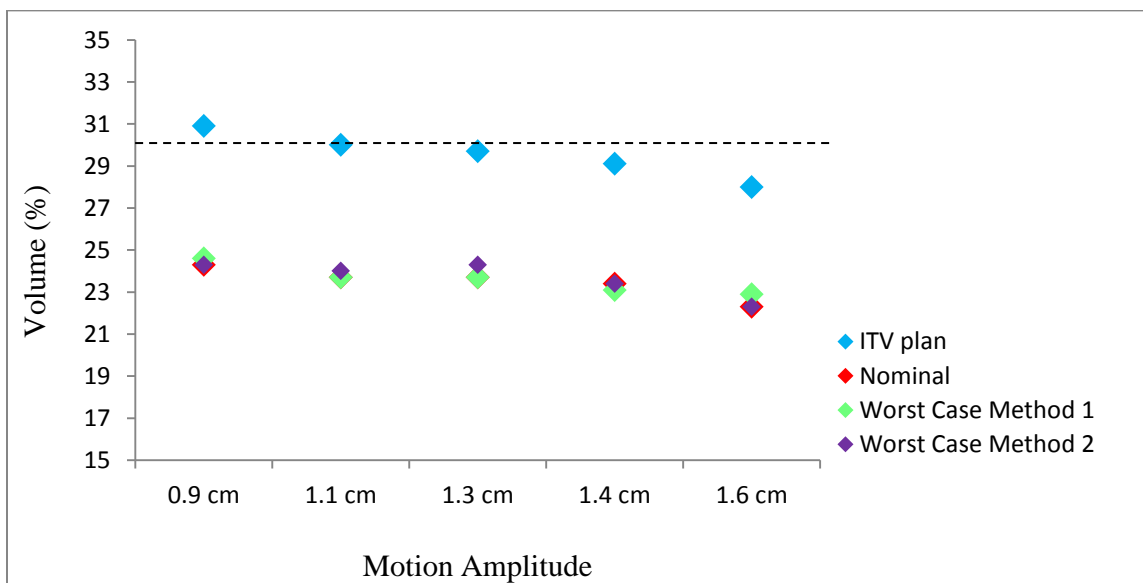


Figure 3.10: V20 of different planning approaches on amplitude variation study. The dashed lines represent the minimum V20 defined by lung cancer radiation therapy protocols in PMH (30%). Method 1 is the average intensity method, and Method 2 is the maximum intensity method

3.3 Study 2: Patient motion variations applied to XCAT phantom images

The nominal 4D plan, ITV plan and the two worst case plans were tested for robustness on motion variations extracted from a respiratory trace measured on a healthy volunteer who was instructed to breathe irregularly (Figure 2.13). The trace was divided into 6 30s segments and accumulated dose for each plan was calculated for each 30s segment. Table 3.5 shows the weight given to each breathing phase at each 30s interval as well as the coefficient of variance of the phase weights across the 6 pdfs. The average coefficient of variance is 0.916. The robustness of the different plans was also tested on the full 180s trace.

Table 3.5: 4DCT phase weightings for each 30 second interval of the patient trace as well as the average, standard deviation, and the coefficient of variance of phase weightings.

phase	0s-30s	30s-60s	60s-90s	90s-120s	120s-150s	150s-180s	Average	Standard deviation	Coefficient of variance
p0	0.05	0.00	0.00	0.00	0.00	0.00	0.01	0.02	2.45
p1	0.13	0.05	0.01	0.01	0.00	0.03	0.04	0.05	1.28
p2	0.19	0.09	0.02	0.04	0.04	0.12	0.08	0.06	0.77
p3	0.15	0.14	0.06	0.10	0.08	0.18	0.12	0.05	0.39
p4	0.18	0.19	0.13	0.17	0.19	0.16	0.17	0.02	0.14
p5	0.27	0.24	0.15	0.16	0.18	0.18	0.20	0.05	0.26
p6	0.03	0.20	0.11	0.15	0.22	0.17	0.15	0.07	0.48
p7	0.00	0.08	0.16	0.20	0.18	0.09	0.12	0.08	0.65
p8	0.00	0.00	0.18	0.15	0.09	0.05	0.08	0.08	0.95
p9	0.00	0.00	0.19	0.03	0.01	0.01	0.04	0.07	1.79

3.3.1 ITV plan

The ITV in Study 2 was created by fusing the GTVs of phases 0-9, and adding 5 mm. The ITV plan was applied to the motion variation scenarios extracted from the healthy volunteer's respiratory trace. Figure 3.11 shows the DVHs of the ITV plan applied to the 30s segments. From Figure 3.11 it can be seen that, with the exception of the 60-90s segment, the CTV was covered by the ITV plan. For the 60-90s segment the minimum dose was 47.8 Gy. Figure 3.12 shows the cumulative dose distribution of the ITV plan on the 60s-90s segment. From this figure, it is noted that the inferior portion of the tumour is not covered by the 95% isodose. Figure 3.13 shows the dose distribution of the ITV plan applied on phase 8; this figure shows that there is cold spot contained within the CTV contours of phase 8.

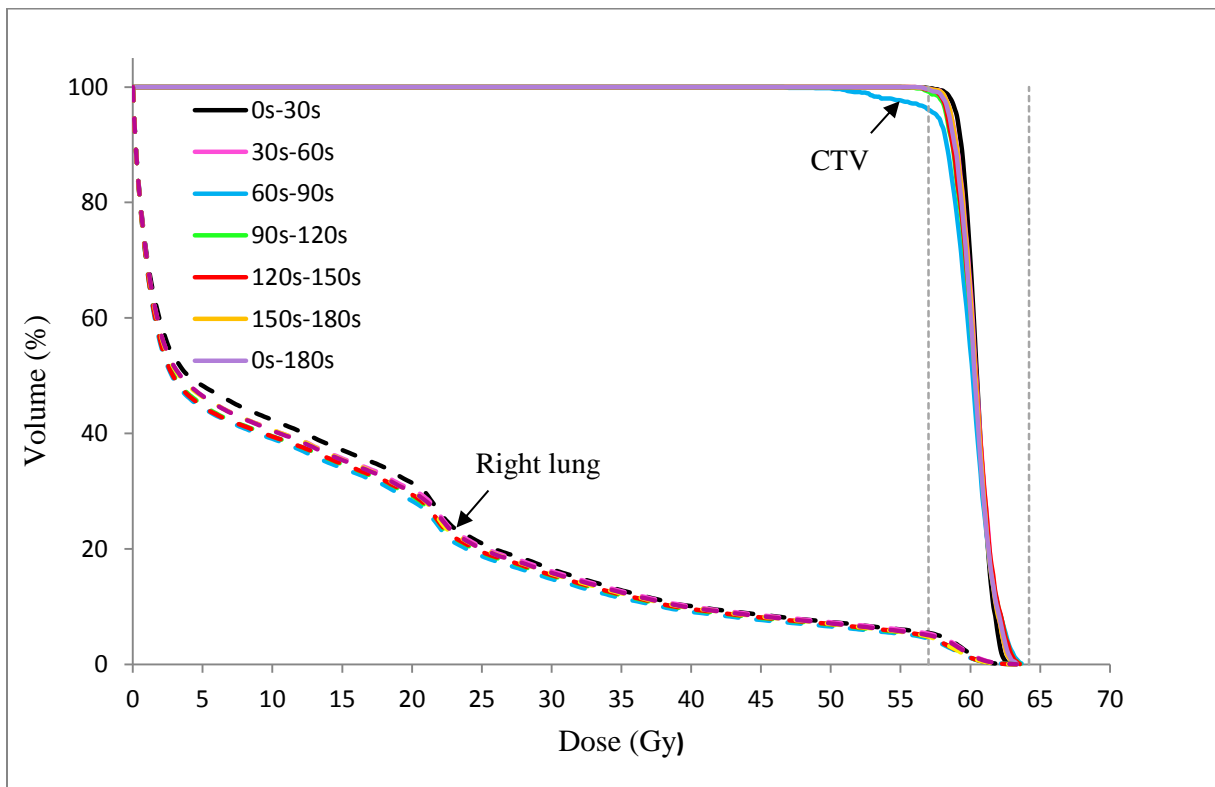


Figure 3.11: Dose volume histograms for the ITV plan applied to other motion variation scenarios showing dose coverage to both the CTV and the right lung.

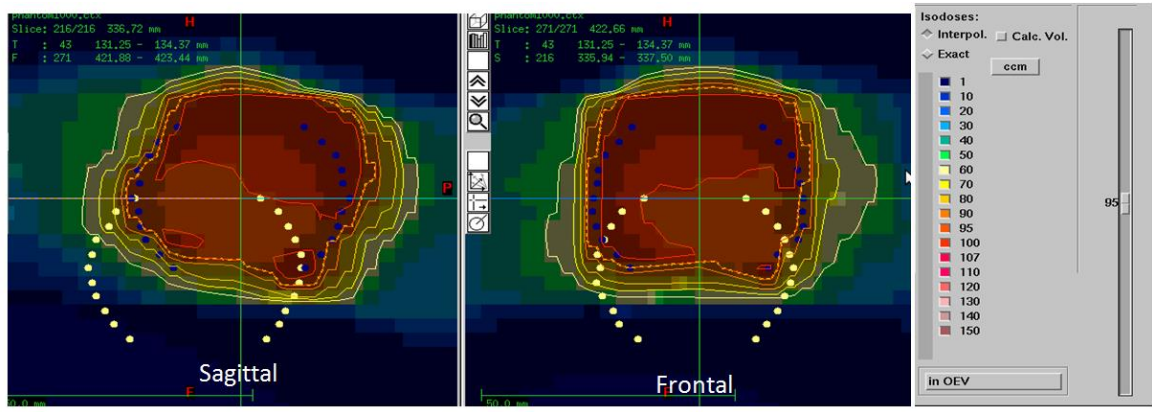


Figure 3.12: Cumulative dose distribution of the ITV plan on the 60s-90s segment. The blue dots represent the CTV contours at exhale, and the yellow dots represent the CTV contours at inhale. The dashed yellow lines represent the 95% isodose (the volume covered by 95% of the prescribed dose).

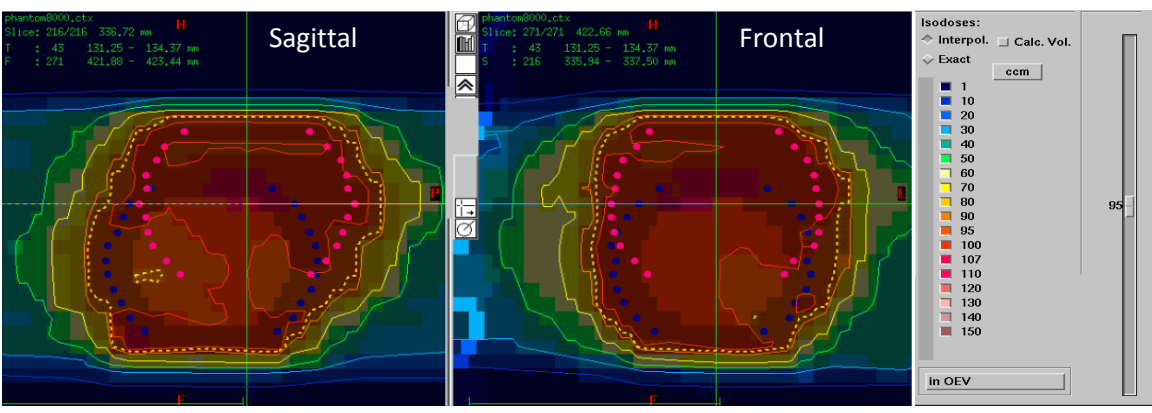


Figure 3.13: Dose distribution of the ITV plan applied on phase 8. The pink dots represent the CTV contours at exhale, and the blue contours represent the CTV at phase 8. The dashed yellow lines represent the 95% isodose (the volume covered by 95% of the prescribed dose).

3.3.2 Nominal 4D plan

A nominal 4D plan was optimized in KonRad on the 0s-30s segment of the motion trace. The optimized plan met both the ICRU criteria and the tight plan criteria. The CTV minimum dose was 59.8 Gy, the maximum dose was 62.1Gy and the D99 was 60.0 Gy. All organs at risk received lower doses than the maximum allowed by the ICRU criteria. 4DDIJs for the 30s segments were created based on the pdfs shown in Figure 2.13. The beam weights from the optimized 0s-30s nominal 4D

plan were then applied to the 4DDIJs of the 6 other segments. Figure 3.14 shows the DVHs of the nominal 4D plan when applied to the 6 30s motion segments as well as the full 180s trace.

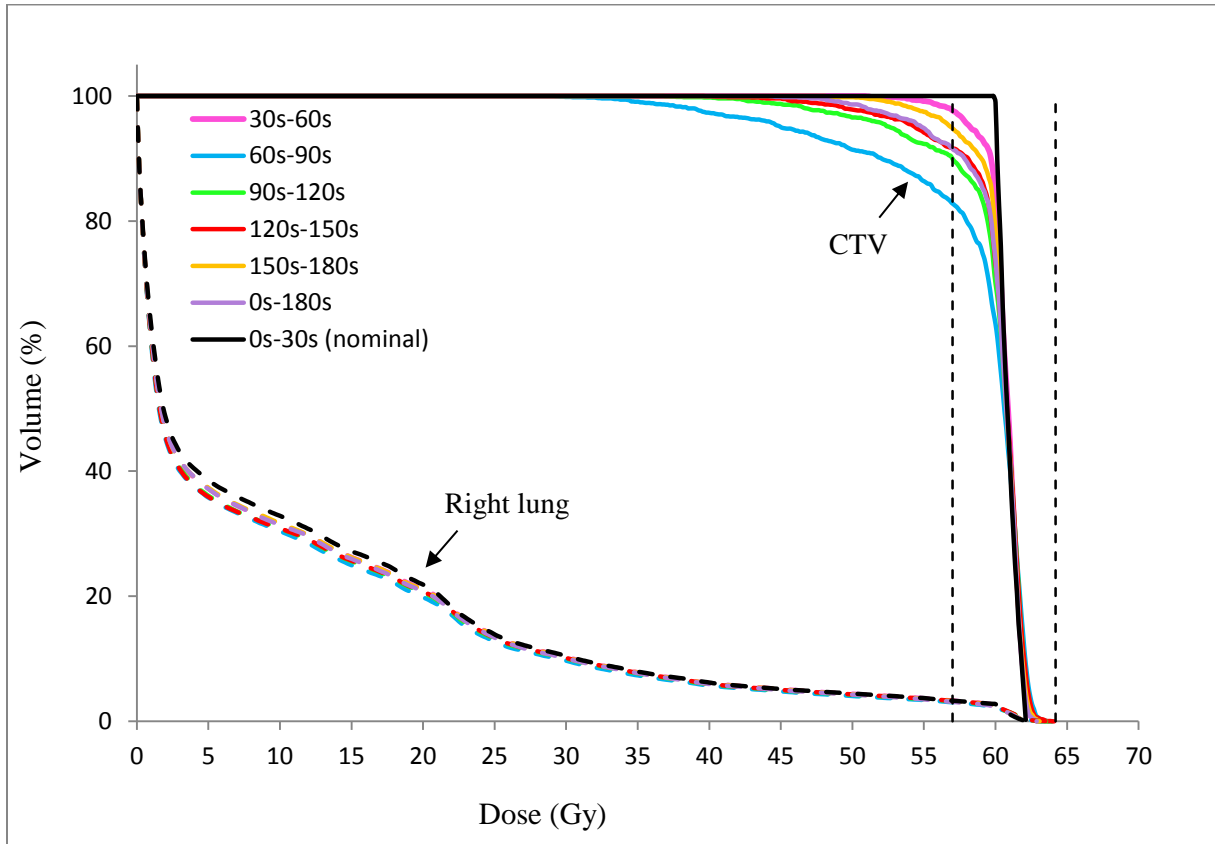


Figure 3.14: Dose volume histograms of the nominal 4D plan applied to 30s segments of the healthy volunteer respiratory trace. Dose coverage of both the CTV and the right lung are shown.

As seen in Figure 3.14, the two cases that yielded the worst CTV coverage are the 60s-90s and the 90s-120s segments. Figures 3.15 and 3.16 show the cumulative dose distribution of the nominal 4D plan applied on the 60s-90s and the 90s-120s segments, respectively. It can be noted that the inferior region of the tumor is under-dosed. When looking at Figure 2.13, it can be noted that during the 60s-90s segment, the tumor spends the least amount of time at inhale (phase 5) when compared other segments.

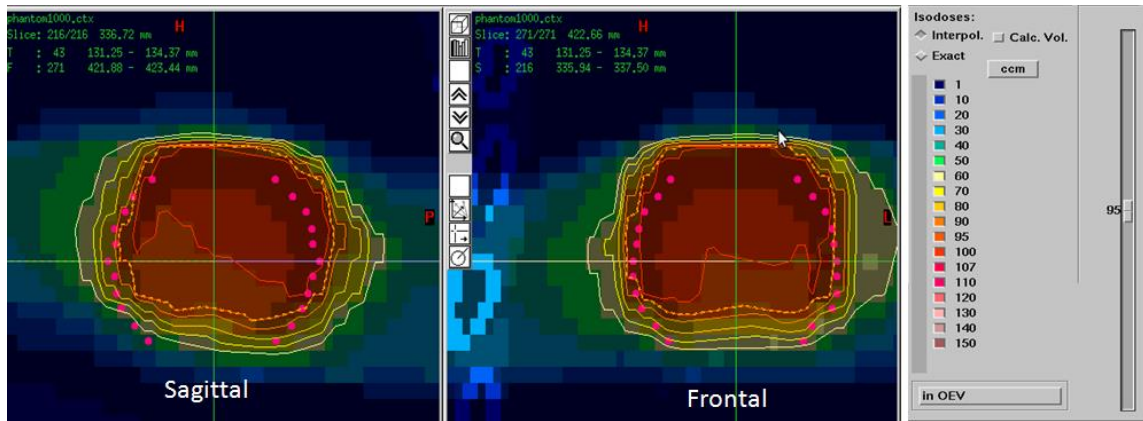


Figure 3.15: Cumulative dose distributions of nominal 4D plan applied on the 60s-90s segment. The pink contours show the CTV and the dashed yellow lines represent the 95% isodose (the volume covered by 95% of the prescribed dose)

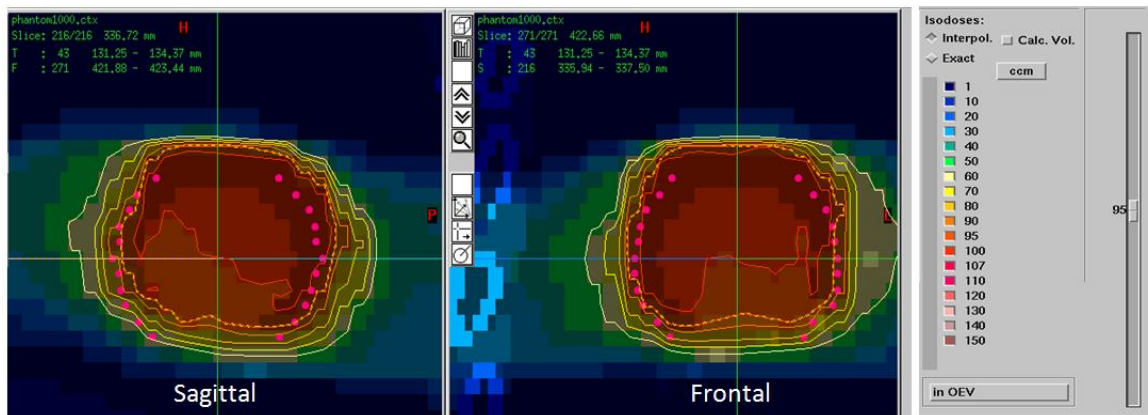
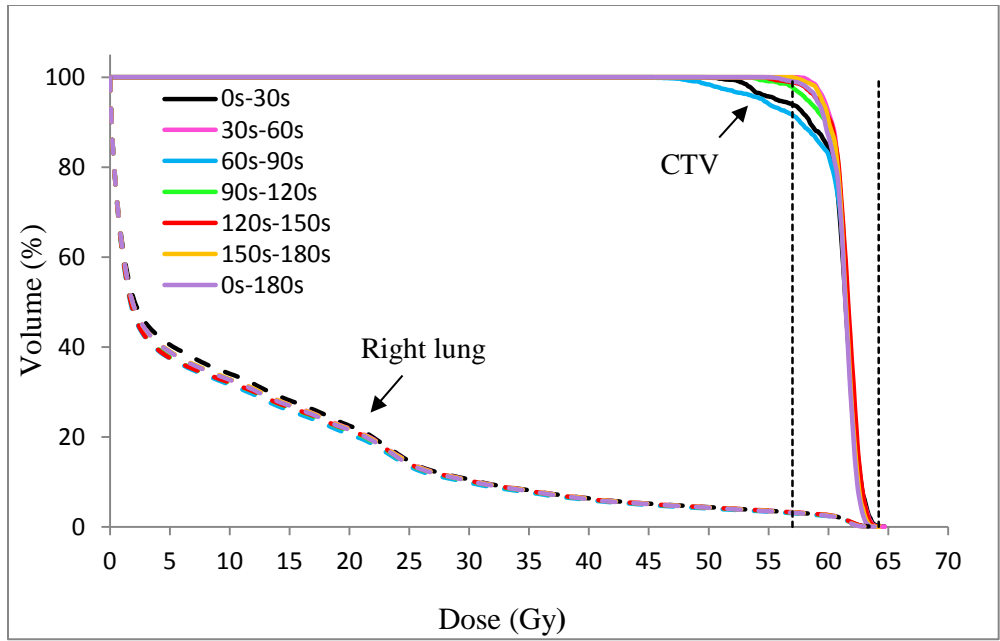


Figure 3.16: Cumulative dose distributions of nominal 4D plan applied on the 90s-120s segment. The pink contours show the CTV and the dashed yellow lines represent the 95% isodose (the volume covered by 95% of the prescribed dose)

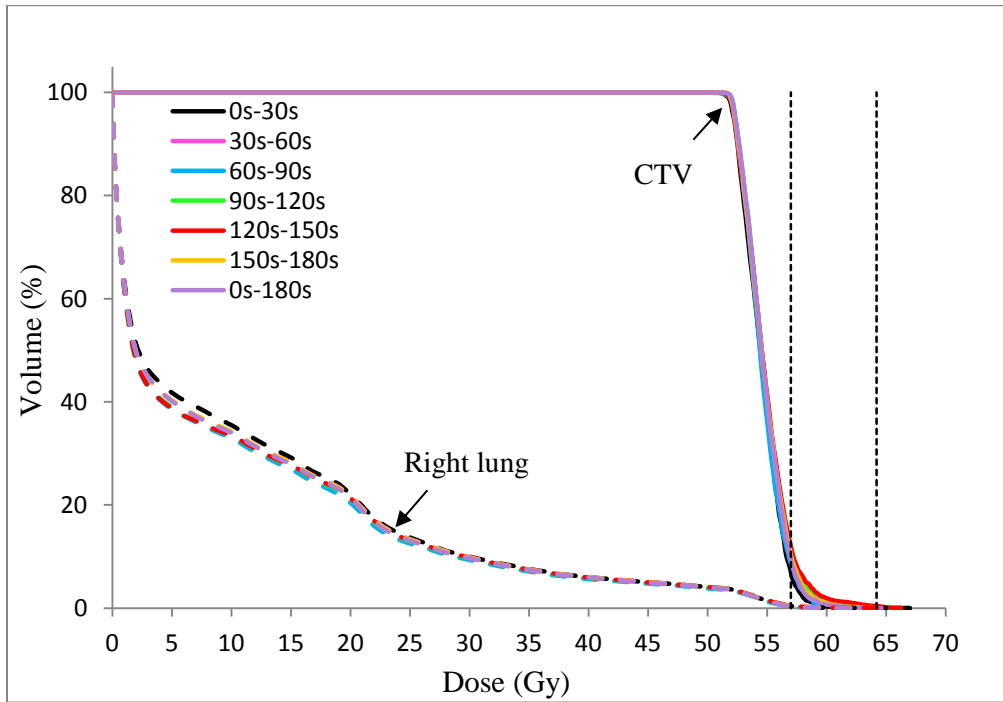
3.3.3 Worst case plan

Two 4D plans were optimized: One on the 0s-30s motion, and one on the 60s-90s motion. The choice of the worst cases was based on the motion pdf outliers in Figure 2.13. Figure 3.17a and 3.17b show the DVHs of the worst case plans using the average intensity method and maximum intensity methods, respectively, applied to each of the 30s motion segments. Figures 3.17a and 3.17b show that both methods of worst case planning were not robust to the motion variations that occurred in the healthy volunteer's respiratory trace. However, there are still differences in the robustness between

the two methods. The average intensity method under-dosed the CTV especially when applied to 0s-30s and 60s-90s segments. The minimum dose to the CTV when using the average intensity worst case planning method applied to those segments was 49.7 Gy, and 45.3 Gy respectively. The average maximum and maximum dose when the average intensity method was applied to all motion variation scenarios was 53.2 Gy and 64.17 respectively. The maximum intensity method was not robust to any of the motion variations. The CTV is under-dosed and over-dosed when the maximum intensity method was applied to all motion variations scenarios. There is also a difference in the dose distribution when using the average intensity method versus when using the maximum intensity method, Figure 3.18 shows the dose distributions of the worst case planning using the average intensity method and the maximum intensity method when applied to the 120-150s segment. Figure 3.18b shows that there is a hot-spot in the inferior region of the CTV.

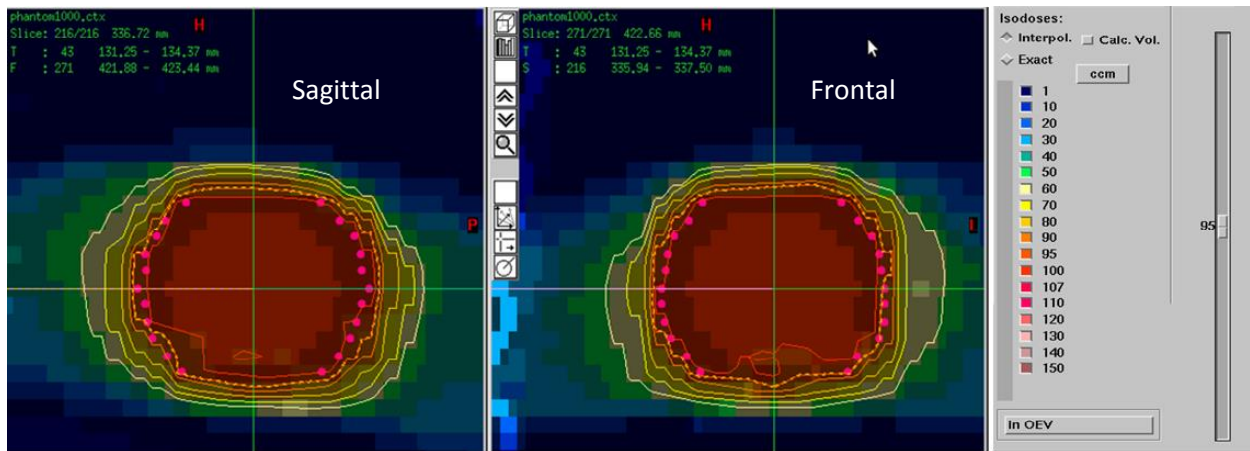


(a)

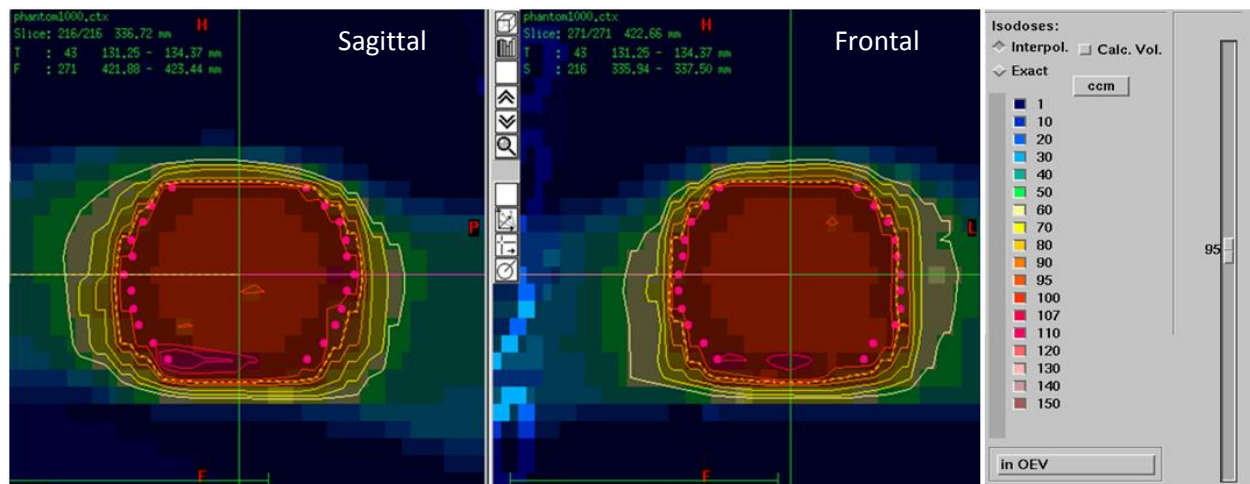


(b)

Figure 3.17: Dose volume histograms of (a) worst case planning using the average intensity method and (b) worst case planning using the maximum intensity method applied on 30s motion segment



(a)



(b)

Figure 3.18: Cumulative dose distributions of worst case plans using (a) using the average intensity method and (b) using the maximum intensity method applied on the 120s-150s segment. The pink contours show the CTV and the dashed yellow lines represent the 95% isodose (the volume covered by 95% of the prescribed dose)

3.3.4 Comparison of dose statistics for different plans

Figures 3.19-3.21 summarize the dose statistics of all the planning approaches when applied to the motion variation scenarios extracted from the healthy volunteer trace. It can be noted that when the nominal plan was applied to other motion variation scenarios, the CTV was under-dosed as the minimum dose criteria was not met. The ITV plan was robust to the 0s-30s (the nominal motion) segment and the 30s-60s segment. The average intensity method of the worst case approach was not robust to any of the motion variation cases. The CTV was under-dosed, as the average minimum dose to the CTV was 53.2 Gy. The maximum intensity method of the worst case approach was not robust to any of the motion variation cases. The CTV was under-dosed in all motion variation cases as the average minimum dose to the CTV was 51.0 Gy.

Figure 3.20 shows the dose delivered to 99% of the CTV when the four planning methods were applied to different amplitude variation scenarios. It is noted that none of the planning methods met the D99 criteria when applied to any motion variation scenario. Figure 3.21 shows the statistics of the volume of the right lung that receives 20 Gy or more. It is noted from this figure that the ITV plan delivers more dose to the CTV bearing lung than other planning approaches. The dashed lines in Figure 3.21 represents the maximum (maximum allowed by PMH lung treatment protocol) volume of lung to be irradiated by 20 Gy or more (30%). As seen in this figure, when the ITV plan is applied to the nominal motion (0s-30s), the V20 lung exceeds 30%.

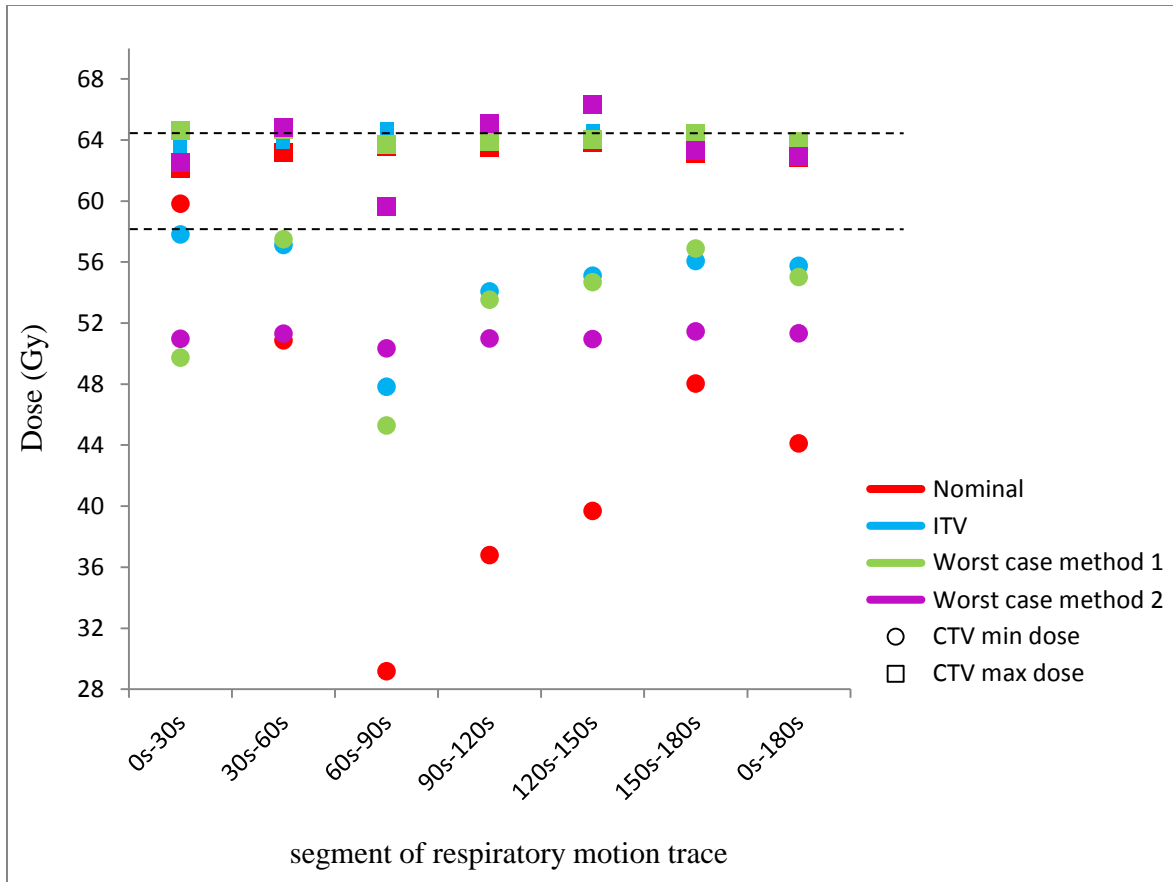


Figure 3.19: Minimum and maximum doses of different planning approaches on motion variation scenarios. The dashed lines represent the minimum and maximum doses defined by ICRU criteria (57 Gy and 64.2 Gy respectively). Method 1 is the average intensity method, and Method 2 is the maximum intensity method

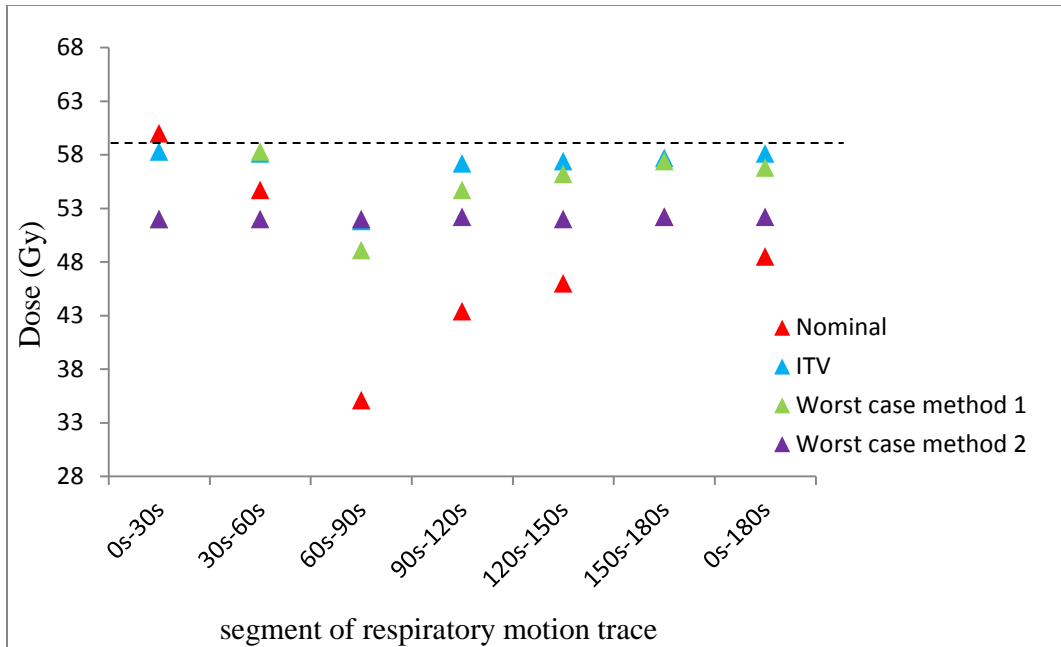


Figure 3.20: D99 of different planning approaches on motion variation scenarios. The dashed lines represent the minimum D99 criteria (59.4 Gy). Method 1 is the average intensity method, and Method 2 is the maximum intensity method

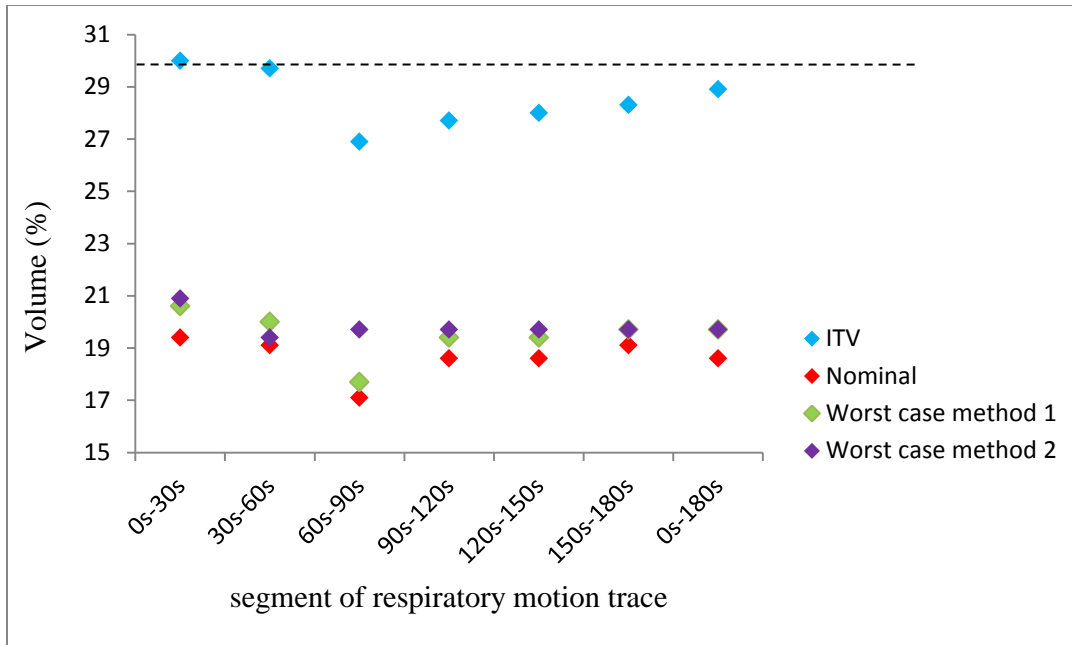


Figure 3.21: V20 of different planning approaches on amplitude variation study. The dashed lines represent the minimum V20 defined by lung cancer radiation therapy protocols in PMH (30%). Method 1 is the average intensity method, and Method 2 is the maximum intensity method

3.4 Study 3: Patient motion variation study

The nominal 4D plan, ITV plan, and the two worst case plans were tested for robustness on motion variations extracted from a respiratory trace measured on a NSCLC patient. The trace was divided into 5 20s segments and accumulated dose for each plan was calculated for each 20s segment. Table 3.6 shows the weight given to each breathing phase at each 20s interval as well as the coefficient of variance of the phase weights. The average coefficient of variance is 0.44. The robustness of the different plans was also tested on the full 180s trace.

Table 3.6: The fraction of time each breathing phase spends in each 20 second interval. The average, standard deviation, and the coefficient of variance are also shown.

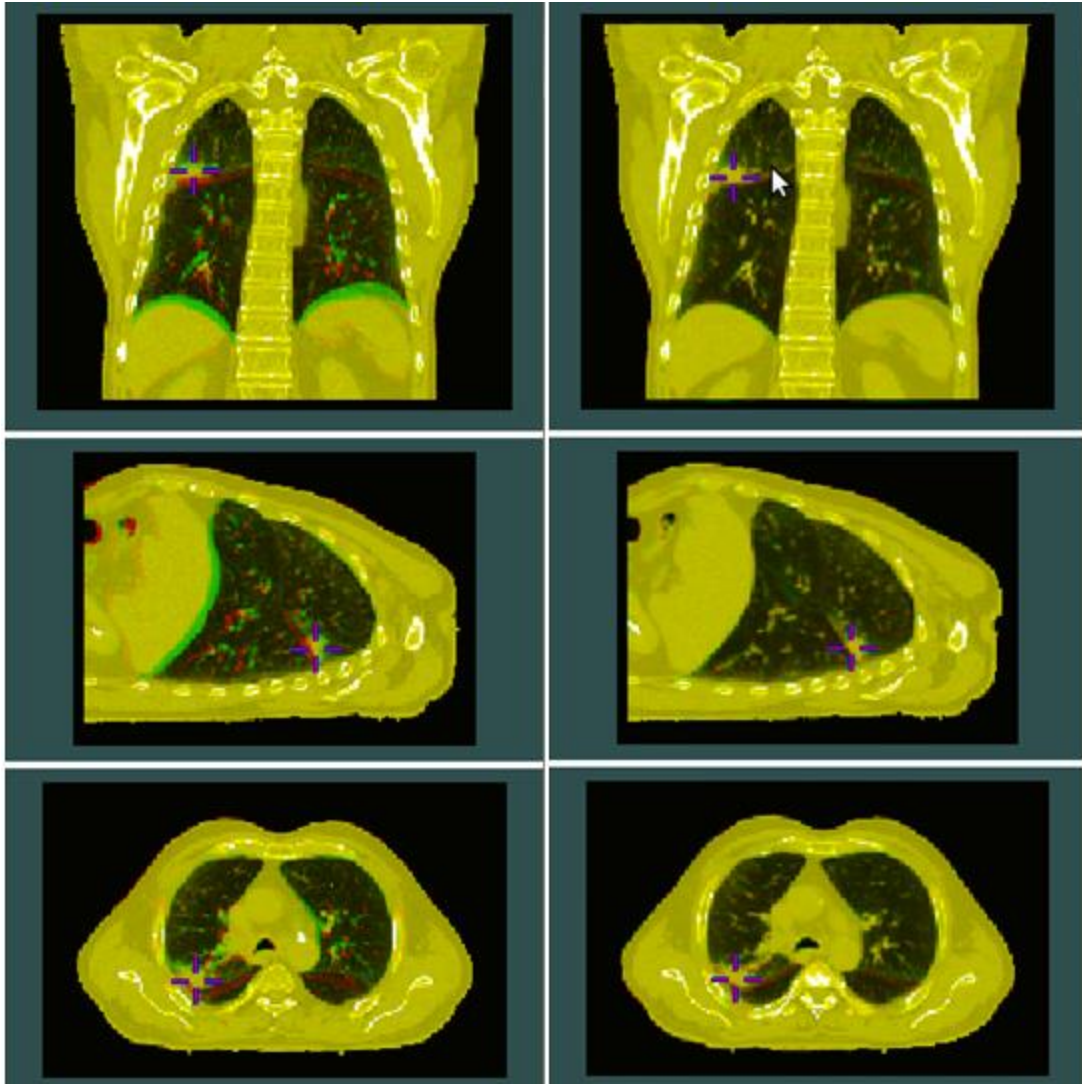
phase	0s-20s	20s-40s	40s-60s	60s-80s	80s-100s	Average	Standard deviation	Coefficient of variance
0	0.06	0.02	0.00	0.03	0.00	0.02	0.03	1.21
1	0.13	0.05	0.04	0.06	0.01	0.06	0.05	0.80
2	0.16	0.15	0.15	0.15	0.11	0.14	0.02	0.13
3	0.25	0.29	0.29	0.30	0.26	0.28	0.02	0.08
4	0.08	0.05	0.03	0.05	0.01	0.05	0.03	0.55
5	0.08	0.08	0.05	0.07	0.03	0.06	0.02	0.33
6	0.08	0.09	0.09	0.06	0.11	0.09	0.02	0.18
7	0.09	0.09	0.11	0.07	0.09	0.09	0.02	0.17
8	0.06	0.10	0.08	0.08	0.09	0.08	0.01	0.18
9	0.00	0.09	0.15	0.12	0.29	0.13	0.10	0.81

3.4.1 Image registration parameters and assessment

Table 3.7 shows the parameters used from the image registration of the CT images of the 9 breathing phases (phases 1 - 9) to the exhale phase (phase 0). The quality of image registration was visually assessed by overlaying the registered image on the target image. Figure 3.22 shows the overlap of the target image on the reference image before image registration and the overlap of the target image on the registered image after registration.

Table 3.7: The optimal parameters used for registration of patient 4DCT images using the ANIMAL software

Target image	Step size (mm)	Lattice diameter (mm)	iterations	Stiffness	Weight	Sub lattice diameter
Phase 0	7.8125	40	30	0.1	0.3	9
Phase 1	7.8125	40	30	0.1	0.3	9
Phase 2	7.8125	30	30	0.2	0.3	9
Phase 3	7.8125	30	30	0.2	0.3	9
Phase 4	7.8125	30	30	0.2	0.3	9
Phase 5	7.8125	30	30	0.2	0.3	9
Phase 7	7.8125	30	30	0.2	0.3	9
Phase 8	7.8125	30	30	0.2	0.3	9
Phase 9	7.8125	30	30	0.2	0.3	9



(a)

(b)

Figure 3.22: (a) Overlap of the patient target image on the patient reference image before image registration. (b) Overlap of the patient target image on the patient registered image after registration

3.4.2 ITV plan

An ITV plan was created based on the ITV contour provided by PMH. The optimized plan met both the ICRU and the tight criteria. The minimum CTV dose was 58.9 Gy, the maximum dose was 62.5 Gy and the D99 was 59.0 Gy. All of the organs at risk received lower doses than the maximum allowed by ICRU criteria. The beam weights from the optimized ITV plan were then applied each of the 20s segments extracted from the patient respiratory motion trace. Figure 3.23 shows the DVHs of the ITV plan when applied to each 20s segment, including the full respiratory motion trace. The ITV plan was not robust to any of the motion variation scenarios as the average minimum dose to the CTV was 53.9 Gy.

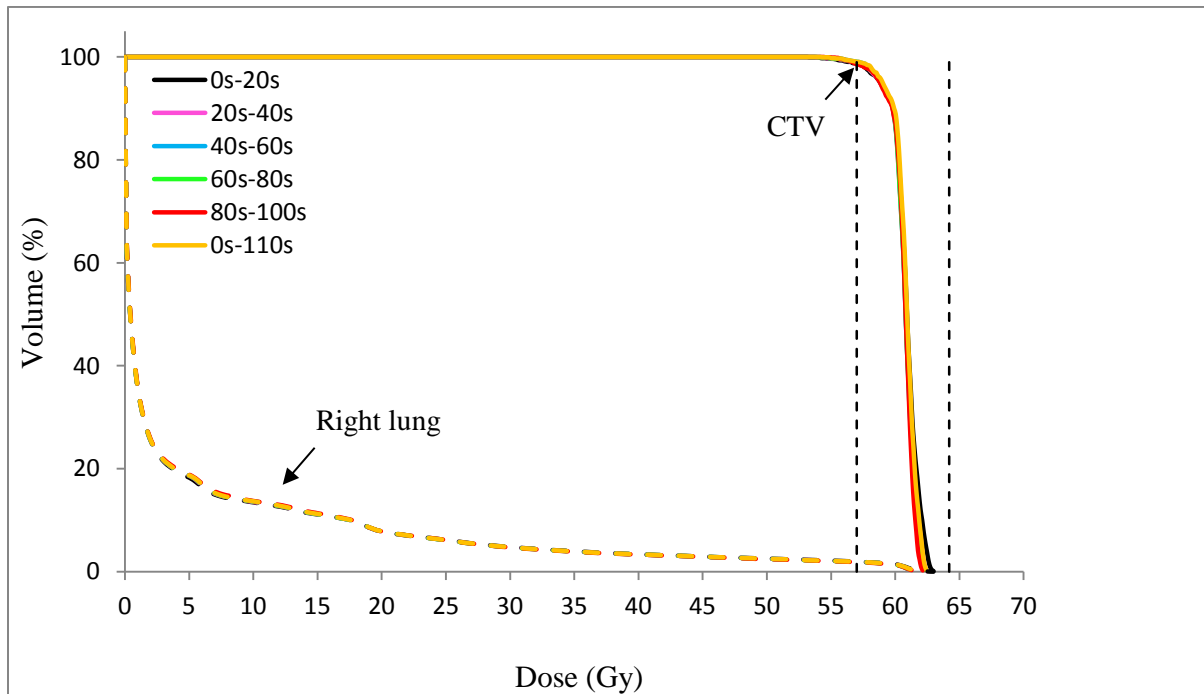


Figure 3.23: Dose volume histograms of the ITV plan applied to the 20s segments of the patient respiratory motion trace showing dose coverage to both the CTV and the right lung.

:

3.4.3 Nominal 4D plan

A nominal 4D plan was optimized in KonRad using the 0s-20s segment of the patient's respiratory motion variation trace. The optimized plan met both ICRU criteria and the tight criteria. The CTV minimum dose was 60.0 Gy, the maximum dose was 61.4 Gy, and the D99 was 60.2 Gy. All of the organs at risk received lower doses than the maximum allowed by ICRU criteria. 4DDIJs for the other 20s motion segments were created based on the pdfs provided in Figure 2.17. The beam weights from the optimized plan were then applied to the 4DDIJs. Figure 3.24 shows the DVHs of the nominal 4D plan when applied to each of the 20s motion segments as well as the full respiratory motion trace (0s-110s).

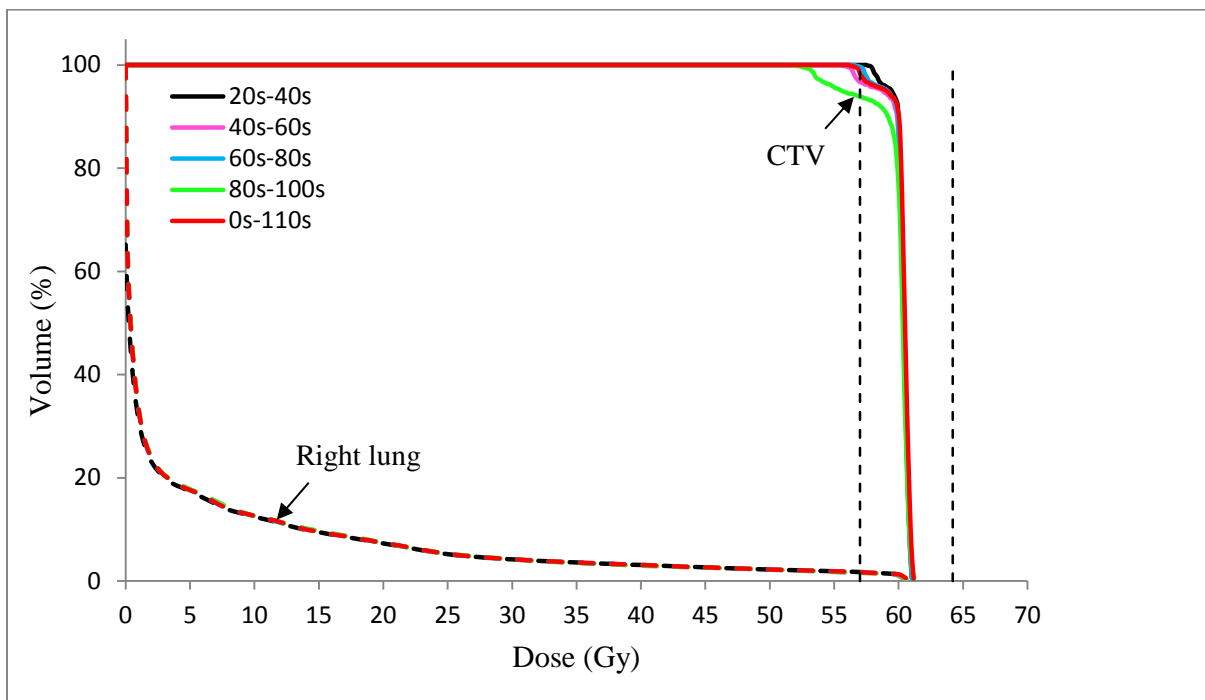
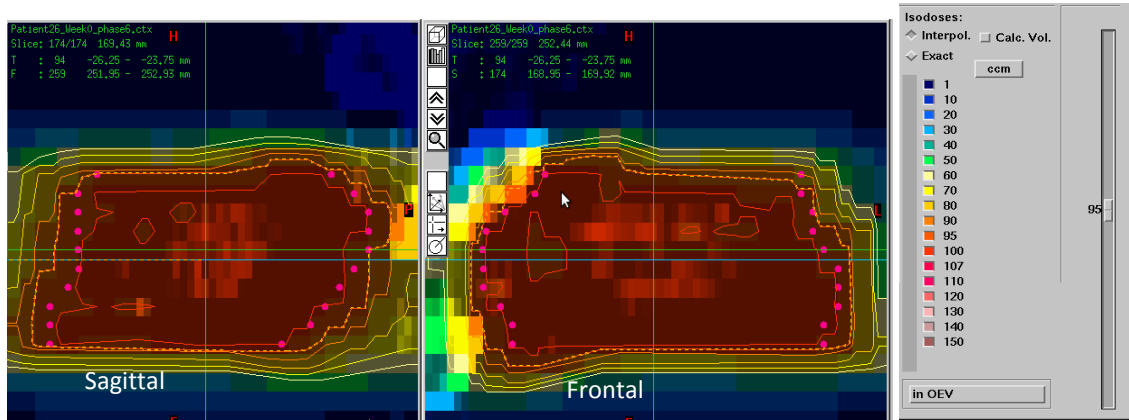
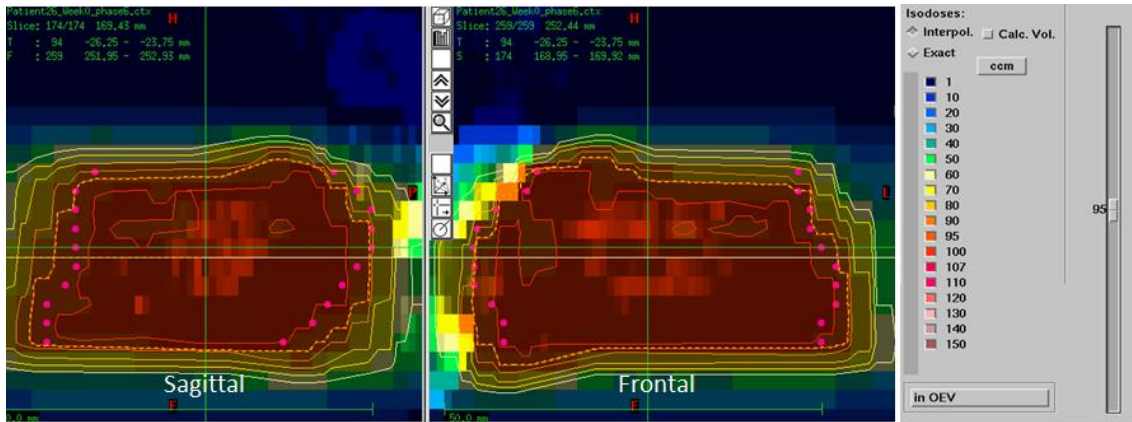


Figure 3.24: Dose volume histograms of the nominal 4D plan applied to 20s segments of the respiratory motion trace. Dose coverage of the CTV and the right lung are shown.

As seen in Figure 3.24, the two cases that yielded the worst dose coverage statistics were the 40s-60s and the 80s-100s segments. Figures 3.25a-3.25b show the cumulative dose distribution of the nominal 4D plan applied to the 40s-60s and the 80s-100s segments, respectively; the superior of the tumor appears under-dosed. When looking at Figure 2.17, in the 40s-60s segment and the 80s-100s segment, the tumor spends the least amount of time at exhale when compared to other segments.



(a)

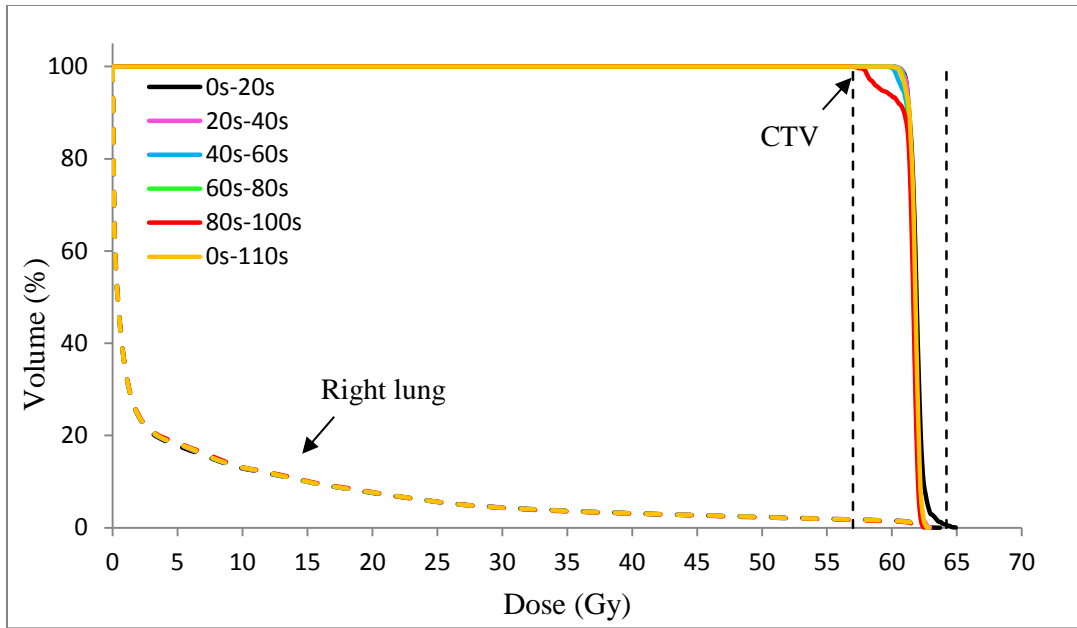


(b)

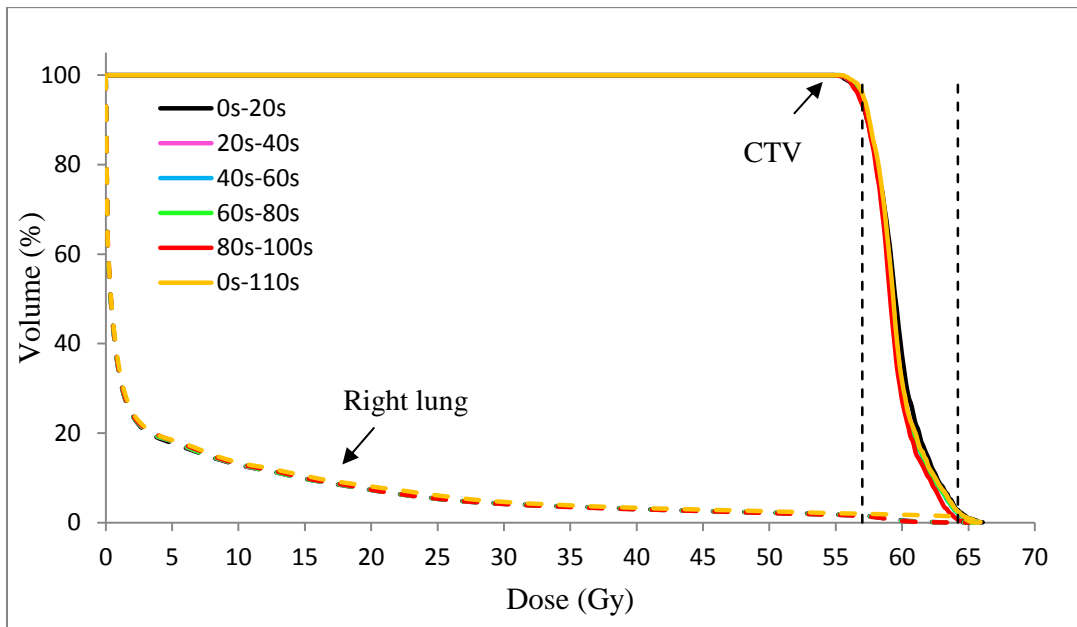
Figure 3.25: Cumulative dose distributions of the nominal 4D plan applied on a) 40s-60s b) 80s-100s segment of the patient respiratory motion trace. The pink dots represent the CTV contours and the dashed yellow lines represent the 95% isodose (the volume covered by 95% of the prescribed dose).

3.4.4 Worst case plans

Figure 2.17 shows that the two most extreme pdfs are the 0s-20s and the 80s-100s (motion outliers). The tumour in the 0s-20segment spends the most amount of time at exhale, and the least amount of time at inhale when compared to other motion pdfs. Conversely, the tumour in the 80s-100s segment spends the least amount of time at exhale, and the most amount of time at inhale. Two 4D plans were optimized in KonRad using the 0s-20s and the 80s-100s pdfs. The beam weights were combined using the average and the maximum intensity methods and then applied to each of the 20s segments as well as the full respiratory motion trace. Figures 3.26a and 3.26b show the DVHs of the worst case plans using the average and the maximum intensity methods, respectively, applied to different motion variations scenarios. There was a difference in the dose distribution between using the average and the maximum intensity methods. For example, Figure 3.27 shows the dose distributions obtained using the average and the maximum intensity methods of the worst case approach when applied to 20s-40s segment. It can be noted from this figure that the maximum intensity method puts more dose on the superior portion of the tumour.

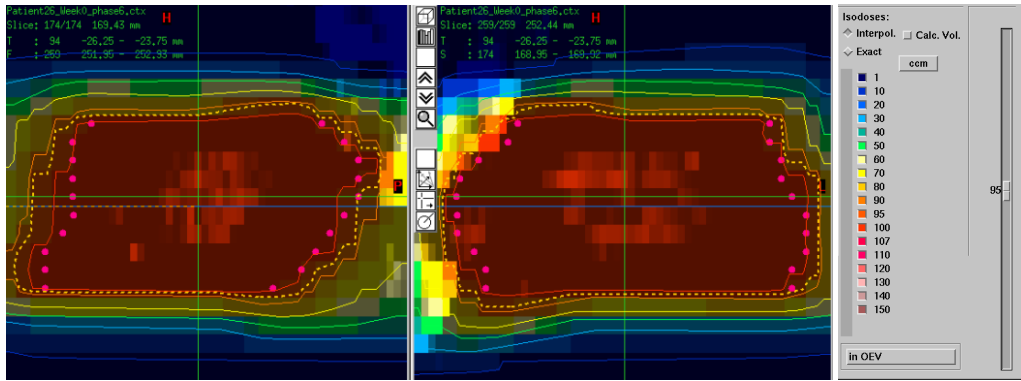


(a)

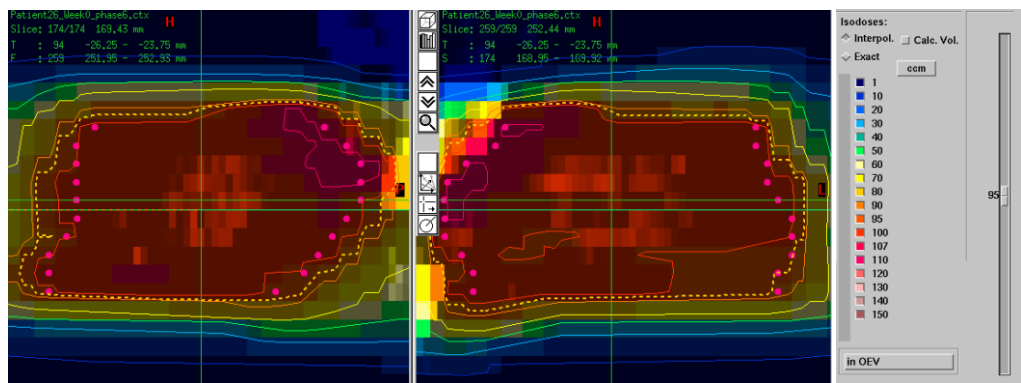


(b)

Figure 3.26: Dose volume histograms of the (a) worst case planning using the average intensity method (b) Worst case planning using the maximum intensity method applied on the patient motion variation scenarios.



(a)



(b)

Figure 3.27: Cumulative dose distributions of the nominal 4D plan applied on the 20s-40s segment of the patient respiratory motion trace. The pink dots represent the CTV contours and the dashed yellow lines represent the 95% isodose (the volume covered by 95% of the prescribed dose) a) using the average intensity method and b) using the maximum intensity method

3.4.4 Comparison of dose statistics for different plans

Figures 3.28-3.30 summarize the dose statistics of all the planning approaches on patient motion variation scenarios using patient image data. It can be noted that when the nominal plan was applied to other patient motion variation scenarios, the CTV was under-dosed as the minimum dose criteria was only met for the nominal (0s-20s) segment. The ITV plan was also not robust to any of the 20s segments as the CTV minimum dose criteria was also not met. Worst case planning using the average intensity method was robust to all of the patient motion variation scenarios, except the 0s-20s segment where the maximum dose to the CTV was 64.9 Gy. The maximum intensity method of the

worst case approach was not robust to any of the patient motion variation cases as the CTV was both under-dosed and over-dosed in all motion variation cases. The average minimum dose to the CTV for the worst case using the maximum intensity method plan was used was 55.0 Gy and the average maximum dose to the CTV was used was 65.7 Gy.

Figure 3.29 shows the dose delivered to 99% of the volume when the four planning methods are applied to different amplitude variation scenarios. It is noted that the worst case plan using the average intensity method met the D99 criterion except for the 80s-100s segment. Figure 3.30 shows the statistics for V20 of the CTV bearing lung. The average V20 to the lung from all planning approaches was 6.5%.

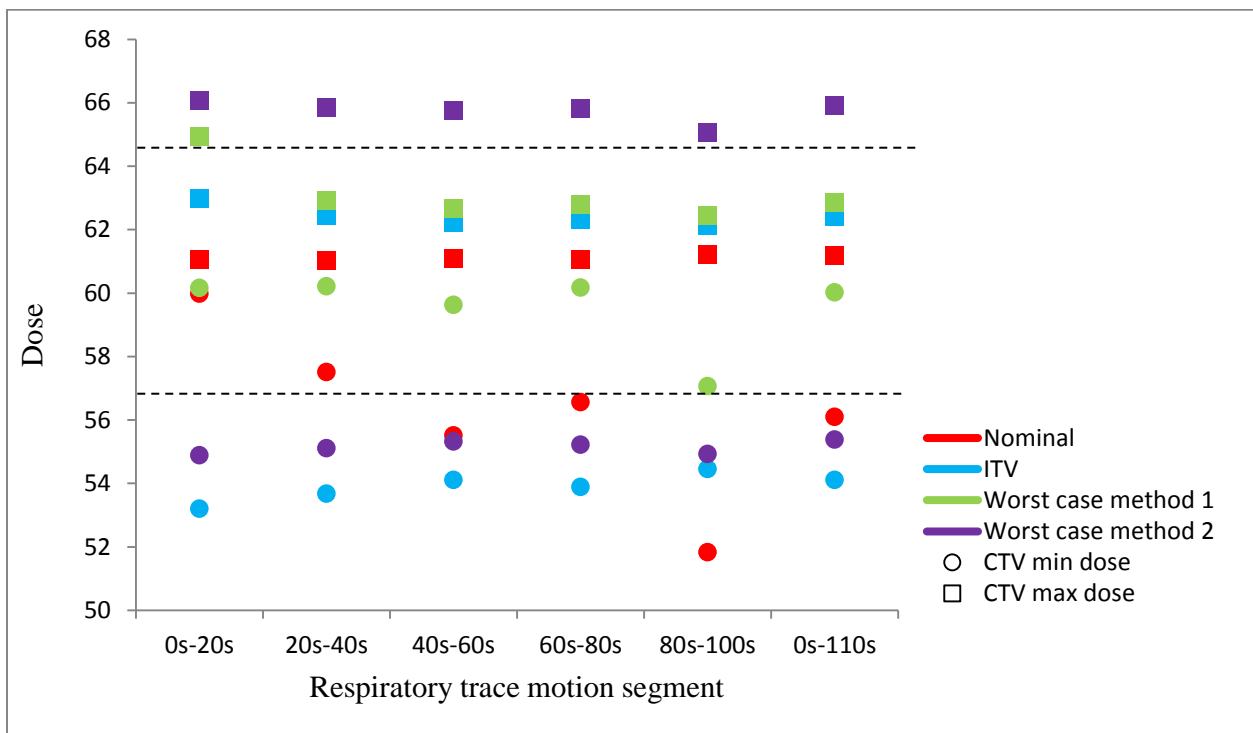


Figure 3.28: Minimum and maximum doses of different planning approaches on patient motion variation scenarios. The dashed lines represent the minimum and maximum doses defined by ICRU criteria (57 Gy and 64.2 Gy respectively). Method 1 is the average intensity method, and Method 2 is the maximum intensity method

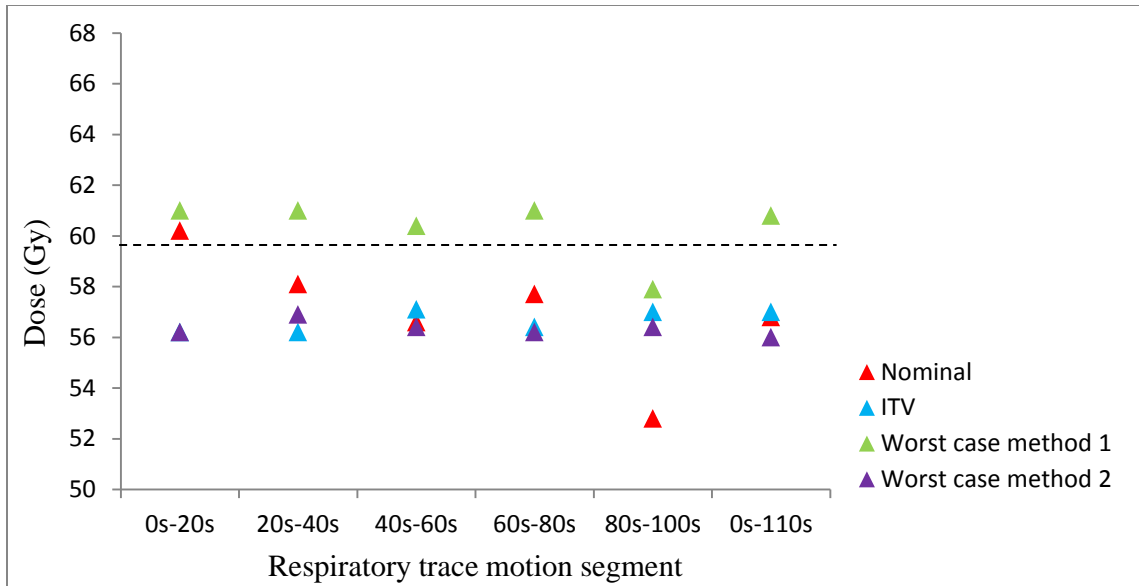


Figure 3.29: D99 of different planning approaches on patient motion variation scenarios. The dashed lines represent the minimum D99 defined by lung cancer radiation therapy protocols in PMH (59.4 Gy). Method 1 is the average intensity method, and Method 2 is the maximum intensity method

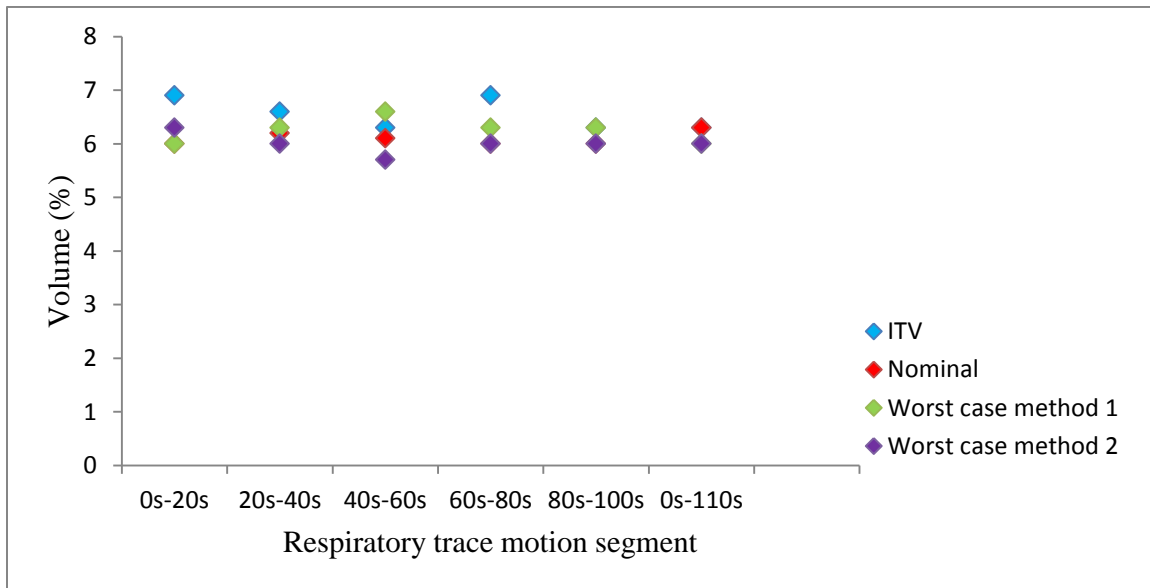


Figure 3.30: V20 of different planning approaches on amplitude variation study. Method 1 is the average intensity method, and Method 2 is the maximum intensity method

3.5 Study 4: Patient inter-fractional motion variations using patient 4DCT data

A nominal 4D plan was created based on the pdf from the full respiratory trace of week 0. This plan was then applied to the week 2, 4, and 7 4DDIJs calculated using the full respiratory traces from each of those weeks. Figure 3.31 shows the results of the nominal plan applied to the different week pdfs. This plan was robust to all inter-fractional respiratory motion variations, except for week 4. The minimum dose to the CTV when applying the nominal plan on week 4 was 56.2 Gy.

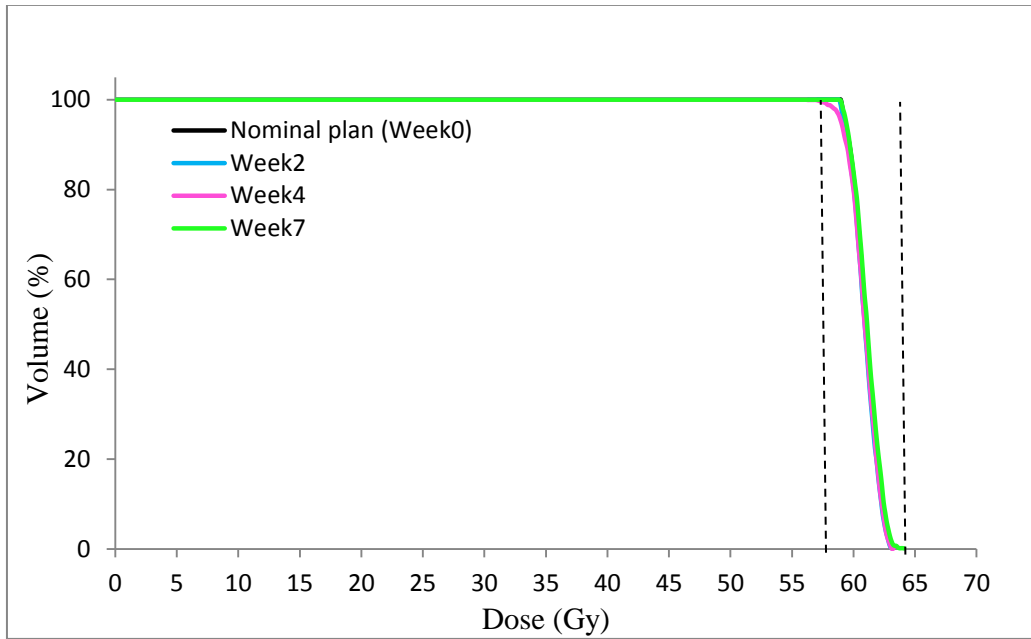


Figure 3.31: Dose volume histograms of the ITV plan applied to the 20s segments of the patient respiratory motion trace showing dose coverage to both the CTV and the right lung.

Chapter 4 Discussion, Conclusions and Future work

4.1 Discussion

The goal of this project was to test the robustness of a novel planning method, which we call the worst case planning approach, to patient intra-fractional respiratory motion variations. The worst case plan is created by optimizing two 4D plans on the worst case motion variation scenarios. Then, the intensity maps of the two 4D worst case plans are combined by either averaging the beamlet intensities (average intensity method) or taking the highest beamlet intensity of the two intensity maps (maximum intensity method). The hypothesis was that the worst case 4D plans developed on clinical patient data would be robust to patient intra-fractional motion variations.

We compared the robustness of nominal 4D plans, ITV plans and worst case plans for three different scenarios: (1) amplitude variations using simulated image data; (2) patient motion variations using simulated image data and (3) patient motion variations using patient image data. Plans were deemed robust if the delivered dose met clinical treatment plan criteria.

The worst case approach using the average intensity method was found to be robust only to the motion variations in Study 3 except for the nominal motion, while the worst case approach using the maximum intensity method was not robust to any of the 3 motion variation scenarios. When comparing the pdfs used in Study 2 with Study 3, we found that the average coefficient of variance of the weight of the breathing phases was 0.92 and 0.44 for Study 2 and Study 3, respectively, which means that the variation in the pdfs was more for Study 2 than for Study 3. This may explain why the worst case planning using the average intensity method was robust for most of the motion scenarios in Study 3 but not for Study 2.

The worst case approach was also compared to the nominal 4D optimization and ITV margin approaches. The nominal 4D plans were only robust to the nominal motion in each study because this approach does not account for uncertainties in respiratory motion. The robustness of the ITV planning approach varied between the different studies. In Study 1 the ITV plan covered the CTV up to the nominal motion amplitude only, since the ITV was contoured from the exhale and inhale GTV corresponding to the nominal motion. In Study 2, the ITV was contoured by fusing the GTVs from all 10 phases. However, the ITV plan was not robust to all motion scenarios. The ITV approach geometrically covers the range of tumour motion but does not consider variations in the dose delivered on different respiratory phases. Further investigation showed that there was a cold spot

inside the CTV when the ITV plan was applied to one of the phases near inhale (phase 8). The ITV plan was optimized on the exhale CT image and the density values of this image are different compared to the other respiratory phase images. These density changes could explain the presence of the cold spot in the dose delivered on phase 8 and why the ITV plan was not robust in Study 2. The ITV plan in Study 3 was also not robust for any of the motion variation scenarios in that study. This may be because the ITV contour that was provided for the patient study was only based on exhale and inhale CTV contours, while the dose was accumulated over all the 10 phases. As CTV contours were only provided for the inhale and exhale phases it was not possible to verify whether the CTV was covered on all respiratory phases. Another reason why the ITV plan was not robust for Study 3 could be attributed to dose perturbations due to density changes, similar to Study 2. The reason why the ITV plan was not robust for Study 3 was not investigated in this project.

In terms of OAR statistics, the ITV planning approach gave more dose to the CTV bearing lung than other planning approaches. The average V20 (volume covered by 20 Gy or more) to the CTV bearing lung by the ITV planning approach was 30%, 31% and 7.9% for study 1, 2, and 3 respectively. On the other hand, the average V20 to the CTV bearing lung by the average intensity worst case method was 26%, 22% and 7.9% for study 1, 2, and 3 respectively. The reader is reminded that V20 of the lungs should not exceed 30%

Throughout this project, it was realized that the uniformity of the intensity map affected the robustness of the resulting worst case plans. More uniform intensity maps resulted in a lower sensitivity to motion variations. As mentioned in Chapter 2, the choice of KonRad constraints affected the uniformity of the intensity map, which in turn affected the robustness of the plan. The average intensity method of the worst case approach generated more uniform intensity maps when compared to the maximum intensity method. This is because the latter method takes the maximum value of the beamlet in one intensity map and the corresponding beamlet in the other intensity map. Therefore, the combined intensity map was also non-uniform. For example, in Study 3, the standard deviation of the static dose to the CTV from the combined intensity map was 2.5 Gy and 5.5 Gy for the average and the maximum intensity methods, respectively. This explains why the maximum intensity method plans were found to not be robust to any of the studies presented in this thesis.

4.2 Limitations to the study

The worst case plan using the average intensity method was robust for most realistic intra-fractional patient motion variations. This method, however, was not investigated on a different range of tumour sizes, locations and motion variations. Furthermore, the tumour size was 11.5 cm³ which is

considered to be a small tumour that would be more likely to be treated with SBRT. Also, our study only tested robustness to intra-fractional motion variations. Preliminary results from applying the nominal 4D plan on inter-fractional patient motion variations found that it was mostly insensitive to those motion variations. This is because the average coefficient of variance in the pdfs for Study 4 was very small (0.33). Further investigations with data from more patients are required to investigate the sensitivity of the nominal 4D planning approach to inter-fractional motion variations and, if required, whether the worst case planning approach would be robust to these types of variations.

It should also be noted that for Study 3 we did not use the prescribed beam angles from the PMH plan data. An attempt was made to optimize 4D plans using the prescribed angles provided to make our plans as close to a realistic clinical case as possible. However, because the treatment planning system used in PMH is different from KonRad, the dose distribution resulting from using the prescribed angles did not cover the CTV with the desired minimum dose. Therefore, a 7 star beam arrangement was created which yielded better dose distribution than the beam arrangement provided by PMH. It would be more clinically relevant to use a smaller number of beams.

Another limitation to Study 3 is that we used phase binned 4DCT images while we assumed that the images were displacement binned to account for amplitude variations. This assumption, however, did not introduce a large error in this project because the difference in tumor displacement between the different phases was small. Displacement binned 4DCTs were not provided for the patient study as the clinical standard is to acquire phase binned 4DCTs

Finally, inter-fractional *anatomical* variations have not been studied in this work. Inter-fractional anatomical variations are likely to be more significant to 4D planning than inter-fractional motion variations but they also affect the magnitude of motion variations. For example, as the patient progresses with the treatment, the tumour usually shrinks, and smaller tumours are more mobile. Furthermore, some tumours are attached to the chest wall during the beginning of the treatment, and when the tumour gets smaller, it might get detached from the chest wall, which causes it to be more mobile.

4.3 Conclusions

This project investigated the robustness of the worst case planning method to simulated and patient intra-fractional motion variations. Two methods to generate the worst case plans were investigated and tested on three different motion variation scenarios. The robustness of the worst case approaches were compared to nominal 4D and ITV plans. The worst case using the maximum intensity method was not robust to any of the motion variation scenarios. The worst case planning using the average

intensity method was found to be robust to the patient motion variations in terms of target coverage, although the target volume was overdosed for the nominal motion. The nominal 4D plan was not robust to any of the studies, because it was not designed explicitly to account for motion variations. In most cases the ITV plan was robust, but this came with the trade-off of a higher lung dose.

In conclusion, the worst case approach using the average intensity method was robust to most intra-fractional motion using clinically realistic data for NSCLC patient. Further investigation on a wide range of tumour sizes, locations and motion variations are needed to evaluate this approach.

4.4 Future work

Further evaluation of the feasibility of the worst case method requires the investigation of inter-fractional motion and anatomical variations. The effectiveness of the worst case method also needs to be investigated on a different range of tumour sizes, locations, and motion variations. To test the robustness of the worst case method on inter-fractional motion and anatomical variations (combined), the pdfs from the full breathing trace for each week could be used. This accounts for inter-fractional motion variations. To account for inter-fractional anatomical variations, the plans could be applied to the 4DCTs from each treatment week.

Since our results indicated that the smoothness of the intensity maps had an important effect on plan robustness, methods to obtain smoother intensity maps should be investigated to potentially improve the robustness of the worst case approach. A possible approach could include using a different treatment plan optimization software which uses different plan constraints that allow better control of intensity map smoothness.

Bibliography

- [1] "Canadian Cancer Society," [Online]. Available: http://www.cancer.ca/Canada-wide/About%20cancer/Cancer%20statistics/PowerPoint%20slides.aspx?sc_lang=EN. [Accessed 15 11 2012].
- [2] K. H. Kernstine, Lung cancer a multidisciplinary approach to diagnosis and management, New York: DEMOSMEDICAL, 2011.
- [3] "American Cancer Society," [Online]. Available: <http://www.cancer.org/cancer/lungcancer-non-smallcell/detailedguide/non-small-cell-lung-cancer-survival-rates>. [Accessed March 2014].
- [4] F. M. Kong and R. K. Ten Haken , "High-Dose radiation improved local control and overall survival in patients with inoperable/unresectable non-small-cell lung cancer: long-term results of a radiation Dose escalation study," *Int J Radiat Oncol Biol Phys*, vol. 63, no. 2, pp. 324-333, 2005.
- [5] F. Khan, The physics of radiation therapy, Philadelphia: Lippincott Williams and Wilkins, 2003.
- [6] E. Weiss , J. Siebers and P. Keall , "An analysis of 6-MV versus 18-MV photon energy plans for intensity-modulated radiation therapy (IMRT) of lung cancer.," *Radiother Oncol*, vol. 82, no. 1, pp. 55-62, 2007.
- [7] Podgorosak, Radiation oncology physics: a handbook for teachers and students, Vienna: International Atomic Energy Agency, 2005.
- [8] "Varian Medical Systems Newsroom," [Online]. Available: <http://newsroom.varian.com/image-gallery?mode=gallery&cat=2473>. [Accessed 16 March 2014].
- [9] A. Recht, M. Ancukiewicz, M. A. Alm El-Din, X. Qi Lu, C. Martin, S. M. Berman, A. E. Hirsch, L. A. Kachnic, A. Katz, S. MacDonald, E. A. Nedeia, M. A. Stevenson, S. N. Powell and A. G. Taghian, "Lung Dose-Volume Parameters and the Risk of Pneumonitis," *JOURNAL OF CLINICAL ONCOLOGY*, vol. 27, no. 24, pp. 3887-3893, 2009.
- [10] Y. Lo , W. McBride and H. Withers, "The effect of single doses of radiation on mouse spinal cord.," *Int J Radiat Oncol Biol Phys*, vol. 22, no. 1, pp. 57-63, 1992.
- [11] C. Taylor, A. Nisbet, P. McGale and S. Darby, "Cardiac Exposures in Breast Cancer Radiotherapy: 1950s-1990s," *International Journal of Radiation Oncology, Biology, Physics*, vol. 69, no. 5, pp. 1484-1495, 2007.

- [12] I. R. 62, "Prescribing, Recording and Reporting Photon Beam Therapy (Supplement to ICRU Report 50)," 1999.
- [13] Z. Allibhai, M. Taremi, A. Bezjak, A. Brade, A. Hope and A. Sun, "The Impact of Tumor Size on Outcomes After Stereotactic Body Radiation Therapy for Medically Inoperable Early-Stage Non-Small-Cell Lung Cancer," *International Journal of Radiation Oncology*, vol. 87, no. 5, pp. 1064-1070, 2013.
- [14] J. Meyer, IMRT, IGRT, SBRT: Advances in the treatment planning and delivery of radiotherapy, Basel: Karger, 2007.
- [15] P. Williams, "IMRT: delivery techniques and quality assurance," *The British journal of Radiology*, vol. 76, pp. 766-776, 2003.
- [16] C. Elith, S. E. Dempsey, M. Findlay and H. M. Warren-Forward, "An Introduction to the Intensity-modulated Radiation Therapy (IMRT) techniques. Tomotherapy, and VMAT," *Journal of Medical Imaging and Radiation Sciences*, vol. 42, pp. 37-43, 2011.
- [17] D. M. Shepard, M. A. Earl, X. A. Li and S. Naqvi, "Direct aperture optimization: A trunky solution for step-and-shoot IMRT," *Med.Phys.*, vol. 29, no. 6, pp. 1007-1018, 2002.
- [18] T. Bortfeld, Image Guided IMRT concepts and clinical applications, New York: Springer, 2005.
- [19] P. J. Keal , G. S. Mageras, J. M. Balter, J. S. Emery, K. M. Forster, S. B. Jiang, J. M. Kapatoes, D. A. Low, M. J. Murphy, B. R. Murray, C. R. Ramsey, M. B. Van Herk, S. S. Vedam, J. W. Wong and E. Yorke, "The management of respiratory motion in radiation oncology report of AAPM Task Group 76," *Med.Phys.*, vol. 33, pp. 3874-3900, 2006.
- [20] I. M. Gagné and D. M. Robinson, "The impact of tumor motion upon CT image integrity and target delineation.," *Med. Phys.*, vol. 31, no. 12, pp. 3378-3392, 2004.
- [21] S. S. Korreman, "Motion in Radiotherapy: photon therapy," *Med. Phys*, vol. 57, no. 23, pp. 161-191, 2012.
- [22] C. J. Ritchie, J. D. Godwin, C. R. Crawford, W. Stanford, H. Anno and Y. Kim, "Minimum scan speeds for supression of motion artifacts," *Radiology*, vol. 185, no. 1, pp. 37-42, 1992.
- [23] T. Bortfeld, S. B. Jiang and E. Rietzel, "Effects of motion on the total dose distribution," *Seminars in Radiation Oncology*, vol. 14, no. 1, pp. 41-51, 2004.
- [24] R. D. Timmerman and L. Xing, Image-guided and adaptive radiation therapy, Philadelphia: Lippincott Williams & Wilkins/ Wolters Kluwer Health, 2010.

- [25] A. F. Abdelnour, S. A. Nehmeh, Y. E. Edri, T. Pan, J. L. Humm, P. Veron, H. Schoder, K. E. Rosenzweig, G. S. Mageras, E. Yorke and S. M. Larson, "Phase and amplitude binning for 4D-Ct imaging," *Phys Med Biol*, vol. 52, no. 12, pp. 3515-3529, 2007.
- [26] L. Wei, P. J. Parikh, J. P. Hubenschmid, J. D. Bradley and D. A. Low, "A comparison between amplitude sorting and phase angle sorting using external respiratory measurement for 4D CT," *Med. Phys.*, vol. 33, no. 8, pp. 2964-2974, 2006.
- [27] J. Hanley, M. M. Debois, D. Mah, G. S. Mageras, A. Raben, K. Rosenzweig, B. Mychalczak, L. H. Schwartz, P. J. Glogger, W. Lutz, C. C. Ling, S. A. Leibel, Z. Fuks and G. J. Kutcher, "Deep inspiration breath-hold technique for lung tumors: the potential value of target immobilization and reduced lung density in dose escalation," *Int. J. Radiat. Oncol. Biol. Phys.*, vol. 45, no. 3, pp. 603-611, 1999.
- [28] K. E. Rosenzweig, J. Hanley, D. Mah, G. Mageras, M. Hung, S. Oner, C. Burman, C. C. Ling, B. Mychalczak, Z. Fuks and S. A. Leibel, "The deep inspiration breathhold technique in the treatment of inoperable non-small-cell lung cancer," *Int. J. Radiat. Oncol. Biol. Phys.*, vol. 48, no. 1, pp. 81-87, 2000.
- [29] D. Mah, J. Hanley, K. E. Rosenzweig, E. Yorke, L. Braban, C. C. Ling and S. A. Leibel, "Technical aspects of the deep inspiration breath-hold technique in the treatment of thoracic cancer," *Int. J. Radiat. Oncol. Biol. Phys.*, vol. 48, no. 4, pp. 1175-1185, 2000.
- [30] M. Stock, K. Kontrisoova, K. Dieckmann, J. Bongers, R. Poetter and D. George, "development and application of a real-time monitoring and feedback system for deep inspiration breath hold based on external marking tracker," *Med. Phys.*, vol. 33, pp. 2868-2877, 2006.
- [31] M. J. Murphy, D. Martin, R. Whyte, J. Hai, C. Ozhasoglu and Q.-T. Le, "The effectiveness of breathholding to stabilize lung and pancreas tumors during radiosurgery," *Int. J. Radiat. Oncol. Biol. Phys.*, vol. 53, no. 2, pp. 475-482, 2002.
- [32] R. M. Underberg, F. J. Lagerwaard, B. J. Slotman, J. P. Cuijpers and S. Senan, "Benefit of respiration-gated stereotactic radiotherapy for stage 1 lung cancer: an analysis of 4DCT datasets," *Int. J. Radiat. Oncol. Biol. Phys.*, vol. 62, no. 2, pp. 554-560, 2005.
- [33] A. M. Berson, R. Emery, L. Rodrigues, G. M. Richards, T. Ng, S. Sanghavi and J. Barsa, "Clinical experience using respiratory gated radiation therapy: comparison of free-breathing and breath-hold techniques," *Int. J. Radiat. Oncol. Biol. Phys.*, vol. 60, no. 2, pp. 419-426, 2004.
- [34] Y. Cui, J. G. Dy, G. C. Sharp, B. Alexander and S. B. Jiang, "Robust fluoroscopic respiratory gating for lung cancer radiotherapy without implanted fiducial markers," *Phys. Med. Biol.*, vol. 52, no. 3, pp. 741-755, 2007.

- [35] K. Ohara, T. Okumura and M. Akisada, "Irradiation synchronized with respiration gate," *Int. J. Radiat. Oncol. Biol. Phys.*, vol. 17, no. 4, pp. 853-857, 1989.
- [36] P. J. Keal, H. Cattell, D. Porkhel, S. Dieterich, K. H. Wong, M. J. Murphy, S. S. Vedam, K. wijesooriya and R. Mohan, "Geometric accuracy of a real time target tracking system with dynamic multileaf collimator tracking system," *Int. J. Radiat. Oncol. Biol. Phys.*, vol. 65, no. 5, pp. 1579-1584, 2006.
- [37] "CyberKnife," CyberKnife, [Online]. Available: www.cyberknife.com. [Accessed 12 Nov 2014].
- [38] T. Neicu, R. Berbeco, J. Wolfgang and S. B. Jiang, "Synchronized moving aperture radiation therapy (SMART): improvement of breathing pattern reproducibility using respiratory coaching," *Phys. Med. Biol.*, vol. 51, no. 3, pp. 617-636, 2006.
- [39] M. Van Herk, P. Remeijer, C. Rasch and J. V. Lebesque, "The probability of correct target dosage: Dose-population histograms for deriving treatment margins in radiotherapy," *Int. J. Radiat. Oncol. Biol. Phys.*, vol. 47, no. 4, pp. 1121-1135, 2000.
- [40] J. W. Wolthaus, C. Schneider, J. Sonke, V. Herk, J. S. Belderbos and M. M. Rossi, "Mid-ventilation CT scan construction from four-dimensional respiration-correlated CT scans for radiotherapy planning of lung cancer patients," *Int. J. Radiat. Oncol. Biol. Phys.*, vol. 65, no. 5, pp. 1560-1571, 2006.
- [41] A. Trofimov, E. Rietzel, H. M. Lu, B. Martin and S. Jiang, "Temporo-spatial IMRT optimization: concepts, implementation and initial results," *Phys. Med. Biol.*, vol. 50, no. 12, pp. 2779-2798, 2005.
- [42] H. Shirato, Y. Seppenwoodle, K. Kitamura, R. Onimura and S. Shimizu, "intrafractional tumor motion: lung and liver," *Seminars in Radiation Oncology*, vol. 14, no. 1, pp. 10-18, 2004.
- [43] J. Sonke, J. Lebesque and M. V. Herk, "Variability of four dimensional computed tomography patient models," *Int. J. Radiat. Oncol. Biol. Phys.*, vol. 70, no. 2, pp. 590-598, 2008.
- [44] J. Sonke and J. Belderbos, "Adaptive Radiotherapy for Lung Cancer," *Seminars in Radiation Oncology*, vol. 20, no. 2, pp. 94-106, 2010.
- [45] C. Cohade and R. L. Wahl, "Applications of positron emission tomography/ computed tomography image fusion in clinical positron emission tomography: Clinical use, interpretation methods, diagnostic improvements," *Seminars in Nuclear Medicine*, vol. 33, no. 3, pp. 228-237, 2003.
- [46] E. Heath, J. Unkelbach and U. Oelfke, "Incorporating uncertainties in respiratory motion into

- 4D treatment plan optimization," *Med. Phys.*, vol. 36, no. 7, pp. 3059-3071, 2009.
- [47] T. Chan, T. Bortfeld and J. Tsitsiklis, "A robust approach to IMRT optimization," *Phys. Med. Biol.*, vol. 51, no. 1, pp. 2567-2583, 2006.
- [48] M. Machtay, K. Bae, B. Movsas, R. Paulus, E. Gore, R. Komaki, K. Albain, W. Sause and W. Curran, "Higher biologically effective dose of radiotherapy is associated with improved outcomes for locally advanced non-small cell lung carcinoma treated with chemoradiation: an analysis of the Radiation Therapy Oncology Group," *Int J Radiat Oncol Biol Phys*, vol. 82, no. 1, pp. 425-434, 2012.
- [49] C. Pokhrel and E. Heath, "A Robust 4D Treatment Planning Approach for Lung Radiotherapy," in *AAPM 55th Annual Meeting*, Indianapolis, Indiana, 2013.
- [50] W. P. Segars, M. Mahesh, T. J. Beck, E. C. Frey and B. M. Tsui, "Realistic CT simulation using the 4D XCAT phantom," *Med. Phys.*, vol. 35, no. 8, pp. 3800-3808, 2008.
- [51] "The DICOM Standard," [Online]. Available: <http://medical.nema.org/standard.html>. [Accessed 28 Oct 2014].
- [52] *Virtuos: Virtual Radiotherapy Simulator: The user manual*, 2002.
- [53] S. Nill, *Development and application of a multi-modality inverse treatment planning*, 2001.
- [54] D. L. Collins and C. Evans, "Animal: Validation and Applications of Nonlinear Registration-Based Segmentation," *Int. J. Patt. Recogn. Artif. Intell.*, vol. 11, no. 8, pp. 1271-1294, 1997.
- [55] E. Heath, D. L. Collins, P. J. Keall, L. Dong and J. Seuntjens, "Quantification of accuracy of the automated nonlinear image matching and anatomical labeling (ANIMAL) nonlinear registration algorithm for 4D CT images of lung," *Med. Phys.*, vol. 34, no. 11, pp. 4409-4421, 2007.
- [56] W. D. D'Souza, S. A. Naqvi and C. X. Yu, "Real-time intra-fraction motion tracking using the treatment couch: a feasibility study," *Phys. Med. Biol.*, vol. 50, no. 17, pp. 4021-4033, 2005.
- [57] W. Elisabeth, S. V. Jeffrey and P. J. Keall, "An analysis of 6-MV versus 18-MV photon energy plans," *Radiotherapy and Oncology*, vol. 82, no. 1, pp. 55-62, 2007.

